Master's thesis

NTNU
Norwegian University of Science and Technology
Faculty of Natural Sciences
Department of Biotechnology and Food Science

Andrea Mandt-Utbøen Holtermann

Viability and Morphology of Human Fibroblasts in RGD-functionalized 3D-Alginate Scaffolds

Qualitative Image Analysis with Focus on the Effects of Microstructuring

Master's thesis in Biotechnology
Supervisor: Berit Løkensgard Strand
Co-supervisor: Aman Sing Chahal
September 2021

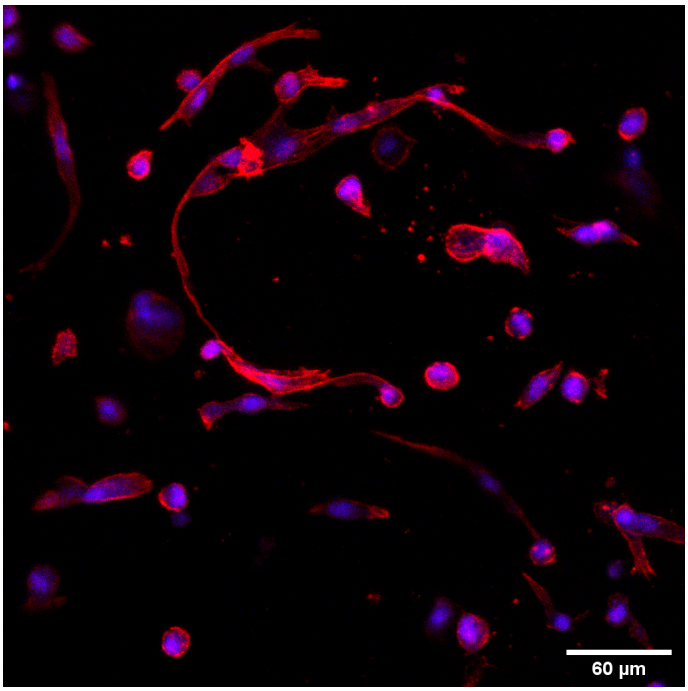

NTNU
Norwegian University of Science and Technology

Andrea Mandt-Utbøen Holtermann

Viability and Morphology of Human Fibroblasts in RGD-functionalized 3D-Alginate Scaffolds

Qualitative Image Analysis with Focus on the Effects of Microstructuring

Master's thesis in Biotechnology
Supervisor: Berit Løkensgard Strand
Co-supervisor: Aman Sing Chahal
September 2021

Norwegian University of Science and Technology
Faculty of Natural Sciences
Department of Biotechnology and Food Science

NTNU
Norwegian University of
Science and Technology

Acknowledgements

This master thesis is a part of the Master's Degree Programme in Biotchnology at the Norwegian University of Science and Technology, and was carried out at the Department of Biotechnology and Food Science.

I want to give my deepest thanks to co-supervisor Aman Singh Chahal for patiently, and with dedication, teaching me everything I needed to know in the lab, and for supporting me all the way throughout the work with this thesis. I want to thank my supervisor Berit Løkensgard Strand for her unique ability to motivate and for always giving helpful advice and feedback. I also want to thank Daria Zaytseva-Zotova for introducing me to working with cells and for inspirational chats in the lab. Thanks to Astrid Bjørkøy for thorough training and help with the confocal microscope. It has been a fun, educational and challenging year. I also wish to thank study consultant Henrik Stamnes Dahl for providing clear information and being helpful with the practical and formal aspects with finishing this degree.

You have all been essential!

Lastly, I wish to thank my family and my friends for always being so caring and for putting up with me. I'm so grateful.

September 10th, 2021

Andrea Mandt-Utbøen Holtermann

Per aspera ad astra

Abstract

The use of three-dimensional (3D) cell culture rather than conventional two-dimensional (2D) cultures is of increasing interest, as it has shown to induce cell characteristics and functions of higher complexity that are more similar to those *in vivo*. This could offer more biologically relevant responses in cell studies, and therefore it is being actively adopted by fields such as cell biology, drug development, cancer research and tissue engineering. Many different 3D scaffolds exist, such as bulk gels, beads, macroporous sponges and foams, fibers and matrices. Hydrogels, based on synthetic or natural polymers, is considered an attractive material due to their similarity to the extracellular matrix surrounding cells. Alginate hydrogels are one such material, popularly used due to its high biocompatibility and extensive ability to form gels of varying mechanical properties. Alginate gels are most typically formed via crosslinking with a divalent cation such as Ca^{2+}. Unmodified alginate hydrogels typically do not support cell culture. To overcome this, chemical modifications can be applied to render this material as bioactive. However, mechanical properties such as stiffness, porosity and structuring are also of importance. For adherent cells such as fibroblasts, ligands for adhesion are crucial. These cells interact with their surroundings by binding to RGD-peptides, either *in vivo* to fibronectin of the extracellular matrix or *in vitro* to RGD grafted onto the culturing material. Attachment allows them to exert force on the material, and thereby also to exhibit movement and spreading by actin filament polymerization and myosin-actin contractility. Fibroblasts are common cells in research and are present in connective tissues throughout the whole body. In this study, the effects of alginate microstructures in 3D scaffolds on the viability and morphology of human fibroblastic cell types were investigated. These cells were primary normal dermal fibroblasts (NHDFs), cell line fetal lung cells (IMR-90) and cell line adult bone marrow cells (HS-5). The cells were cultivated for up to 21 days in a porous alginate foam and a homogeneous gel, both containing 1% (w/v) Ca^{2+}alginate (75% functionalized with RGD-containing peptide GRGDSP), and analyzed after 1, 7 and 21 days using light microscopy, fluorescent labeling and confocal laser scanning microscopy and cytotoxicity tests based on LDH-release. No major differences in viability and cytotoxicity between foam and hydrogel were observed for any of the cell types. The NHDFs were generally more viable than the other cell types, and interacted more with the material, which could be related to them being primary cells. Morphological effects were seen in the form of actin extensions, with more organized cytoskeleton in cells exposed to the foam. Over time IMR-90 and HS-5 seemed to prefer cell-cell interaction, possibly due to inherent incompatibilities with the material properties.

Sammendrag

Bruk av tredimensjonal (3D) cellekultivering istedenfor konvensjonell todimensjonal (2D) kultivering er av økende interesse, ettersom det har vist seg å kunne indusere mer komplekse egenskaper og funksjoner hos celler, som ligner mer på de i kroppen eller vev (*in vivo*). Dette kan bidra til responser av høyere biologisk relevans i cellestudier, og derfor er bruken av dette økende innen cellebiologi, legemiddelutvikling, kreftforskning og vevsteknikk. Mange ulike systemer for 3D-cellekultivering finnes, eksempelvis geler, mikrokapsler eller perler, makroporøse svamper og skum, fibre og andre 3D-matrikser. Hydrogeler, basert på enten syntetiske eller naturlige polymerer, er et attraktivt materiale på grunn av likheter med den ekstracellulære matriksen som finnes rundt celler i vev. Hydrogeler baser på alginat er populære på grunn av høy biokompatibilitet og god evne til å danne geler med varierende mekaniske egenskaper. Alginatgeler lages ofte ved tverrbinding med et divalent kation, som for eksempel Ca^{2+}. Hydrogeler av umodifisert alginat er mindre anvendelige i cellekultur, men kjemisk modifikasjon kan gjøre materialet bioaktivt. Mekaniske egenskaper slik som stivhet, porøsitet og strukturering er også av betydning. For forankringsavhengige celler slik som fibroblaster er ligander som tillater forankring essensielt. Slike celler interagerer med omgivelsene ved å binde til RGD-peptider, enten til fibronektin i den ekstracellulære matriksen *in vivo* eller til cellekulturmaterialer modifisert med RGD. Binding tillater cellene å utøve kraft mot materialet, noe som tillater bevegelse og spredning av cellen ved polymerisering av aktin filamenter og kontraksjon utøvd av aktin og myosin i cellen. Fibroblaster finnes i kroppens bindevev, og er mye brukt i forskning. I denne studien undersøkes effektene av alginat-mikrostrukturer i 3D-kultivering på levedyktighet og morfologi hos menneskelige fibroblaster. Cellene som ble studert var primærceller fra dermis (NHDF), og cellelinjene IMR-90 og HS-5, henholdsvis med opphav i lungeceller fra embryo og stromale beinmargceller. Cellene ble dyrket opptil 21 dager i et porøst alginatskum og i en homogen gel, begge bestående av 1% Ca^{2+}alginat (75% funksjonalisert med RGD-inneholdende peptid GRGDSP), og analysert etter 1, 7 og 21 dager med bruk av lysmikroskopi, fluorescensfarging og konfokal laserskannemikroskopi, og test av cytotoksisitet baser på frigjort LDH. Ingen store forskjeller i levedyktighet og cytotoksisitet mellom skum og hydrogel ble observert i noen av celletypene. NHDF-cellene var generelt mer levedyktige enn de andre cellene, og interagerte mer med materialet, som muligens kan være relatert til at de er primærceller. Effekter på cellemorfologi ble observert i form av forlengelser av aktin, som i skum var preget av mer organisert cytoskjelett. Over tid foretrakk IMR-90 og HS-5 celle-celle-interaksjon, som kan skyldes inkompatibilitet med materialegenskapene.

Abbreviations

2D	*Two-dimensional*
3D	*Three-dimensional*
AM	*Acetoxymethyl ester*
AT	*Adenine-thymine*
ATCC	*American Type Culture Collection*
AU	*Adenine-uracil*
bp	*Base pairs*
CLSM	*Confocal laser scanning microscopy*
-COOH	*Carboxyl*
D1	*Day 1 (after seeding cells and casting gels)*
D21	*Day 21*
D7	*Day 7*
DAPI	*4',6-diamidino-2-phenylindole dihydrochloride*
DMEM	*Dulbecco's Modified Eagle Medium*
DNA	*Deoxyribonucleic acid*
dsDNA	*Double stranded DNA*
ECM	*Extracellular matrix*
EDTA	*Ethylenediaminetetraacetic acid*
EthD-1	*Ethidium homodimer-1*
F	*Fraction*
FBM	*Fibroblast basal medium*
F_G	*Fraction of guluronate*
FGM	*Fibroblast growth medium*
FITC	*Fluorescein isothiocyanate*
FN	*Fibronectin*
FP	*Fluorescent protein*
G	*α-L-guluronic acid*
GAG	*Glycosaminoglycan*
GC	*Guanine-cytosine*
GDL	*Glucono delta lactone*
GFP	*Green fluorescent protein*
GRGDSP	*Gly-Arg-Gly-Asp-Ser-Pro (RGD-containing peptide)*
HA	*Hyaluronan*
HBSS	*Hank's Balanced Salt Solution*

HDF	*Human dermal fibroblast*
HEPES	*4-(2-hydroxyethyl)-1-piperazineethanesulfonic acid*
HPMC	*Hydroxypropyl methylcellulose*
HPV	*Human papilloma virus*
HS-5	*Cell line of human bone marrow stromal fibroblast-like cells*
HSC	*Hematopoietic stem cell*
IC	*Inosine-uracil*
IFF	*International Flavors & Fragrances*
IMR-90	*Cell line of normal human fetal lung fibroblast (Institute for Medical Research-90)*
INT	*Iodotetrazolium chloride*
INT	*Iodonitrotetrazolium (tetrazolium salt)*
LAF	*Laminar air flow*
LDH	*Lactate dehydrogenase*
M	*β-D-mannuronic acid*
MMP	*Matrix metalloproteinase*
MSC	*Mesenchymal stromal/stem cell*
M_w	*Molecular weight*
NH	*Indole nitrogen*
NHDF	*Normal human dermal fibroblast*
-OH	*Hydroxyl*
P	*Passage number*
PBS	*Phosphate-buffered saline*
PEG	*Polyethylene glycol*
PFA	*Paraformaldehyde*
RGD	*Arg-Gly-Asp (tripeptide)*
RNA	*Ribonucleic acid*
RT	*Room temperature*
SMC	*Smooth muscle cell*
ssDNA	*Single stranded DNA*
T75	*Tissue culture flask (treated surface area 75cm^2)*
TCP	*Tissue culture plastic*
UP LVG	*Ultrapure low viscosity guluronate (alginate)*
UV	*Ultraviolet*

Contents

1 INTRODUCTION

We live in a three-dimensional world. We can sense the ground under the soles of our feet, feel whether it's raining, or the sun is shining on our heads. We can smell our food and recognize signs of danger. These are all important cues to tell us how to act and adapt in order to survive. The cells we are built from live in such a world too – the three-dimensionality that is inherent to our tissues and organs. When cells are studied *in vitro*, they are removed from their natural microenvironment. While cells contribute to the construction of their environment, they also adapt themselves according to their surroundings. There is a mutual feedback interaction made possible through receptors on the cell surface, the cell's way of sensing its world. Hence, when the cellular environment changes, the cell is bound to adapt to these changes. Traditionally, culturing of cells on two-dimensional (2D) tissue culture plastic (TCP) has been the standard. However, current knowledge from research indicates culturing in three-dimensional (3D) materials might be more biologically relevant [1], especially for studying specific cell types or cell states [2]. Cells proliferate well in 2D, but there is a desire to allow the cells to express characteristics more similar to those *in vivo*. This can possibly be better achieved by making *in vivo*-like models by tailoring materials according to requirements of the cells. 3D materials that mimic the natural environment of cells offer a lot of possibilities within fields such as drug development and toxicology [3]. Due to this, there seems to be an ongoing shift from 2D cultivation on flat TCP to 3D encapsulation of cells in materials that more accurately mimic the natural cellular environment [3, 4].

1.1 3D cell culturing

To obtain a more biologically relevant model for cell studies, cells can be cultured in 3D instead of the traditional 2D monolayer on flat surfaces of glass or tissue culture plastic (TCP) [1, 3, 5-7]. Several studies on the topic indicate that 3D cultured cells exhibit characteristics more similar to those *in vivo* (Figure 1) [2, 4, 8]. 2D cultivation is inexpensive and easy to use, but it puts cells in a state very different from their origin and exposes cells to stimuli unrelated to *in vivo* conditions [3, 9]. On flat surfaces, adhesive cells maximize their adhesion and have the tendency to look, behave and respond differently than in their natural cellular environment [5, 9]. Fibroblasts for example, which naturally are non-polar, will adopt a flat morphology with an artificial apical-basal polarity in 2D culture [6, 10], with most of the cell surface connecting either to the well plate or cultivation media [9]. 3D cultured cells seem to have more complex morphologies that are more comparable to their native appearance in tissue [9].

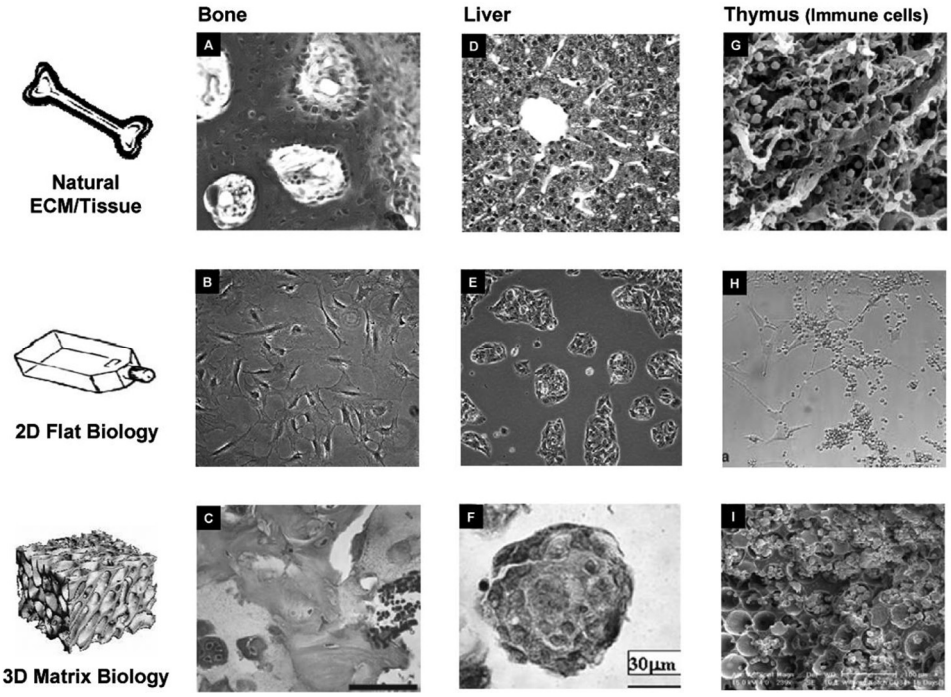

Figure 1: Morphological differences between cells of bone (**A**, **B** and **C**), liver (**D**, **E** and **F**) and thymus (**G**, **H**, **I**), in their natural state, 2D cultivated and 3D cultivated. 2D cultivation gives the cells a stretched morphology, while 3D cultivation reveals a morphology closer to *in vivo* [8].

Cultivation of cells in 3D involves seeding of cells in a scaffold where they can interact with their microenvironment in all directions. The goal is to create a cellular environment that is more similar to that of the native tissue [5, 11], and by that providing tunable models that allow for studying interactions between cells and their environment [1, 3, 5]. 3D culturing can be a useful tool in e.g. cell biology [2, 12], cancer research [13] and tissue engineering [5]. Furthermore, drug development and toxicology studies can be improved by the potentially more relevant cellular responses [1, 3, 5]. 3D models can also lead to a reduced need for animal trials [5], which are not always able to predict the responses of human cells [14].

Several studies suggest that 2D is not sufficiently selective to dissect differences between cells [2, 12]. By cultivation in 3D collagen gels, differences between dermal fibroblasts from different patients that could not be observed in 2D culturing, have been observed [2]. Another study indicated that 3D culturing of normal and malignant breast cells revealed phenotypical differences that were not expressed when grown in 2D [15]. 3D cultivation has also shown to promote normal growth of epithelial cells with epithelial polarity [6], and exhibition of natural phenotypes in hepatocyte primary cells [3]. The higher relevance of information from 3D cultured cells compared to 2D has also been shown in gene expression profiles [7, 9]. This has been seen in breast cancer research [7, 16], and in studies on fibroblasts [17]. In a study by Li

et al. (2003), gene expression profiles of smooth muscle cells (SMCs) grown on a 2D surface and in a 3D collagen matrix showed to differ in expression of 99 genes [17, 18].

1.1.1 The gel-like extracellular matrix

In their natural state, most cells are surrounded and structurally supported by the extracellular matrix (ECM) (Figure 2), which is a hydrated gel-like network of proteins and polysaccharides. It comprises of glycosaminoglycans (GAGs), such as hyaluronan (HA), fibrous proteins, such as collagens, and glycoproteins such as fibronectin (FN). The ECM allows cells to attach and communicate with their environment and other cells [1, 3, 19]. Interaction between the ECM and cells is important for regulation of cell survival, proliferation, morphology, migration [4, 5, 19-21] and the generation of traction forces [22]. The components of the ECM are produced and secreted by the cells in the matrix. Important ECM-producers are epithelial cells and mesenchymal cells such as fibroblasts. Cells organize, remodel and degrade their ECM, mainly through the integrin attachment. The ECM composition is adapted to the functions of the cell types, and therefore varies between different tissues [1, 4, 19].

GAGs are often linked to proteins, forming proteoglycans that serve as a hydrated polysaccharide "gel" in which the other ECM-components are embedded in. This gel-like mesh permits diffusion of nutrients, hormones, cytokines, enzymes, and other metabolites [1, 19]. FNs have an important role in organizing the matrix and in the attachment of cells to the matrix [1, 19, 23], and they also function as tracks which the cells can use to migrate [19]. The FN protein contains a peptide sequence of Ar-Gly-Asp (RGD), which functions as a ligand and a binding site for integrins on the cell surface. Integrins are transmembrane protein dimers that function as cell receptors [19]. In addition to attaching the cell to the matrix, integrins transmit both mechanical and molecular signals both ways through the plasma membrane. Intracellularly, the integrins are connected to the cytoskeleton, which mainly consists of actin filaments [1, 19, 24].

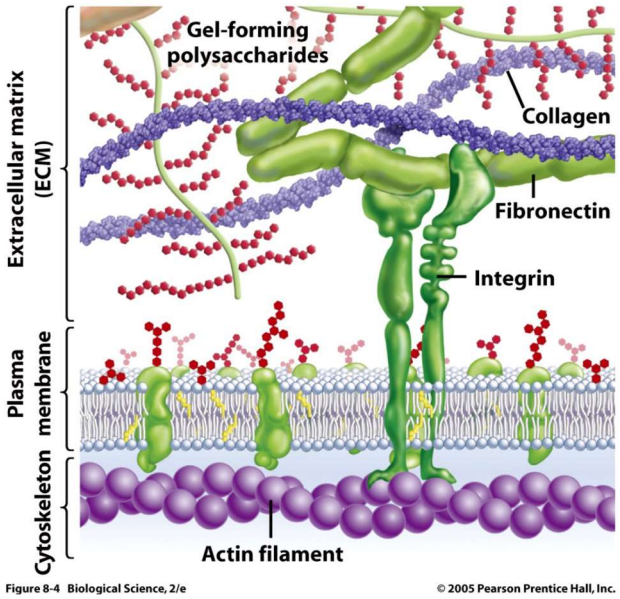

Figure 2: Main composition of the natural extracellular matrix (ECM). A sequence of amino acids (RGD) in FN functions as a ligand for the transmembrane cell receptor integrin, allowing cell attachment and signaling to the cytoskeleton [1, 19, 23]. Illustration from *Biological Science*, 2005 Pearson Prentice Hall, Inc [25, 26].

1.1.2 Scaffolds for 3D culture

As 3D cultivation is a growing field, there exists a lot of different scaffolds, both based on synthetic, semi-synthetic and natural materials [4, 5]. There are 3D systems for cells both with and without a matrix scaffold [27]. In systems without a scaffold, the cells have to create their own ECM without physical support or porosity, such as in tumor spheroids [28]. 3D scaffolds however, may include different types of approaches to imitate the ECM [27]. Common formats of scaffolds include gels, beads, matrices, fibers, and porous materials [9, 29, 30]. Hydrogels have been applied widely to create 3D scaffolds for cells, due to their similarities with the gel-like ECM [5, 31, 32]. These are hydrated polymer networks [33] that exist as scaffolds in different sizes and shapes [29]. They can be made from polymers that are either synthetic, such as polyethylene glycol (PEG), or natural, such as hyaluronan (HA) or alginate [31]. Entrapment of cells in a 3D hydrogel often involves the cells being mixed in a precursor solution, then entrapped in the gel by either non-covalent or covalent cross-linking [3, 31]. In addition to being similar to the ECM, hydrogels are easy to handle and their properties such as degree of diffusion and degradation can be controlled through processing [34]. Regarding natural polymers for hydrogels, these can be derived from either animal tissue [31] or non-animal sources [27, 35]. Animal-tissue-derived hydrogels are naturally compatible with animal cells [31], seen for instance with laminin-rich ECM gels [36] and Matrigel^{TM}. The latter is a 3D gel that contains matrix proteins and glycoproteins from mouse sarcoma cells, and that showed to successfully

support cultivation of cells exhibiting natural morphology and behavior [4, 30, 31, 37]. However, with animal-derived materials there are concerns regarding availability, batch-to-batch variation, the possibility of pathogen transmission and immunogenicity, which makes such materials less attractive [4, 31]. This draws attention towards non-animal derived natural polymers, such as polysaccharides like alginate, as a viable alternative. Alginate hydrogels have been widely applied in the field of 3D cell culture and tissue engineering due to their biocompatibility and favorable gelling properties [27, 35].

Mimicking the ECM is an important part of creating suitable 3D scaffolds for cells [5], and has led to extensive ongoing research on the subject [4]. The composition and stiffness of a mimicked ECM can be adapted to imitate the natural cellular environment of the cell type of interest. In that way, the cell's native morphology and function can be better achieved [3] and understood [38]. This involves creating functional materials with suitable physical properties, e.g. regarding degree of stiffness and porosity, and with modifications that are able to support attachment and enable interaction [24].

A variety of cell types are often referred to as being adhesion dependent. This implies that anchoring of the cell to a solid or semi-solid interface is crucial for its survival [3, 9, 24]. Cells of connective tissue, including soft tissues and bone, are adherent cells that require attachment to the ECM in order to survive, spread and proliferate [3, 39]. In such cells, lack of attachment often results in cells gravitating towards apoptotic programming [24, 40]. Such apoptosis can depend on lack of attachment sites, the present integrin types and changes in the mechanical force of surroundings [41]. The ECM is a dynamic environment that undergoes phases of formation and degradation. Cells themselves form their cellular environment [1, 4, 19] by secreting ECM components as well as degrading enzymes such as matrix metalloproteinases (MMPs) and GAG-hydrolases. Therefore, the degradability of the hydrogels used for cell immobilization matters [3]. Hydrogels can be produced with varying degree of stability. This can be adjusted by modifying the gels with segments that are susceptible to hydrolytic or enzymatic degradation [33, 34]. In a study by Bott et al. (2019), human dermal fibroblasts (HDFs) cultivated in PEG-hydrogels modified with MMP-degradability and RGD-peptides for cell adhesion exhibited their tissue-typical spindle-shape morphology and created cell-cell networks. Cells in gels with only the RGD-grafting remained mostly round with only sporadic spreading, and cells in gels without RGD did neither spread nor proliferate. However, in spite of being functionalized for RGD-binding and MMP-cleavage, high material stiffness with elastic modulus more than 1200 pascals (Pa) seemed to impede the fibroblast's ability to move

and proliferate, acting as a barrier [2]. Also, regarding gel stiffness, HDFs seeded on top of a HA/FN-based gel have shown to adopt a more stretched and organized cytoskeleton and proliferate more in stiffer substrates (4270 Pa), similar to on TCP. However, cells seeded on softer materials (550 Pa and 95 Pa) migrated faster and had a less dense cytoskeleton with signs of buckling and spots [38]. A similar observation of coherence between material stiffness and cytoskeletal organization has been reported with hepatocytes [42].

For hydrogels, it is desired that they have pores that allow transport of small molecules, oxygen, nutrients, and waste, while preventing diffusion of large molecules. The diameter of pores of the surface of a hydrogel crosslinked with calcium usually varies between 5-200 nm [43]. Macroporous scaffolds such as sponges and foams give more surface area for attachment and proliferation [30, 31, 44], and have shown to be especially beneficial in growing bone cells [44]. Such scaffolds usually allow a well spread, spatially organized cell seeding. However, these scaffolds are often considered to be between 2D and 3D, as the increase in surface area gives similarities with flat 2D cultivation [31].

To find an appropriate 3D system for cell studies, one must aim for a culture system that allows for an accurate and accessible investigation of the cell in such materials, while also considering the cell requirements and study aim. Some of the methods that have been mentioned here are 2D culturing on TCP or on top of a gel, 3D culturing by entrapment inside a gel or gel beads, 2.5D culturing in macroporous scaffolds and spheroid 3D culture without scaffold. Mesenchymal stromal cells (MSCs) have shown to have improved maintenance of functional characteristics in culture when hydrogel cell-matrix interactions are provided, compared to TCP culture [45, 46]. They have been tested in many different materials, and have shown improved secretion, migration, proliferation and cell-cell interaction in a macroporous scaffold with average pore size around 120 mm, compared to in a nanoporous hydrogel (average pore size 5 nm) [46, 47]. In a review by Weschler et al. (2021) on how hydrogel material properties affect the secretome of MSCs, an overview on different current hydrogels scaffolds and their advantages in MSC culturing is provided (Figure 3) [46]. The figure shows some important cons of culturing on TCP, on top of hydrogel, inside of hydrogel, in microspheres, such as beads, in porous scaffolds and spheroids [46].

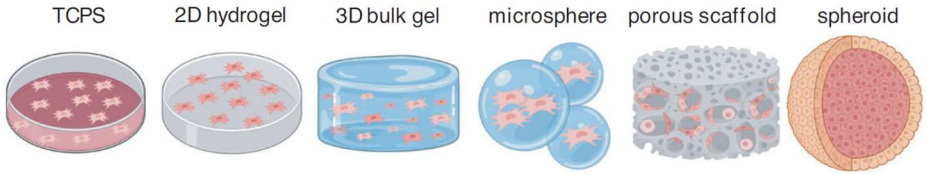

	TCPS	2D hydrogel	3D bulk gel	microsphere	porous scaffold	spheroid
Increases proliferation	↑↑	↑	↑	–	↑	↑↑
Promotes secretory properties	–	↑	↑	↑	↑↑	↑↑
Facilitates cell-cell interactions	–	–	↑	↑	↑↑	↑↑
Provides user control over cellular microenvironment	–	↑	↑↑	↑↑	↑	–
Improves in vivo survival	–	–	↑↑	↑↑	↑	↑

Figure 3: Different culture systems compared by their ability to improve certain desirable properties, graded by no improvement (-), some improvement (↑) and higher improvement (↑↑). The qualitative assessment is based on results from cultivation of MSCs. Figure by Wechsler et al. (2021) [46].

1.2 Alginates as 3D scaffolds

Alginates are natural biopolymers in the form of polysaccharides. They can be extracted industrially from brown seaweeds such as *Laminaria* spp., *Ascophyllum nodosum*, *Ecklonia* spp., *Macrocystis* spp. and *Lessonia* spp. [48], but are also produced by some bacteria like *Pseudomonas* sp. and *Azotobacter vinelandii* [7, 49]. Isolated alginates are converted into water-soluble alginate salts, such as sodium (Na) alginate [48]. Due to their gelling abilities, alginates are widely used in pharmaceuticals and in foods [7] as thickeners and gelling agents [48]. Alginates have shown to be biocompatible and are therefore suitable as biomaterials in biomedical applications. Alginates for such purposes are ultra-purified, removing any contaminants and leads to materials of low toxicity and immunogenicity [7, 50]. Some applications that alginate-based biomaterials have been used for are immobilization of cell and enzyme systems [51], proliferation of mammalian cells [7], tissue engineering [52], cell encapsulation [53, 54] and drug or cell delivery [55].

Alginates are linear, unbranched polymers of the uronic acids β-D-mannuronic acid (M) and α-L-guluronic acid (G), linked by (1,4)-glycosidic bonds. G is the C5-epimer of M [56]. The polymers occur as long chains with a pattern of blocks of M, blocks of G and sequences with alternating M and G (Figure 4) [48, 57-60]. The order and fraction (F) of M, G or MG depends on the source the alginate was isolated from [56].

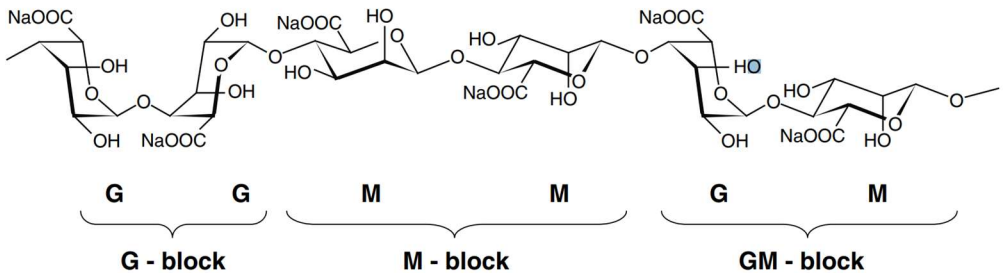

Figure 4: Chemical structure of a sodium alginate chain built from monomers of α-L-guluronic acid (G) and β-D-mannuronic acid (M). Figure retrieved and modified from *Alginates: Biology and Applications* (2009) by Rehm [49].

Soft alginate-based hydrogels can be prepared by cross-linking the alginate chains with divalent cations such as calcium (Ca^{2+}) barium (Ba^{2+}) and strontium (Sr^{2+}) [7, 48, 61]. Most divalent cations can be used, except for magnesium (Mg^{2+}) [60]. Alginate in combination with Ca^{2+} for preparation of viscous solutions and gels is widely used [56]. When Ca^{2+} ions react with alginate, they attach to G-blocks in different alginate chains and forms interactions between them, creating a network [48, 56]. The calcium ion exchanges the sodium ion, because its binding to the chain is of higher affinity [48]. However, also blocks of MG are able to form stable crosslinks with Ca^{2+}, both with other blocks of MG and of GG, as shown in Donati et al. (2005) [62]. Grant et al. (1973) visualized the interaction between polysaccharides and divalent cations, such as alginate and Ca^{2+} ions, in the "egg box model" (Figure 5), the ions being eggs placed in the empty spaces of the alginate chain egg-box [48, 63].

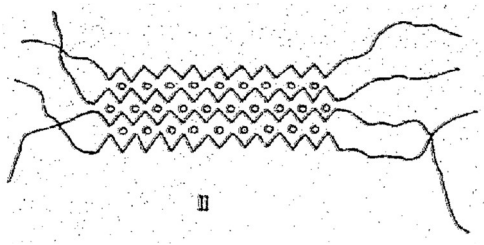

Figure 5: The egg-box model. Divalent cations (dots) fit in the alginate chains as eggs in a box. Original drawing from Grant et al. (1973) [63].

To make a gel, the water-soluble alginate salt must first be hydrated [48]. Then, there are different methods for gelation. Two main methods based on ion crosslinking are internal setting and external setting. In the latter, there is an external reservoir that contains the cross-linking ions. The crosslinking and gelation are initiated from the outside and proceeds inwards in the alginate solution by diffusion of the ions [48, 64]. This method is suitable for creating smaller materials [48], such as alginate beads [61, 65]. To entrap cells by this method, alginate solution

containing cells can be dripped into a calcium solution [7]. In the internal setting (Figure 6), the crosslinking ion is released homogeneously in the alginate, in a controlled manner [48]. This can be performed by mixing a calcium salt, such as $CaCO_3$ [51], of low solubility in the alginate solution. The calcium ions can be released by adding an acid to the mix. For this, the slowly hydrolyzing acid glucono delta lactone (GDL) can be used as a proton (H^+) donor [51, 64].

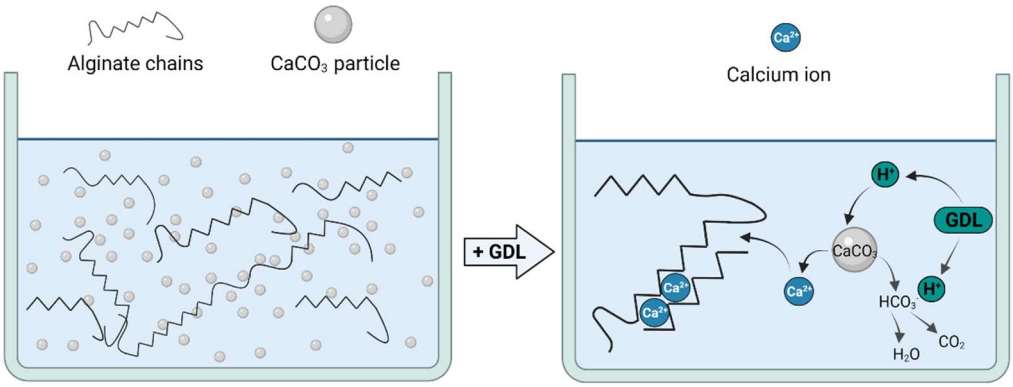

Figure 6: Internal gelation of alginate by cross-linking with Ca^{2+}, in the presence of $CaCO_3$ and GDL. Addition of GDL causes the release of calcium ions from bound form in $CaCO_3$. The calcium ions attach to and crosslink the alginate chains in the solution as shown in detail to the right in the figure. Illustration inspired by figure in Nobile et al., 2008 [66]. Created in BioRender.com.

Alginates can form gels at mild conditions, which makes it possible to entrap cells and proteins without disturbing biological activities considerably [67]. They can gel at RT and are heat-stable [48]. Alginate hydrogels offer a gel porosity that allows diffusion of small water-soluble molecules [67-69]. In a study by Boontheekul et al. (2005) the pore size of 1% (w/v) alginate gels was around 5 nm [70]. The gelling ability and chemical properties of the formed gel depend on, the content of G-blocks, availability of cross-linking cations and molecular weight of the chains [7, 48, 51, 56, 61]. The viscosity of the gel depends on e.g. the length and ion affinity of the alginate chains [56] and the gel composition [48]. Alginates with high G-content, which are the ones mostly applied for gel formation [7], have a high ability to form gels by Ca^{2+} crosslinking [56]. High-G alginates are often used when a high gel strength is desired. They have been said to be low on immunogenicity, compared to high-M alginates, and are often preferred for immobilization materials. [71]. However, this is debatable, for instance as shown in an *in vivo* biocompatibility study by Tam et al. (2011) [72] on injected alginate beads in mice, where high M-alginate resulted in lower degree of fibrosis, compared to the high-G alginate [72, 73].

Many different alginate hydrogel scaffolds for 3D cell culture exist. Some main types are beads, gels and foams [5]. As mentioned, alginate gel beads have been used for cell entrapment. One of the most researched medical applications of alginate is the use of alginate gels in cell therapy in diabetes treatment, often in the form of microencapsulated insulin-producing islet cells for *in vivo* transplantation [74-76]. In this study, discs of internally gelled (Figure 6) alginate were used with cells seeded inside. Cells can also be seeded on top of such alginate gels, e.g. as shown with myoblasts in a study by Rowley et al. (1999) [77]. Alginate foams containing alginate solution were also used here. In these foams, the alginate solution is crosslinked by precipitation of calcium ions from the foam structure (Figure 7). Alginate foams and sponges are macroporous scaffolds. Their porosity may facilitate cell-cell connections and led to better diffusion of nutrients, oxygen and waste compared to an ecapsulation material without this support structure [7, 78, 79]. High porosity foams that are able to support cell infiltration can be produced by steps of internal gelation, gas foaming [80] and freeze drying [7, 80, 81].

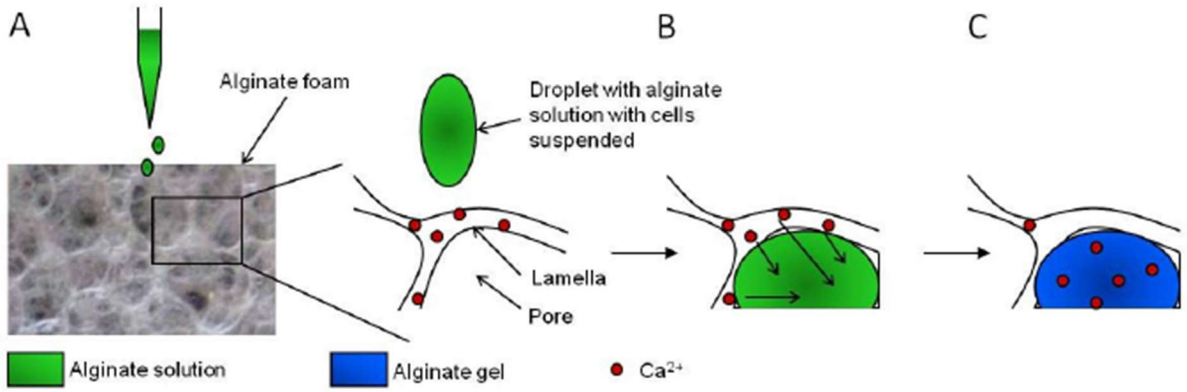

Figure 7: Gelation of alginate foams. Calcium ions diffuse from the foam walls (lamella) (**B**) into the pores upon addition (**A**) of alginate solution and causes cross-linking (**C**). The cells are in solution and will be entrapped when the gelation occurs [5, 31]. Illustration copied from review article by Andersen et al. (2015) [5].

Cultivation of fibroblasts in alginate sponges has shown that the cells were immobilized inside pores and were able to proliferate. Their morphology remained spherical, as opposed to the flat morphology that is seen in monolayer cultivation [79]. Due to their increased mass transport and cell infiltration, macroporous scaffolds are especially of interest in tissue engineering [82, 83]. Porous alginate hydrogels for tissue engineering have been used for encapsulation of a hepatocarcinoma cell line (hepG2) and showed increased proliferation and larger cell spheroids under porous conditions [82].

The foams used in this study (Figure 8) come as gamma-sterilized, dry discs prepared in well plates, and turn into hydrogels upon rehydration with alginate solution. Unfortunately, NovaMatrix® did not provide any specifications regarding the dry alginate foams due to their termination in production. However, it is likely that the foams used for experiments in this thesis are similar to those used by Andersen et al. (2014) [31] in their study. Those were produced from 2% (w/w) alginate by ionically gelling with $CaCO_3$ and GDL then aerated and air-dried. The foams were 2 mm thick before drying [31]. Foam pore sizes can vary from 225-400 µm, regarding dry foam density (DFD) and alginate concentration (% w/w). Low density and low alginate concentration give larger pores. Foaming agents used were polysorbate and hydroxypropyl methylcellulose (HPMC) [29, 31]. Cells are seeded using alginate solution as a carrier, and gelation occurs when the solution with the cells comes in contact with the pore walls. Andersen et al. (2014) used these foams with 0.1%-1% alginate and obtained seeding efficiency of cell line murine fibroblasts (NIH:3T3) between 95-115%, compared to 18% without alginate [31].

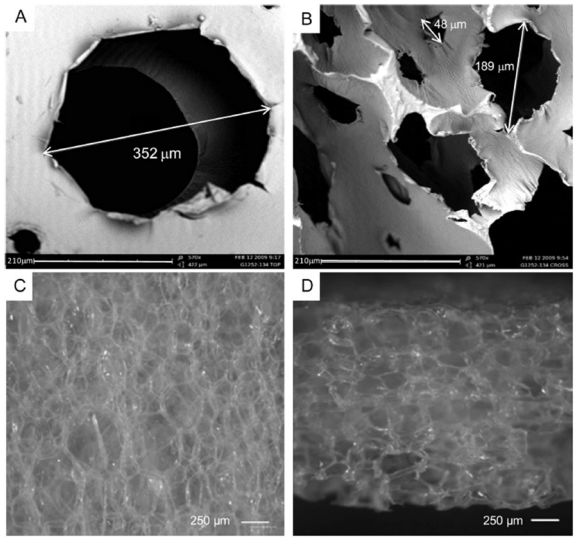

Figure 8: Dry alginate foams with interconnected pore network. Details and size of pores is shown in scanning electron microscopy (SEM) images (**A** and **B**), showing pore diameters of 352 µm, 189 µm and 48 µm. Light images show foam surface seen from above (**C**) and cross section (**D**). Scalebars in C and D are 250 µm. From Andersen et al. (2012) [29].

Foams are considered to be something between 2D and 3D, because the cells can spread on the surface of pore walls, similarly to the attachment to a surface in monolayer 2D culture [4, 5]. However, in the sponges used by Prestwich (2007) described as 2.5D, the cells are added suspended in media [4]. In the foams used in this study, the cells were mixed with alginate solution priorly. The use viscous alginate solution as carrier for cells can be highly beneficial

in reducing the number of cells that otherwise could end up colonizing the bottom of the well plate, as seen with the increased cell seeding efficiency in Andersen et al. (2014) [31].

For cells to be able to survive and thrive in alginate materials, the materials must be modified [7]. The free hydroxyl (-OH) and carboxyl (-COOH) in the alginate allows for chemical modifications and thereby functionalization of the alginates [7, 84]. Oxidation with periodate is commonly performed on alginates. Periodate opens the ring structure and forms a dialdehyde, increasing the flexibility of the chain. This enhances degradability [7, 71]. Oxidation of alginates with periodate (IO-anion) gives more reactive groups [85] and facilitates attachment of substituents or cross-linkers [7]. The degree of oxidation allows for control of degradability [70].

For enabling cell attachment to the material, the alginate can be grafted with RGD [7]. RGD-coupling of alginate has shown to promote both adhesion and proliferation of murine osteoblast cells [86], chondrocytes [87] and myoblasts cells [77, 88]. Alginates cannot interact with mammalian cells on their own, but by covalently coupling RGD-cell adhesion ligands at free -COOH groups in the chains this is made possible. Such grafted polymers offer the possibility to explore specific cell receptor-ligand interactions [77, 89]. In addition to chemical modifications, material properties of the alginates like stiffness, degradability and topography can also affect the biological activity [7]. Degradability can be modified by grafting the alginate with MMP-cleavable peptides, allowing the cells to enzymatically degrade and remodel the gel matrix. This has shown to increase degree of cell elongation and cellular networks of MSCs [90]. Apart from degradation by cells, the stability of alginate gels is affected by presence of transition metal ions, oxygen, and pH. Exposure to acid or alkaline conditions are primary reasons for depolymerization [91].

Regarding the specifications for alginates used in this study, these were ultrapure unmodified alginate products from NovaMatrix®, with proposed applications in tissue engineering, medical devices, drug delivery and cell encapsulation [92]. The raw material for their alginates is the large brown macro algae *Laminaria hyperborea* [93, 94]. The unmodified alginate was used in mix with RGD-grafted alginate to make alginate solutions with cell adhesion possibility.

1.3 Cells of interest

Three different human-derived adherent cell types were used in this study, whereof two were cell lines and one was primary cells. The primary cells were normal human dermal fibroblasts (NHDFs). The cell lines were human lung fibroblasts (IMR-90s) and human bone marrow

stromal fibroblast-like cells (HS-5s). Fibroblasts are a heterogenous family of mesenchymal-derived cells [95-97]. The fibroblasts have many morphological similarities with mesenchymal stem cells (MSCs) [98], also called mesenchymal stromal cells. MSCs are a heterogenous group of multipotent progenitor cells with a fibroblast-like spindle morphology, that can differentiate into cell types such as osteoblasts, chondrocytes, marrow stromal cells and adipocytes [46, 99-104]. The fibroblasts are found in all tissues of the body [96], where they reside in the interstitial spaces of organs [105]. They have important functions in secreting ECM-components and interacting with the ECM [105-107], and are abundant in connective tissue [19, 97]. Fibroblasts are important players in injury responses [105]. Upon damage in tissues, fibroblasts migrate through the connective tissues and rebuilds or remodels where necessary [108]. As mentioned in Section 1.1.1, the ECM is essential in mechanical support of cells, and facilitates adhesion and migration, which all are crucial functions for cell survival and proliferation. Disorders such as fibrosis and cancer are associated with malfunctions in the cell-ECM interaction [106]. The importance of understanding functions of fibroblasts has made them very common in cell biology studies [109], and they are widely used both in form of primary cell cultures and immortalized cell lines [97].

Fibroblasts were first described as a cell type by Rudolf Virchow in 1858 [110, 111]. They are known for having spindle-like elongated morphology [97], at least in inactive form [107]. However, morphology and functions of the fibroblast varies according to tissue and state of the tissue (Figure 9) [95, 96]. This “topographic differentiation” is shown also by different gene expression profiles of fibroblasts in different anatomical locations [112]. Fibroblasts significantly change their native characteristics when they are cultivated on flat surfaces [1, 17]. Studying these cells only in 2D therefore might lead to biological properties being missed. Grown in 2D, their ECM receptors assemble on the ventral side towards the culture surface and the cell adopts a highly spread, flat shape with large lamellipodia and high degree of stress fibers [17, 113]. (Stress fibers and formation of lamellipodia are further explained in Section 1.3.2.) On the other hand, in 3D cultivation, the receptors are spread all over the cell, and this can give a more global interaction that might allow a highly elongated and less flat-spread morphology [17, 113, 114].

Cultured fibroblasts have shown to differentiate into myofibroblasts, especially when grown in low cell densities. Myofibroblasts have smooth-muscle-like features and have an important role in wound healing by contracting the wound [95, 115-117]. There are studies and reviews that have indicated that there are many phenotypical similarities between fibroblasts and MSCs,

including when it comes to abilities in differentiation into tissue specific cell types [98, 118, 119]. However, they seem to have some differences in gene expression and regulation. The exact relation between the two groups of cells is a complex topic of debate, indicating that there still is a need for further characterization of these cells [98]. This will therefore not be addressed further in this thesis, where fibroblastic cells are in focus.

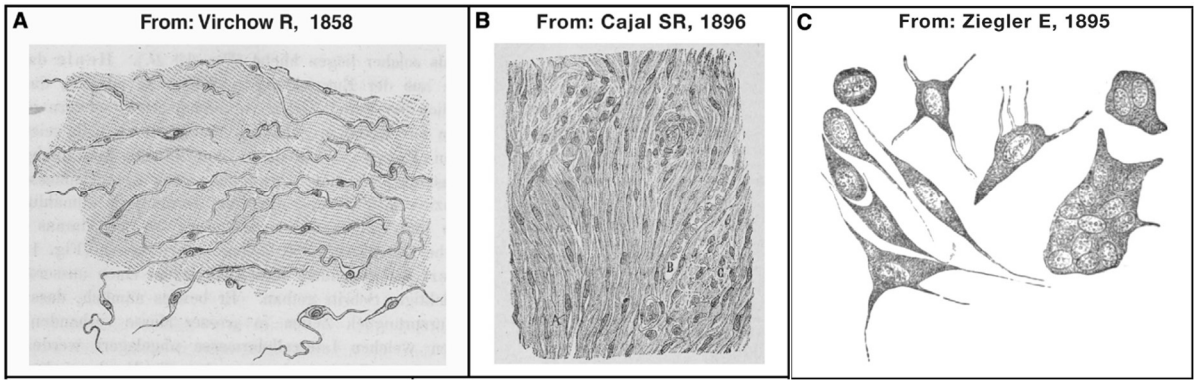

Figure 9: Early drawings of fibroblasts by Rudolf Virchow, Ramón y Cahal Santiago and Ernst Ziegler, showing **A**) spindle-shaped cells in pig embryo connective tissue, **B**) fusiform cells in keloid scarring, and **C**) various forms of fibroblasts in new connective tissue upon tissue healing [110, 111, 120, 121].. Obtained and modified from review by Plikus et al. (2021) [110].

The home of the fibroblasts, the connective tissue, is one of the four types of animal tissue. It consists of cells scattered through an ECM that varies from liquid to gel-like to almost solid, and is found across adipose, cartilage, bone, and blood bearing organs [122]. The main roles of connective tissue includes mechanical support, holding tissues and organs in place [107, 122]. It also functions as nutrients storage, holds blood vessels and allows movement of cells and nutrients [107]. Resident cell types are fibroblasts, adipocytes and mast cells, but it is also often home to free blood cells. Different types of connective tissue vary in composition, type and content of ECM-components and cells [107]. Connective tissue comprises loose connective tissue and dense connective tissue [107, 122]. Loose connective tissue is found in lamina propria of digestive- and respiratory tracts and epithelial linings of organs, where it permits diffusion of fluids and movement of cells. Dense connective tissue provides mechanical support and are collagen rich. It can be either irregular or regular, based on whether the thick collagen bundles are randomly arranged or arranged unidirectionally. The irregular is found in dermis of skin, and encapsulates organs, and its fibroblasts are usually inactive and compressed. The regular is found mostly in tendon and has fibroblasts that usually exhibit spindle-shape [107].

All three cell types used in this study are adherent human fibroblasts or fibroblast-like cells derived from dermis of skin, lung tissue or bone marrow. The fibroblasts from dermis, NHDFs (Figure 10), were primary cells from adult human skin. According to supplier (Lonza) they are suitable for applications such as ECM protein analysis, wound healing, collagen metabolism, cosmetics, skin therapy and skin models. They are guaranteed 15 population doublings [123].

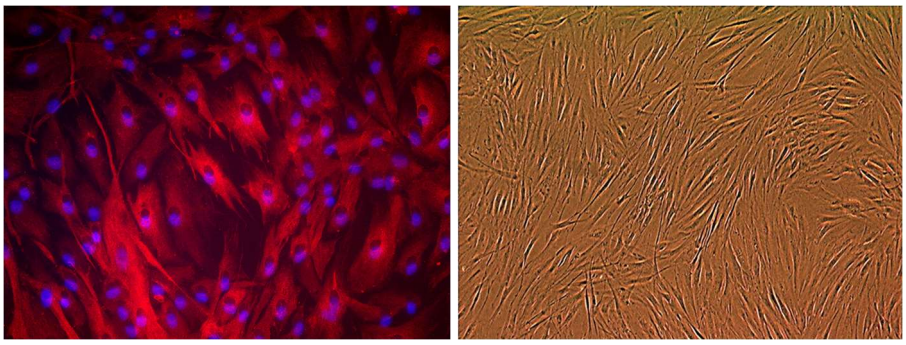

Figure 10: Adult NHDFs in culture, stained with immunohistochemistry in 24-wellplate (left) and in culture at high density showing a uniform morphology (right). Images by suppliers (Lonza Products) [123].

Dermis is the middle layer of skin, between the upper layer of epidermis and bottom layer of subcutaneous fat [124]. It makes up the largest part of the skin and provides mechanical support [124, 125]. The dermal fibroblasts (Figure 10, Figure 11) are either papillary, reticular or follicular, and have functions in remodeling and repairing wounds and maintaining the skin physiology [125]. Dermal fibroblasts are widely used in research, and is often considered the most suitable cell type for studying cell metabolism under normal conditions, during development and aging, upon disease or exposure to agents [126].

Figure 11: Dense irregular connective tissue of human dermis showing a fibroblast (dark area) surrounded by ECM high in collagen fibers (light area). Magnification is x10 000. Image from *Ultrastructure Atlas of Human Tissues* (2014) [107].

Figure 12 shows IMR-90 in 2D culture. IMR-90 is a fibroblast-like cell line originating from human lung tissue. It was derived by W.W Nichols et al. in 1975 from the lungs of a 16-week-

old aborted female fetus, for use in research [127-129]. The cell line is banked in large quantities in support of the National Institute on Aging (NIA) research and details were obtained from American Type Culture Collection (ATCC). According to ATCC the cell line is for laboratory research only, and suitable for 3D cell culture and in use as a transfection host. The IMR-90 cell line is reported to be capable of 58 population doublings [127-129].

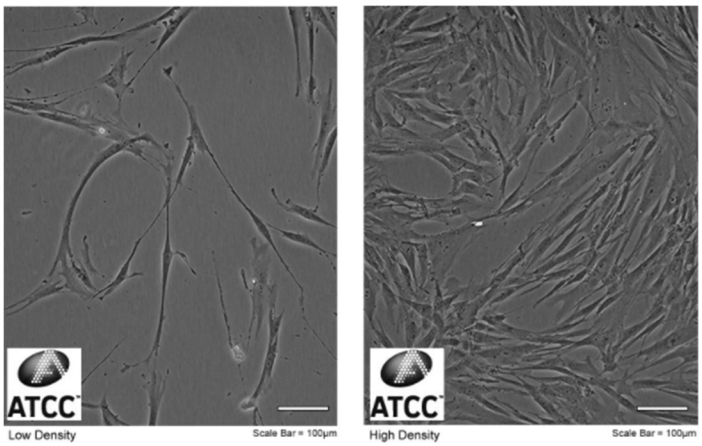

Figure 12: Light microscopy images of IMR-90s in culture with low density (left) and high density (right). Scalebars are 100 µm. Images from ATCC [127].

Lung tissue, belonging to the respiratory organ system [122], consists of the upper and lower system. The nose, paranasal sinuses and pharynx belongs to the upper, while the lower system comprises trachea, bronchi and bronchioles [130]. Connective tissue gives stability and helps in the functions of the lung [131]. It is found in the interstitial spaces, parenchyma, and the most common cells in this interstitium are fibroblasts [132]. The lung fibroblasts are usually located close to the lung epithelium or endothelium [105], and have functions in the elasticity that is needed for breathing [110]. They are important for supporting the alveolar structure, both by proliferating and by repairing damage [133]. Diseases in the connective tissue can give many different complications [134]. In lung diseases such as asthma, fibrosis and chronic obstructive pulmonary disease (COPD), there are changes in the fibroblasts in terms of numbers and characteristics [105]. As mentioned, IMR-90 is from a 16-week-old embryo [127-129]. The developmental stage of lungs in a 7–17-week-old embryo is called the pseudoglandular stage, and involves differentiation of epithelial cells, and development of airways, bronchioles, pulmonary arteries and veins. The lung is still immature at this point. While still in development, airways are lined by undifferentiated cells and the interstitial space is large and has low vascularization [130].

Different from the other cell types, the HS-5 cell line (Figure 13) has been transformed with a virus for immortalization. The cell line origin is stroma of bone marrow from a 30-year-old

male, and it was isolated by Fred Hutchinson Cancer Research Center in 1995. According to ATCC, usages for this cell line are in laboratory research purposes only [135]. The cell line is suitable for 3D cell culture and immunology studies, as feeder layer in *ex vivo* bone marrow cultures or in colony forming assays. The virus used for immortalization was human papilloma virus (HPV)-16 E6/E7, and the cell line was transformed with the HPV-sequences using a retrovirus vector. HS-5 is the fifth of 27 clones that were isolated. These details on the cell line was obtained as recorded by ATCC [135]. The immortalization was performed using a recombinant retrovirus containing the E6/E7 genes of the HPV. These genes interfere with tumor suppressor proteins, which causes prevention of cell cycle arrest. Of the 27 immortalized clones, HS-5 and HS-21 are fibroblast-like. HS-5 appears relatively small and forms a network of overlapping cells, that are similar to astrocytes. In high densities, HS-5 forms a dense net [136].

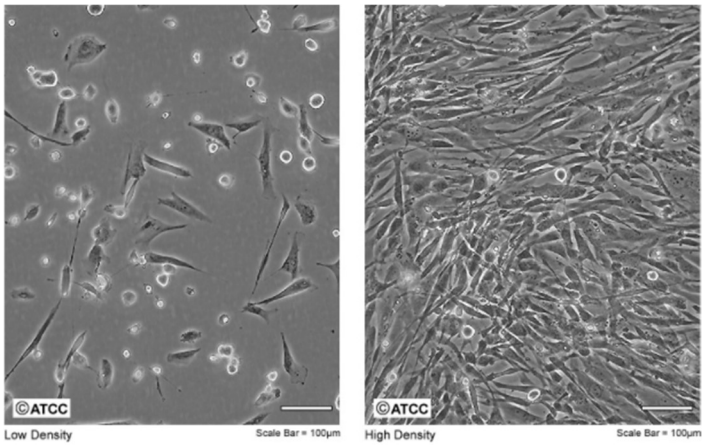

Figure 13: Light microscopy images of HS-5 in culture with low density (left) and high density (right). Scalebars are 100 µm. Images from ATCC [135].

Bone marrow is a large organ located in the cavities of bones, where it is supported by porous bone microarcitectures [137, 138]. It belongs to the immune and lymphatic organ system [122] and houses may different cell types in a viscous microenvironment. The soft bone marrow tissue [138] provides structural and physiological support for hematopoietic cells [139]. Bone marrow is the main source of the hematopoietic stem cells (HSCs), which differentiates into different blood- and immune cells, giving a continual renewal of these cells in blood [137, 138]. Adult bone marrow also contains MSCs, which are able to differentiate into bone, cartilage and adipocytes [138].

HS-5 is a fibroblast-like cell that secretes different stimulating factors and interleukins (ILs), which makes it able to support proliferation of HSCs when these are co-cultured [104, 136]. An evaluation of HS-5, HS-27 and primary bone marrow MSCs by Adamo et al. (2020), it was

found that bone-marrow derived commercial cell lines such as HS-5 and HS-27 are good candidates as disease models for MSCs. The findings suggested HS-5 to have an expression pattern similar to bone marrow-derived MSCs, and therefore might function as a model for reproducing properties of these. As cell lines are easier to manipulate in vitro compared to primary MSCs, these findings have many advantages. The same study showed that the HS-5 cells had higher ability to differentiate into osteoblasts than adipocytes [104]. Similarly, Kabrah et al. (2015) also showed that HS-5 is suitable as an alternative for MSCs in a 3D model [140].

1.3.1 Primary cells and cell lines

An important difference between NHDF, IMR-90 and HS-5, is that the former are primary cells while the two latter are cell lines. Primary cells are cells that have been isolated directly from the tissue of interest, not yet sub-cultured. Therefore, they usually still exhibit many of their natively differentiated properties when cultured *in vitro* [141-144]. For instance, fibroblasts will continue secretion of collagen, epithelial cells will form epithelial-like sheets, embryonic skeletal muscle form muscle fibers, and nerve cells will form axons. Studying these cells *in vivo* can be difficult, so this is very favorable [141]. Fibroblast-like primary cells usually grow well and fast in culture [142]. Primary cells can be passaged for weeks or months. However, their capacity for division is finite and they will eventually die. Normal human somatic fibroblasts can usually divide 25-40 times before they stop [141] due to replicative cell senescence [141, 142, 144, 145]. Replicative cell senescence is caused by continual shortening and uncapping of the ends of the chromosomes (telomeres) and leads to the cells having a limited replicative life span. The telomeres are repeated DNA-sequences with protein caps on the end of chromosomes. This shortening leads to a decline in cell division rate and other changes in cell characteristics [141, 145-147], and is therefore an important limitation with the use of primary cells [142]. In addition, primary cells are sensitive and have specific requirements when it comes to cultivation media and supply of growth factors and nutrients, which can be challenging. Some primary cells will differentiate along their native lineage after each passaging (self-replication), while others, like primary hepatocytes, instead tend to dedifferentiate and lose their characteristics [144].

Replicative senescence seems to be a tumor suppressor mechanism, in the way that tumors often have mutations that allow them to overcome this. Many malignant tumor cells can replicate continuously, as well as some stem cells [141, 145-147]. The obstacle of replicative senescence can be overcome by creating immortalized cell lines by transformation. Telomerase is an enzyme that maintains the telomers, but which is not expressed in human somatic cells. By

transforming human cells with the gene that encodes telomerase, immortalization can be obtained. Such transformed cell lines can grow in higher densities in culture than normal primary cells, and they can sometimes also grow without needing attachment. Cell lines can be generated from cancer cells, or by transforming normal cells [141]. There are different ways to transform cells for immortalization, for example transfection with tumor-inducing chemicals, or with viruses, such as the viral HPV E6/E7 genes, or by transfection with human telomerase [141, 144]. There are many different cell lines that exist, and one of the most famous is the first one created, the HeLa cells, originated from human epithelial [141].

Immortalized cell lines are available and can be expanded almost without limitation [148]. However, they are likely to differ more from *in vivo* state than primary cells do [141, 148]. Pan et al. (2009) compared mouse primary hepatocytes to a mouse hepatoma cell line (Hepa1-6). Even though many important signaling pathways were maintained in the cell lines, many proteins were down-regulated and there were differences in characteristic metabolic pathways, the immune system and in ECM-synthesis. The cell line showed a shifting focus to proliferative functions. However, the study only involved primary cells at a specific time point and a specific cell line [148]. Though cell lines don't guarantee an accurate resemblance of primary cells, they have been very important in, among other things, vaccine research, drug development and testing, gene studies and tissue engineering, due to their availability and ease of use. They also allow avoidance of the ethical concerns with obtaining cells from human and animal tissue [149].

1.3.2 Cytoskeletal response to the microenvironment

Different tissues have different properties regarding stiffness and elasticity (Figure 14). Skin, muscle and brain are examples of soft tissues that have elasticity due to the presence of the adherent cells in the ECM. Tissue cells can sense the stiffness of their environment, and evidence suggests that this information affects the properties of adhesion and cytoskeleton behavior [24]. It seems that the stiffer the surroundings are, the higher the stiffness of the cell is [150].

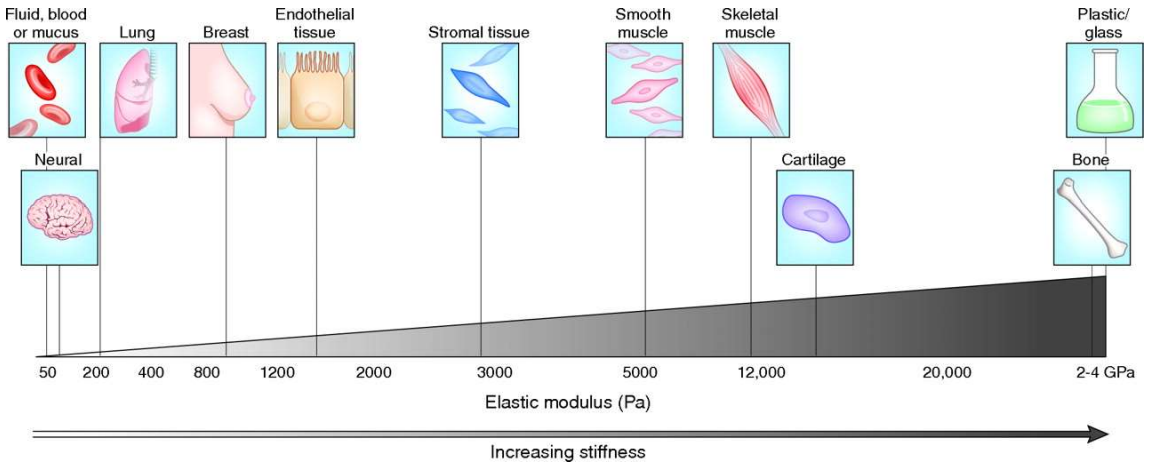

Figure 14: Stiffness in terms of elastic modulus of tissues in the human body, measured in pascals (Pa). Brain and lung are amongst the softest tissues, while stromal tissue (fibroblasts) is closer to the middle. Most tissues are not nearly as stiff as stiff as plastic and glass, which are commonly used substrates for 2D cell culturing. Figure from Cox and Erler (2011) [150, 151].

The interaction between cells and their surrounding matrix depends on signaling that is ligation-induced, such as binding of integrin to fibronectin-RGD and traction-induced, based on mechanical stimuli [38]. However, these go together, since the mechanical signaling is transduced via the binding of integrin [109]. Through mechanotransduction, integrins translate mechanical cues from the extracellular environment to internal signaling. Human MSCs have shown to sense their mechanical environment this way. When cultured on substrates with tissue-specific matrix properties, MSCs differentiated into specific cell types. With stiffnesses around 100 Pa, 10 000 Pa and 25 000 Pa, they showed differentiation towards neurons, skeletal muscle cells and bone cells, respectively [45]. This indicates that modified matrices can be used to differentiate MSCs. For bone cells, microporous scaffolds might be better, while for soft tissue cells, hydrogels might be more suitable [3].

The way cells can sense the stiffness of a material they have attached to, is through pulling forces. The pulling triggers an internal response in the cell and causes recruitment of integrins and other proteins to the binding site. This response is strong when the attached matrix is rigid, while attachment to a soft matrix will give less tension in the cell and a lower response [19]. For a cell to be able to move, it must have the possibility to exert such a traction on the ECM, adjacent cells or a culturing substrate [39]. The pulling forces are imposed by actin-myosin contractions in the cytoskeleton [24], and allow the cell to move along extracellular fibers [109]. Adherent cells apply force to their surroundings, and respond to their surroundings through cytoskeletal organization [24]. Changes in the cytoskeleton triggers pathways in the cell and causes changes in the cell [109] according to the microenvironment [42].

The cytoskeleton is a fibrous protein network that extends throughout the cytoplasm of the cell. It provides mechanical support, anchorage, and transport for cell organelles, and consists of actin filament, intermediate filaments, and microtubules. Actin filaments, found all over the cell, consist of two intertwined strands of globular actin units [109]. It is the actin filament that exert pulling forces [109]. Actin filaments occur as single filaments, in linear bundles, 2D networks and 3D gel-like structures (Figure 15). Cell movement and morphology are regulated by the formation of actin filament, which occurs through a nucleation driven process [108]. This involves a complex reorganization of the cytoskeleton [42, 108]. The cells spread or move by protrusion of the cell membrane by actin filament nucleation, dynamic attachment to the extracellular material and actin-myosin contraction. In the latter step, the cell can be drawn forward. The cell protrusions can have different shapes, but common in fibroblasts are filopodia and lamellipodia. Filopodia are spike-like, one-dimensional projections and contain a core of long, bundled actin filaments. These allow the cells to explore the environment. Lamellipodia are two-dimensional, sheet-like structures with crosslinked actin filaments [108].

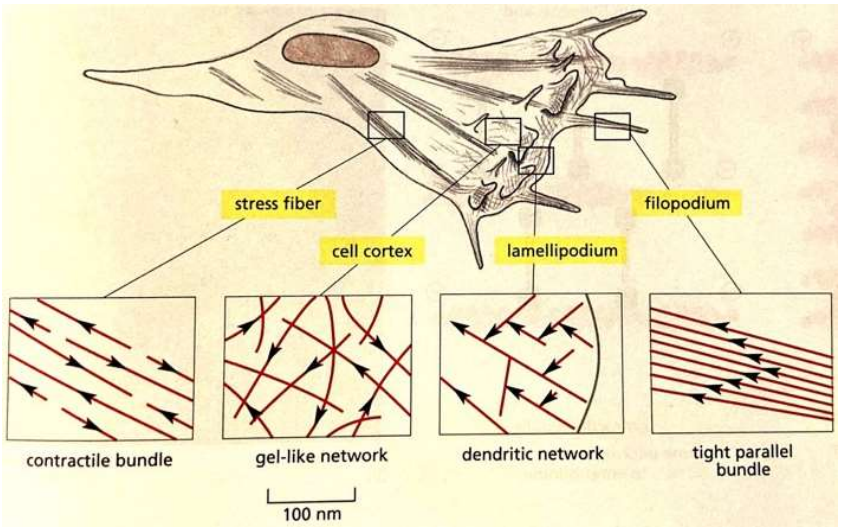

Figure 15: The different actin filament (red) arrangements in a cell, here illustrated by a fibroblast crawling on a 2D tissue-culture dish. The arrows on the actin filaments points towards the minus end of the filament, which is the slow-growing end [108].

The stress fibers are contractile actin filament bundles that terminate in the focal adhesion, connects with the ECM and exert tension [108, 152]. The focal adhesion is the area of attachment where the actin filament is linked with the ECM. In a dynamic manner, these adhesions are formed at the leading edge and disassemble at the back as the cell moves forward [108, 153]. Focal adhesions appear as integrin associates with ECM-ligands, which leads to further clustering of integrins and other proteins. This allows the transmission of information between ECM and cell cytoplasm [6, 152]. Through the tension caused by actin-myosin

activity, the strong interaction in the focal adhesions exerts a pull on the substratum the cells are attached to and allows movement of the cell [108, 152]. Focal adhesions eventually become elongated structures, aligned with the stress fibers [153].

The extent to which cells generate stress fibers and focal adhesions is largely dependent on the properties of the substrate itself [17, 18, 24, 38, 42, 113, 150]. For instance, SMCs have shown to have less stress fibers and focal adhesions *in vitro* in a 3D matrix than in 2D culture [18]. Because of this, in addition to receptor-ligand interactions, cell functions will also depend on mechanical properties of their environment, such as stiffness, but also topography and architecture [154]. Properties on the nanoscale (less than 1 μm), microscale (1-1000 μm), like porosity and pore size, and macroscale (bigger than 1 mm), like scaffold dimension, can be of importance [155]. The size, geometry and topology of pores are physical cues that can guide cell morphogenesis, and which also are important for the spatial organization cells. Grooves and roughness in surfaces have shown to affect cell orientation and can also improve attachment of some cells. Fibroblasts have shown to prefer smooth surfaces, while osteoblast-like cells prefer rougher surfaces [156]. In a bone marrow cell line (SR-4987) the spatial development was investigated by culture in three different porous materials, two different porous cellulose beads (100 μm and 500 μm pore size) and a polyester fibrous material. This resulted in growth that was globular, spread, and thin and long, respectively [156, 157].

1.4 Methods for studying cells cultivated in 3D scaffolds

In this study, viability and morphology was studied using light microscopy, confocal laser scanning microscopy (CLSM) and a cytotoxicity test based on release of the cytosolic enzyme lactate dehydrogenase (LDH). CLSM was chosen as the main method of analysis due to its suitability for studying cells in three dimensions. CLSM requires fluorescence staining prior to imaging and was used here for differentiating live from dead cells, and for staining specific parts of the cell. Light microscopy was used for studying the cells while they were still alive, and the cytotoxicity test complements the viability imaging.

Light microscopy requires no fixing or staining, and therefore allows studying cells while they are alive. In bright-field light microscopy, the image is formed directly by light passing through the specimen [158]. To improve contrast when examining unpigmented cells, phase-contrast can be applied. One can also stain the cells, but this would involve killing them [158]. The light microscope can separate details that are 0.2 μm apart. If they are closer, they will appear as a single object. When using the light microscope, the focus is on a particular plane of choice in

the specimen. However, the complete specimen is illuminated at all times, and this might cause an out-of-focus blur [158].

Instead of illuminating the whole specimen, confocal laser scanning microscopy (CLSM) involves a pinpoint illumination. Single spots of specific planes of the specimen are exposed to light by passing laser light through a pinhole [158], allowing out-of-focus light to be excluded [109, 159]. By this, CLSM offers the ability the create sharp images of high resolution and contrast [109, 160]. CLSM combined with fluorescence is one of the most widely used tools for studying cells in 3D cultures [159, 161]. An important advantage with CLSM is that it allows imaging of optical sections of the specimen [109, 160, 162] – which can be reconstructed into a 3D image [109, 159, 160]. However, the applicability of CLSM in cell culture depends on the transparency of the specimen. Transparent materials are the most suitable [159, 163-165].

CLSM with fluorescence works by pinpoint laser illumination of a fluorescently stained or tagged specimen of interest, which will lead to emission of fluorescence [158]. It is the fluorescent molecules in the specimen that emit this light. The emitted light is collected by an objective lens [160] before it passes through a second pinhole and reaches a detector [158, 160]. The second pinhole makes sure any emitted light from other parts of the specimen is excluded. The laser scans through a chosen point of the specimen, back and forth horizontally, which results in a two-dimensional image of the plane of focus [158]. The image is made pixel by the help of oscillating mirrors that deflect the laser beam across the specimen [158, 160, 162]. Images can be in the form of a slice of a single optical section, or as a series of images that capture the whole thickness of the specimen. The latter is called a Z-stack and enables 3D visualization [158, 160].

CLSM is usually combined with fluorescence microscopy. This allows localization of specific compartments, proteins or other molecules of cells and tissues [109, 158] with high precision, by the use of specific fluorescent. It can also be used for co-localization of differently stained molecules [158, 160], such as for example cytoskeletal networks in combination with nucleic acids in the nuclei [158]. The fluorescent probes can be in the form of dyes, or dyes conjugated to antibodies, [109, 158], and will absorb and emit light of specific wavelengths [109]. The light emitted is of longer wavelength than the absorbed light, due to lowered of energy (Figure 16). Light of wavelengths from 400 nm (violet) to 700 nm (deep red) are visible to the human eye. The fluorescently tagged specimen is illuminated with the wavelength it absorbs, using light passed through an excitation filter. The fluorescence is excited, and the emitted light is passed through an emission filter of specific wavelength. The filters are adapted to only let through

wavelengths that excite, and are emitted, by the fluorescence of interest [158]. This results in a specific fluorescence emission that localizes the compartment of interest.

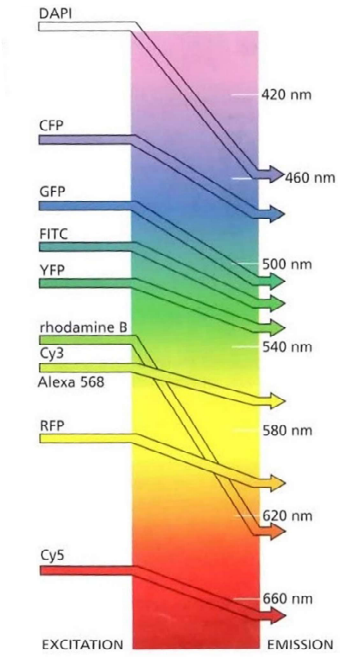

Figure 16: Common fluorescent probes with their respective maximum excitation and emission wavelengths, shown along with the colors on the light spectrum. Illustration is from *Molecular Biology of the Cell* 6th edition [158].

Several fluorescent probes can be used in the same specimen, and images of these can be merged. Commonly used stains are green-fluorescent fluorescein, excited by blue light, and red fluorescent rhodamine, excited by green-yellow light. A widely used derivative of fluorescein is fluorescein isothocyantae (FITC) [158]. 4',6-diamidino-2-phenylindole dihydrochloride (DAPI) is a blue-fluorescent stain that absorbs ultraviolet (UV) and is widely used for DNA-labeling [158, 166]. Other examples of fluorescent proteins (FPs) are CFP, GFP, YFP and RFP which respectively are cyan, green, yellow and red. New fluorescent dyes such as Cy3, Cy2 and Alexa dyes are well adapted to fluorescence microscopy. However, a problem with Alexa dyes and other organic probes is that the dyes will bleach when illuminated over time. Such light damage or weak degree of staining are sources of poorer image quality [158].

1.4.1 Fluorescent labeling

One way to study cell morphology is to stain the cytoskeleton and nuclei, which will localize the cells by the nuclei and show how they have been shaped by stretching of the actin filament. This was performed in this study by staining cells with blue-fluorescent DAPI and red-fluorescent Alexa 568 Phalloidin. The viability of cells can be qualitatively visualized by

staining dead and living cells. In this study, green-fluorescent calcein-acetoxymethyl ester (calcein-AM) and red-fluorescent ethidium homodimer-1 (EthD-1) were used for this.

All living cells have ubiquitously intracellular active esterases [167], which are enzymes that catalyze esters into its alcohol and acid through hydrolysis [168]. Calcein-AM is an uncharged, lipophilic molecule that passively permeates the cell membrane. When it enters a living cell, it will be hydrolyzed by esterases into green-fluorescent calcein, and the cell will appear green in the microscope [167, 169, 170]. Calcein is polyanionic and negatively charged, causing it to be cell impermeant and well retained in the cytosol of living cells with intact membranes [171, 172]. It is a structural derivative of fluorescein [173], a commonly used green fluorescent dye excited by blue light [158], and these have similar fluorescence properties [173]. The excitation spectrum is around 494-495 nm, and it emits wavelengths of 515-530 nm [167, 169, 170]. A dead cell without this intracellular enzymatic activity will not be stained green.

While calcein-AM stains live cells green by indicating esterase activity, the dye EthD-1 stains dead cells red by indicating loss of plasma membrane integrity [167, 174]. EthD-1 is a polycationic dimeric molecule [175] enters cells with a damaged plasma membrane. In the cell it will bind to nucleic acids with high affinity [176]. It is not able to enter cells with an intact membrane [167]. The structure of the dye consists of two aromatic phenanthridinium rings, which both function as chromophores [177]. EthD-1 is an intercalating dye, which forms stable complexes with nucleic acids such as double stranded DNA (dsDNA) and single stranded DNA (ssDNA) by inserting one of its aromatic rings between base pairs (bp) [175, 178, 179]. One EthD-1 molecule will cover 4 bp, and totally the ratio is 1 EthD-1 per 4-5 bp [179]. Upon binding, the fluorescence of EthD-1 is increased 40 times, comparing the EthD-1 alone to the EthD-1-dsDNA complex [179]. A low intrinsic fluorescence with large enhancement upon binding is typical for intercalating dyes, and this is caused by reduced free rotation of the molecule upon binding [178]. The dead cells will appear as bright red fluorescent. EthD-1 has excitation around 495 nm when exposed to light [167], while it emits light of wavelength from 610-700 nm [175], with maximum around 630-635 nm [167, 180]. When excited with light at 495 nm, calcein-AM and EthD-1 treated cells with have emission of fluorescent light at respectively around 515 nm and 635 nm, giving them distinctive signatures of fluorescence [180].

DAPI is a common blue-fluorescent probe used for staining nuclear, chromosomal DNA. It absorbs ultraviolet light and emits bright blue fluorescence [158, 166], and is widely used as a counterstain [181, 182]. Upon interaction with cells, DAPI will preferentially bind to dsDNA

in sequences that are rich in the nucleobase pair adenine-thymine (AT). The DAPI molecule attaches to the minor groove [183, 184], which is one of the two repeated grooves created by the coiling of the DNA double helix [185]. DAPI is hydrophobic [186] with flat aromatic rings that fit into the minor groove. It inserts itself sideways into the groove, displacing the hydrogen spine in the dsDNA helix [187, 188]. The binding has been found to be formed by hydrogen bonds with bases in DNA and electrostatic van der Waals interactions with phosphates in DNA [186, 189]. The hydrogen bond is formed between the indole nitrogen (NH) in DAPI and the thymine (T) base in DNA. The structure when bound to DNA is very similar to that of the DNA alone, said to be nearly isomorphous [187].

The binding of DAPI to DNA results in a fluorescent complex [183], with a high quantum yield of 0.92, compared to 0.04 of unbound DAPI. The quantum yield is the ratio of emitted photons to absorbed photons and is therefore a measure of the efficiency of the probe. This means that there is a large increase in fluorescence upon binding [184], around a 20-fold enhancement. The increase in fluorescence is said to be caused by removal of water from both the DAPI molecule and the minor groove of DNA, upon hydrogen bond formation [182, 190]. DAPI is cell-impermeant, so cells must be permeabilized and fixed beforehand to allow entrance of DAPI into the cell [191, 192]. Reported excitation for DNA-bound DAPI varies between 350-405 nm (405 nm is violet light) [181, 182], with maximum around 358 nm (UV) in dsDNA-DAPI complexes according to Sbirkova-Dimitrova et al. (2017) [186]. Emission maximum is around 460-461 nm (blue) [182, 186]. By fluorescence microscopy, DAPI probes can therefore be excited with ultraviolet light and detected with a blue/cyan emission filter [186].

The dye Alexa Fluor 568-phalloidin is a conjugate of the dye Alexa Fluor 568 and phalloidin [193, 194]. Phalloidin is a toxin produced by the deadly toxic mushroom *Amanita phalloides*. It is a bicyclic, water-soluble heptapeptide that selectively binds tightly along the sides of actin filaments in cells [108, 193-195]. This binding is non-covalent [195] with site in the cleft between subdomains of the actin monomers [196]. The toxicity of phalloidin is due to its polymer-stabilizing effects. It prevents the filaments from depolymerization [108], hindering the dissociation of monomers at the ends of the actin filament [196]. The stabilization is due to hydrophobic interactions and [195] strong hydrogen bonds [197]. The normal function of actin filaments is based on a dynamic balance between filament-state and monomer-state, and disturbances in this balance results in toxic effects in living cells [108].

Because of its affinity to actin filament, phalloidin is widely used for studying actin filament in cells [108, 193, 194]. If isolated, phalloidin can be fluorescently labeled and used as a probe to

label and visualize actin filaments in tissues and cells [108, 193-195], as with the Alexa Fluor™ 568 phalloidin probe in the morphology assay in this study. Alexa 568-phalloidin is photostable and fluoresces with bright red-orange, with wavelength maxima for excitation at 578 nm and emission at 600 nm [193, 194]. It is not cell permeable, so the cells must be fixed and permeabilized before staining [194, 197]. Alexa dyes are relatively new fluorescent dyes developed specifically for use in fluorescence microscopy [158], with nomenclature based on the approximate wavelength maximum in nm of the particular dye [198]. They are generally more fluorescent and photostable than their more commonly used analogs, such as fluorescein, rhodamine and Cy3. Alexa dyes can withstand pH changes between 4-10, which is a benefit [198]. Phalloidin can be conjugated with different fluorophores to label actin filament, depending on for example other present fluorophores if the particular assay involves co-staining [199]. This is mainly done to prevent any overlap in emissions, enabling differentiation between dyes more accurately.

1.4.2 Cell preservation and permeabilization

Preserving and permeabilizing the cells the way they are at a given moment allows them to be stored, labeled and imaged as desired. This was important for the DAPI/Phalloidin morphology assay that was applied in this study. Fixation involves preservation of the cells by stabilizing their structure. This is often performed with aldehydes, such as formaldehyde, which is a common fixative [200]. Upon reaction with cells, formaldehyde reacts with proteins by cross-linking them, resulting in entrapment of the cell constituents in a matrix of crosslinked proteins. The solution used in this study is made from paraformaldehyde (PFA), which is a polymer of formaldehyde that is commonly used for making formaldehyde solution [200, 201]. Triton X-100 is a non-ionic detergent [202] used for permeabilization of the cell membrane [201]. Treatment of cells with Triton X-100 allows access to intracellular features [201] by permeabilizing the cell membrane through solubilization of membrane lipids [202, 203]. As other detergents, Triton X-100 is amphiphilic, which means that it has both hydrophilic and hydrophobic properties. The molecule is small with an uncharged polar end (hydrophilic) and a non-polar end (hydrophobic). When the detergent is added to cells, the hydrophobic part of the detergent binds to membrane proteins in the hydrophobic region of the cell membranes. The binding leads to disruption of hydrophobic interactions and displacement of lipids with detergent molecules. Often, detergent-protein complexes are formed, in which detergent molecules attach to the protein with their hydrophilic parts facing out. These complexes can be

found in solution [203]. The possibility of extraction of proteins along with the lipids when using Triton X-100, or other such detergents, can be a disadvantage [201].

1.4.3 Cytotoxicity

Cytotoxicity is an important evaluation of studies *in vitro*. There are many ways to assess the viability and cytotoxicity of cells, commonly based on factors such as cell membrane permeability and enzymatic activity. In this study, the viability was assessed qualitatively with a Live/Dead assay using CLSM. In addition, a colorimetric cytotoxicity test based on release of lactate dehydrogenase (LDH) was run. Using two different assays for studying cell survival is an advantage and can increase reliability of the results if they indicate the same. There are many different colorimetric tests in addition to the LDH assay, such as MTT assay and MTS assay [204]. An advantage with the LDH-assay is that it is applied on the cultivation media from the experiment, and therefore can be applied without killing the cells. In addition, it is reliable and simple to perform. LDH based cytotoxicity assays can be applied for quantitatively assessing both cell-mediated cytotoxicity and cytotoxicity mediated by agents, compounds, or materials [204, 205].

LDH is a cytosolic enzyme that will be released into the culturing media if cell membranes are damaged. High levels therefore indicate membrane lysis or cell death. The amount of LDH activity in the collected media is determined by enzymatic test that includes two enzymatic reactions (1. Step and 2. Step, Figure 17) [204, 205]. If there is LDH in the collected media, NAD^+, added by the catalyst (diaphorase), will be reduced to $NADH/H^+$ in the conversion (oxidation) of lactate to pyruvate. (Lactate is supplied by sodium lactate in an added dye solution). Then the enzyme diaphorase in the catalyst will transfer H/H^+ from $NADH/H^+$ to a tetrazolium salt, iodonitrotetrazolium (INT). This causes the pale yellow INT to be reduced to formazan salt, which is red and can be colorimetrically detected [204, 205].

Measured absorbance of the media will therefore correlate with the degree of conversion of INT into formazan, which is dependent on the amount of LDH activity that results in $NADH/H^+$. An increase in amount of formazan, indicated as red coloring of the samples, correlates with increased amounts of LDH activity, and then also the number of dead cells [205].

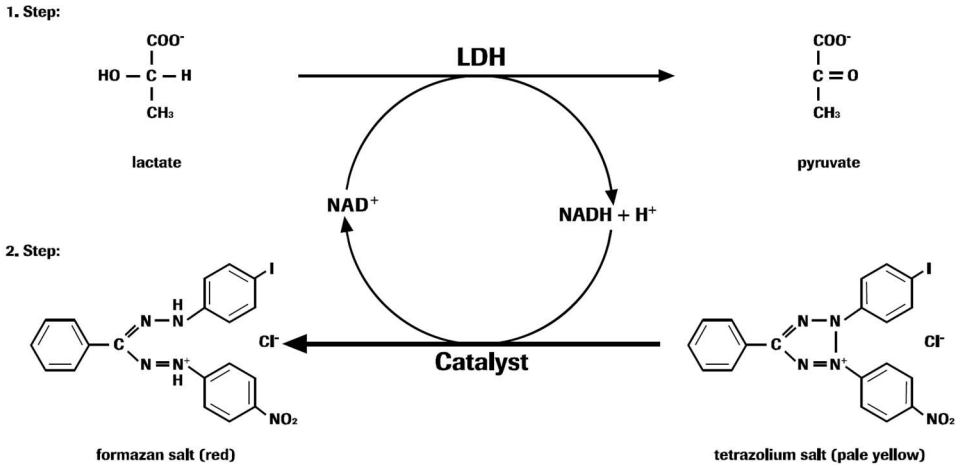

Figure 17: The two enzymatic steps that makes the basis of the LDH Cytotoxicity test. Lactate, in the form of sodium lactate, and NAD^+ is supplied respectively by the dye solution and the catalyst. Any present LDH will catalyze the conversion of lactate into pyruvate, producing $NADH+H^+$. Diaphorase catalyzes the reduction of pale yellow tetrazolium salt (INT) into red formazan salt, using $NADH/H^+$ and producing NAD^+. Figure is acquired from the product protocol for the Cytotoxicity Detection Kit^{PLUS} (LDH) supplied by Sigma-Aldrich®/Roche Diagnostics GmbH [205].

Formazan as a measure of LDH, has a quite broad absorption maximum around 500 nm [205], but absorbs maximally at 492 nm and is measured quantitatively at 490 nm [204, 205]. The precursor to formazan, INT, has almost no absorption around this wavelength. Figure 18 is adapted from the Cytotoxicity Detection Kit^{PLUS} (LDH) protocol (provided by Roche Diagnostis GmbH) and shows the absorbance spectra of a culturing media (RPMI 1640, 1% bovine serum albumin (BSA)) with the reaction mixture of Cytotoxicity Detection Kit, in the absence (dotted line) and presence (stippled line) of LDH [205].

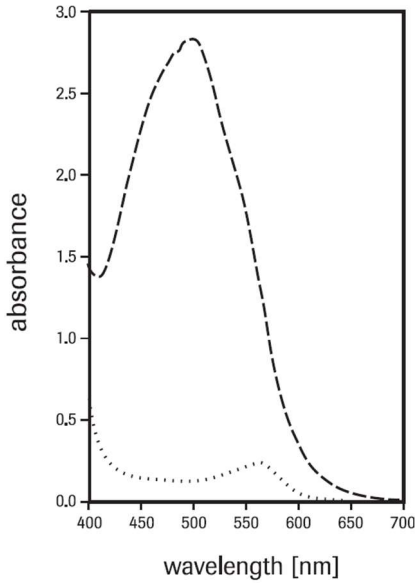

Figure 18: Absorption spectra in media (RPMI 1640) with 1% BSA, with reaction mixture of a LDH Cytotoxicity Detection Kit^{PLUS}, with (stippled line) and without (dotted line) presence of LDH, showing the difference when formazan is formed and not. Acquired from protocol by Sigma-Aldrich®/Roche Diagnostics GmbH [205].

A disadvantage with the LDH cytotoxicity test is that some compounds, e.g. serum, have inherent LDH activity, which can cause high background readings. The use of serum-free or low-serum media is therefore recommended. Background controls are therefore important to include [204].

1.5 Aim and research questions

The main aim of this study is to investigate short- and long-term effects of 3D microstructures on fibroblast viability and morphology. This was performed by exploring differences between cells cultivated in two different alginate-based 3D hydrogel scaffolds: a porous foam and a homogeneous hydrogel. Cell research using 3D culturing instead of 2D culturing has shown to have advantages in terms of offering models that can achieve more physiologically relevant responses from the cells. However, there are many properties of the 3D culture systems that affect the cells. These can be based on chemical properties, such as grafting and modifications of the 3D material, but also on mechanical properties such as stiffness, porosity and topography. In addition, cells of different tissue origin are expected to inherently respond differently to the material properties.

Here, the effects of microstructuring on three different human cell types were studied – primary NHDFs, cell line IMR-90 and cell line HS-5 in two different 3D scaffolds, both containing RGD-functionalized alginate. The cell viability and morphology were assessed after 1, 7 and 21 days, mainly using qualitative image analysis, along with a quantitative cytotoxicity test. In this study, the effects of microstructuring were explored by addressing the following research questions:

- How is the distribution of alginate within foams?
- Do the alginate foams promote viability and/or induce morphologies in cells differently than in the cells seeded in gels?
- Do the cell types respond differently to the foam and/or hydrogel?
- How is the viability and morphology on the short term compared to long term?
- Do the results of viability staining correspond to the cytotoxicity tests?

2 MATERIALS AND METHODS

2.1 Cultivation of NHDF, IMR-90 and HS-5 cells

Three different adherent cell types were tested in this study; primary cells of NHDF (Lonza® CC-2511™), cell line IMR-90 (ATCC® CCL-186™) and cell line HS-5 (ATCC® CRL-11882™). Prior to experiments, cells were cultivated (Figure 19) in sterile T75 flasks (VWR® Tissue Culture Flask, 75cm^2, Surface Treated, Vented cap) with cell-specific culture media. All cells were kept in a CO_2 incubator (5% CO_2 atmosphere, 37°C, Thermo Scientific Heracell™ 150i) and media was changed every 2-3 days. Prior to use, all cells were stored in cryovials (~500,000 cells/vial), cryopreserved (-70°C). To start cultivation, the cryovials were thawed and cells immediately seeded in T75 flasks with media (37°C). All cell work was performed under sterile conditions in a laminar air flow bench as required (LAF-bench, ESCO Class II Biohazard Safety Cabinet). Handling of cells, medium or chemicals for cell treatment was performed in a LAF-bench, and all equipment was disinfected with ethanol (70%) before use. Medium and solutions for cells were preheated in water bath (Grant GD100, 37°C).

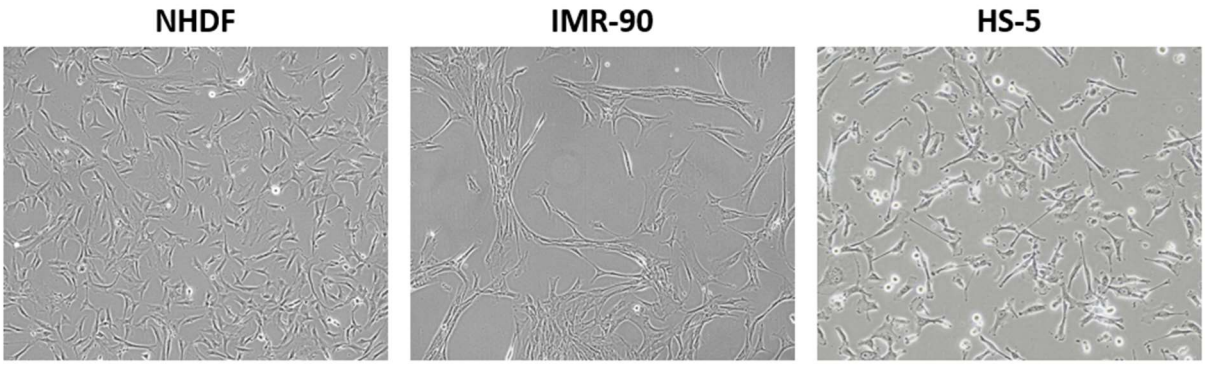

Figure 19: Light microscopy images of the 2D cultivated NHDF, IMR-90 and HS-5 in T75 flasks, imaged with a 10x objective. The cells appearance and confluency were monitored consistently.

All cells were cultured and passaged as needed to perform experiments. Passaging of flasks was generally performed at 70-90% confluency. Normally one flask was split into two new flasks. Cell splitting was performed with chemicals described in subsections for each cell type (2.1.1-2.1.3). The workflow for splitting cells involved washing of cells, detachment of cells, collecting of cells and centrifuging (Eppendorf® Centrifuge 5804 R) to generate a cell pellet. After cell counting with a light microscope (Nikon Eclipse Ts100, Nikon Eclipse Ts2) and hemocytometer (Bürker, counting chamber), total cell number and required volume of cell suspension to acquire the desired seeding cell density was calculated. Seeded cell density for T75 flasks was usually between $0.2x10^6$ and $0.5x10^6$ cells/flask. In the following three

subchapters (2.1.1-2.1.3), the specific culture conditions pertaining to each cell type is outlined in detail.

2.1.1 Normal human dermal fibroblasts (NHDF, Primary cells)

NHDFs (CC-2511) are primary cells derived from the dermis of human adult skin, with biosafety level 1. The cells tested negative of any infections, and guaranteed 15 population doublings from the supplier [123]. For these cells, a fibroblast growth medium (FGM™-2 Fibroblast Growth Medium-2 BulletKit™, Lonza® Clonetics®, CC-3132) was used, containing fibroblast basal medium (FBM™, CC-3131) with addition of fibroblast growth media supplements and growth factors (FGM™-2 SingleQuots™ Kit, CC-4126). Components of the total medium are shown in Table 1.

Table 1: Components of the complete FGM used for cultivation of NHDFs in this study.

Component	Concentration (%)
FBM	~97.75
Fetal Bovine Serum (FBS)	~1.96
-Human Fibroblast Growth factor B (rhFGF-B)	~0.098
Insulin, Recombinant Human	~0.098
Gentamicin sulfate + Amphotericin-B (GA-1000)	~0.098

For passaging, sterile Hank's Balanced Salt Solution (HBSS) was used to wash the cell monolayer, removing any remains of media. Trypsin-Ethylene Diamine Tetraacetic acid (Trypsin-EDTA) solution (1x, sterile-filtered, BioReagent, 0.5 g porcine trypsin and 0.2 g EDTA*4Na/L HBS, with phenol red [206]) was used to detach cells from flask. Trypsin neutralizing solution (TNS) (PBS with 5% FBS, without Ca/Mg, stored at -20°C) was used for collecting the cells, and FBM for resuspension of the cell pellet.

2.1.2 Human lung fibroblasts (IMR-90, Cell line)

The IMR-90 (CCL-186) cell line originates from lung tissue of a 16-week-old female fetus. These cells are capable of 58 population doublings before senescence, and categorized as biosafety level 1 [127]. The culturing media used was low glucose Dulbecco's Modified Eagle's Medium (DMEM, 1000 mg/L of glucose and sodium bicarbonate ($NaHCO_3$), w/o L-glutamine, Sigma-Aldrich®, Lot # RNBH2448, D5546) with addition of supplements and growth factors (Table 2).

Table 2: Components of the complete low glucose DMEM used for cultivation of IMR-90s.

Component	Concentration
DMEM, low glucose (1 mg/mL)	86%
FBS (100%)	10%
L-glutamine (200 mM)	2 mM
Pen Strep (10000 U/mL)	100 U/mL
NEAA (100%)	1%
Na pyruvate (100 mM)	1 mM

For passaging, sterile Phosphate-buffered saline (PBS, Dulbecco's Phosphate Buffered Saline, Biowest®, w/o Magnesium, w/o Calcium, Sterile Filtered, Batch: MS00QY) was used for washing the cell monolayer, removing any residual media and dead cells. Trypsin-EDTA was used to detach the live cells from the flask. Low glucose DMEM was used for collecting the cells and for resuspension of the cell pellet.

2.1.3 Human bone marrow stromal fibroblast-like cells (HS-5, Cell line)

The HS-5 (CRL-11882) cell line originates from bone marrow/stroma of an adult male. These cells have been immortalized by being HPV-16 E6/E7 transformed, implying that the cells contain human papilloma viral sequences, and is therefore classified as biosafety level 2 [135]. Medium used for HS-5 was high glucose DMEM (4.5 g/L D-glucose, w/o L-glutamine, w/o pyruvate, Gibco, Lot 2265772), with added supplements (Table 3).

Table 3: Components of the complete high glucose DMEM used for cultivation of HS-5s in this study.

Component	Concentration
DMEM, high glucose (4.5 g/mL)	86%
FBS (100%)	10%
L-glutamine (200 mM)	4 mM
Pen Strep (10000 U/mL)	100 U/mL
Na pyruvate (100 mM)	1 mM

As with the IMR-90 cells, PBS was used to wash the HS-5 cell monolayer as well. Trypsin-EDTA was used to detach the live cells from the flask, as with both NHDF and IMR-90. High glucose DMEM was used for collecting the cells and for resuspension of the cell pellet.

2.1.4 Cell preparation before experiment

In preparation for experiments, cells were cultivated and passaged at least once. Passage number of cells used for experiments were between P6 and P13. When preparing the cells for experiments, passaging was performed as described previously (overview in Table 4), and instead of resuspending cell pellets in culturing media, a custom prepared buffer (3DLife buffer)

was used. 3D Life Buffer was used to prevent any interferences with the production of the hydrogel itself, which the use of media may cause considering the presence of phosphate and proteins in media. 3DLife buffer preparation is described in Section 2.2.1.

Table 4: Overview table of cell types NHDF, IMR-90 and HS-5, and their pertaining media and passaging chemicals.

Cell	Biosafety level	Media	Wash	Detachment	Collecting solution
NHDF	1	FGM	HBSS	Trypsin-EDTA	TNS
IMR-90	1	DMEM, low glucose	PBS	Trypsin-EDTA	DMEM
HS-5	2	DMEM, high glucose	PBS	Trypsin-EDTA	DMEM

For experiments, cells were resuspended in 3D Life buffer and diluted appropriately in order to obtain the required cell concentration. Separate cell suspensions were made for adding to the alginate solution for foams and for hydrogels.

Composition of the alginate solutions will be described in Section 2.2. Preparation of the alginate solutions and cells before experiments, as well as procedure for cell seeding and scaffold casting are described Section 2.3.

2.2 Alginate scaffolds: Foams and hydrogels

Two different forms of alginate scaffolds were tested for 3D cell culturing in this study: a hydrogel and a foam. The alginate solution for these were produced in-house using ultrapure low viscosity high G (UPLVG) sodium alginate (PRONOVA™, BP-0907-02, F_G=0.682, F_{GG}=0.572, $N_{G>1}$=16 M_w=237 kDa) and UPLVG grafted with tripeptide Arg-Gly-Asp (RGD) to enable cell attachment to the material. The RGD-grafting was in the form of the peptide Gly-Arg-Gly-Asp-Ser-Pro (GRGDSP). The UPLVG was purchased from NovaMatrix®, IFF Nutrition & Bioscience, Sandvika, Norway. UPLVG-GRGDSP (Batches: 06/06/2018, 10/06/2020, 16/11/2018, M_w=237 kDa, D_{ox} 8%, D_S 5%) was provided by Daria Zaytseva-Zotova and Anita Akbarzadeh at NTNU. The hydrogel comprised of in-house produced alginate solution, while the foam comprised of in-house produced alginate solution added to a dry alginate foam sheet (PRONOVA™ UP, gamma sterilized), also produced by NovaMatrix®. All alginates from NovaMatrix® are isolated from the large brown macro algae *Laminaria hyperborea* [93, 94]. In theory both the scaffolds used here are hydrogel based, but they will be referred to as "foam" and "hydrogel". UPLVG will be referred to as unmodified alginate, while UPLVG-GRGDSP will be referred to as RGD-grafted alginate.

The foams and hydrogels consisted of 1% (w/v) alginate. 75% of the total alginate was RGD-grafted, while 25% was unmodified. The alginate concentration and content of RGD were selected based on previous experiments conducted by the group. For preliminary studies of the foams (without cells), a fluorescent alginate (LF200S, S21483, F_G=0.677, F_{GG}=0.567, $N_{G>1}$=14, M_w=298 kDa), prepared by Joachim S. Kjesbu at NTNU, was used. The LF200S had been conjugated with fluoresceinamine. Only one type of fluorescent alginate was used and will be referred to as LF200S in this thesis. LF200S was also used for some additional studies (Section 2.10). Table 5 presents a complete overview of alginates used in this study.

The 1% alginate solutions were made from 2% (w/v) stock solutions of the RGD-grafted alginate and the unmodified alginate. Stock solutions were made by dissolving the alginates overnight in 3D Life buffer (4°C, 15 rpm) in a rotator (Grant Bio PTR-60 360° Vertical Multi-Function). The stock solutions were stored in fridge (4°C) until use. The next Sections 2.2.2 and 2.2.3 presents the scaffolds used in this study (foam and hydrogel). Section 2.3 provides details on the preparation and casting of the 1% alginate solutions with cells.

Table 5: Overview on alginate products used in the experiments presented in this thesis. The table highlights the form, batch, fraction of guluronate (F_G), molecular weight (M_w) and other important properties.

Product name	Form	Comment	Batch	F_G	M_w (kDa)
PRONOVA™ UP LVG Sodium Alginate	Powder	Unmodified Stored in fridge (4°C)	BP-0907-02 (05/2018)	0.682	237
UP LVG-GRGDSP	Flake	RGD grafted/ Peptide-coupled Stored in freezer (-21°C)	06/06/2018 16/11/2018 25/05/2018-10/06/2020 01/2021	-	97
PRONOVA™ UP Alginate Foam	Foam sheet	Gamma-sterilized Stored in RT	96-well plate: BU-1410-37 (first batch) BU-1407-15 (new batch) BU-1407-17 (new batch) 24-well plate: BU-1407-18	-	-
LF200S	Flake	Fluorescent Stored in RT	S21483	0.677	298

2.2.1 3DLife buffer

To prepare alginate solutions, working-solutions for reagents, and cell suspensions for experiments, a customized buffer (3DLife buffer) was used. This was an adapted 4-(2-hydroxyethyl)-1-piperazineethanesulfonic acid (HEPES) buffer. All components of the buffer are outlined in Table 6. All dry ingredients were dissolved in Milli-Q (MQ) water. The final pH was adjusted to 7.4 by adding sodium hydroxide (NaOH, 1M) dropwise. The buffer was stored in fridge at 4°C).

Table 6: Recipe for the 3DLife buffer (1x), used to dissolve alginate, prepare working-solutions, and make cell suspension for experiments. Table shows the ingredients with their chemical formula and concentration (mM) in 1x buffer.

Concentration in 1x buffer (mM)	Component	Manufacturer
25	HEPES	PanReach/AppliChem VWR® Chemicals
14	$Na_3Citrate$ **x** $2H_2O$	VWR Prolabo BDH
56	Fructose	Norsk Medisinaldepot
70	Sodium chloride	VWR AnalaR NORMAPUR

2.2.2 Foam

Dry alginate foams were delivered in sterile 96-well plates, and three different batches of foams were used in experiments (BU-1410-37, BU-1407-15, BU-1407-17). The foams come as dry, porous sheets laying in the bottom of the wells of 96-well plates and readily rehydrate upon the addition of 1% alginate solution (Figure 20). Recommended by NovaMatrix®, 10 µL of alginate solution was utilized for all cell-based experiments with foams. Gelation is completed in 10 minutes.

Figure 20: Appearance of the foam scaffold used in this study. To the left is a dry alginate foam as they come delivered from NovaMatrix®, taken out of the 96-well plate. To the right, a foam supplemented with 10 µL 3DLife buffer for demonstration of foam appearance after absorption of liquid.

Components of the 1% alginate solution for foams are shown in Table 7. For gelation within the foams, nothing additional had to be added to the 1% alginate solution, because Ca^{2+} is integrated in the dry foams.

Table 7: Concentration of components added to dry foams, in stocks and final solution.

In 1x 3DLife buffer:	STOCK	FINAL
Alginate solution (75% RGD-grafted, 25% unmodified)	2%	1%
Cell suspension	1.538 x 10^6 cells/mL	0.769 x 10^6 cells/mL

2.2.3 Hydrogel

The hydrogel (Figure 21) is homogeneous, without the microstructure and porosity of the foam. The 1% alginate solution was added a suspension of calcium carbonate ($CaCO_3$) (360 mM, d=0.7µm, VIcality) and a solution of D-(+)-Gluconic acid delta-lactone (GDL) (Sigma-Aldrich, Lot: 011M0035V), and was casted directly into empty wells in 96-wellplates in optimized volumes (65 µL/well).

Figure 21: Appearance of the hydrogel scaffold used in this study. This 1% alginate gel (65 µL) was casted in removable rubber wells on a glass plate for testing gelation, without cells.

For gelation to occur, GDL and Ca^{2+} was used for crosslinking. The composition of the hydrogel is shown in Table 8. A suspension of $CaCO_3$ was used in order to supply the gelling ion (Ca^{2+}) for the hydrogel gelation. To prepare suspension, the powder had been heat-sterilized (180°C, 2 h) and resuspended in sterile 3DLife buffer (0.2 µm filter sterilized). GDL solution was added to the 1% alginate-cell mixture at the very end. Gelation starts 15 minutes after addition of GDL and takes 2 hours.

Table 8: Composition of hydrogels, with concentration in stocks and final solution.

In 1x 3DLife buffer:	STOCK	FINAL
Alginate solution (75% RGD-grafted, 25% unmodified)	2%	1%
$CaCO_3$ suspension	360 mM	18 mM
Cell suspension	3.077 x 10^6 cells/mL	0.769 x 10^6 cells/mL
GDL solution	180 mM	36 mM

2.2.5 Assessment of alginate distribution in foams

In order to evaluate the distribution of alginate across the pores of the alginate foams, fluorescent alginate LF200S was used. Both a 0.5% and 1% solution of LF200S were tested to determine whether the polymer content and viscosity of the alginate solutions affected the distribution across the foams. For these tests, 24-wellplate foams (BU-1407-18) were used due to ease of handling. The foams are electrostatic and was therefore first put in place with forceps if they were not laying at the bottom of the well. Solutions were added dropwise (100 µL/well, n=6), in a manner such that the entire foam was covered uniformly. The foams were imaged at three timepoints (15 min, 48 h and 7 days) with confocal laser scanning microscopy (CLSM) as outlined in Section 2.6.

2.3 Experimental design

To investigate the effects of microstructuring in 3D alginate culturing scaffolds, three different cell types were cultivated in porous alginate foams and homogeneous alginate hydrogels for up to 21 days (Figure 22). The cells were seeded inside the scaffolds, which both were based on RGD-functionalized alginate. The experimental procedure was the same for all cell types, timepoints and for both scaffolds, except that the LDH Cytotoxicity test was performed only at D1 and D7. The experiments were divided in two: short-term (D1 and D7) and long-term (D21) studies. D1 and D7 were conducted in parallel using two separate 96-well plates, while long-term studies were conducted independently. Foams and hydrogels were casted on the same plate. This approach was adopted for all three cell types.

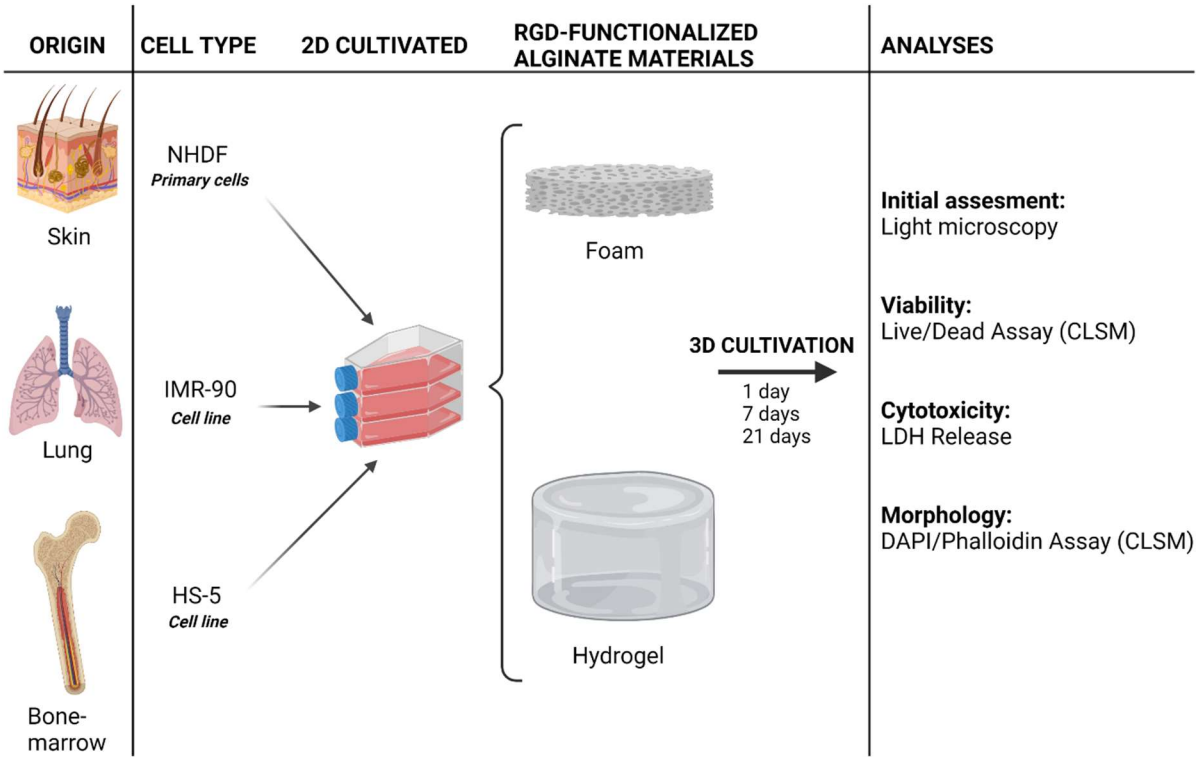

Figure 22: Experimental overview. Initially, one type of primary cells and two types of cell lines were cultivated in T75 flasks for expansion of cell numbers. Before use in experiment, the cells were passaged at least once into new T75 flasks. Each cell type was seeded in two types of 3D alginate materials: foams and hydrogels. The cells were cultivated for up to 21 days, and analysed at short-term and long-term with light microscopy, CLSM (assessing viability and morphology), and with a cytotoxicity test based on LDH release. Illustration created in BioRender.com.

The cells were analyzed at D1, D7 and D21 with light microscopy, a Live/Dead viability assay, a LDH cytotoxicity test and a DAPI/Phalloidin morphology assay. Imaging with light microscopy, collection of culture media for the LDH Cytotoxicity test and Live/Dead staining was performed under sterile conditions while the cells were still alive. The Live/Dead stained cells were visualized with CLSM. The colorimetric LDH Cytotoxicity test was performed on the collected media, and absorbances were measured with a plate reader. Staining with DAPI/Phalloidin was performed on fixed and permeabilized cells. Morphology was visualized with CLSM. All methods of analysis are described in detail in Sections 2.4, 2.5 and 2.6.

2.3.1 Preparation of alginate solutions and cell suspensions

2% alginate stock solutions were prepared as described in Section 2.2. Under sterile conditions in a LAF-bench, the 2% solutions and 3DLife buffer were filter sterilized with syringes (Terumo, Belgium) and 0.2 µm pore sized syringe filters (GE Healthcare, Life Sciences, Puradisc^{TM} 13 mm Whatman^{TM}, UK). This was to ensure sterility, as bacteria cannot pass this pore size. 1% alginate solutions for foams and hydrogels were prepared according to Table 7

and Table 8, respectively. The $CaCO_3$ suspension was vortexed, added to the alginate solution for hydrogels and mixed thoroughly. Cells and GDL were not added until the cell suspensions were ready. Meanwhile, the alginate solutions were kept in fridge at 4°C. The cells were split as described in Section 2.1. The cell pellet was resuspended in sterile 3DLife buffer (37°C). Separate cell suspensions for foams and hydrogels were diluted to respectively 1.538 x 10^6 cells/mL and 3.077 x 10^6 cells/mL.

2.3.2 Casting procedure

The alginate solution for foams was added cells and mixed, giving a 1% alginate solution. The solution was added onto the dry foam sheets (PRONOVA™ Alginate Foams) in 96-well plates (10µL/well, n=15), giving 7700 cells/well. The solution was mixed between each casting to avoid cell sedimentation. The plate was kept in incubator (5% CO_2 atmosphere, 37°C) for gelation. After 10 minutes, cell specific culturing media (150 µL) was added carefully to the foams to avoid flipping or harm. GDL solution (180 mM) was prepared by dissolving in 3DLife buffer, mixing for 30 s and filter sterilization (0.2 µm filter). The alginate solution for hydrogels was added cells and mixed, and then added GDL and mixed, giving a 1% alginate solution. The hydrogels were casted in empty wells (65 µL/well, n=15) on the same plate as the foams (Figure 23), giving 50 000 cells/well. The solution was added in the middle of the wells, using cut off pipette tips to reduce loss of solution. The 96-well plate was put in incubator for 2 hours. The hydrogels were added culture media dropwise (150 µL) and put back in incubator for 30 min.

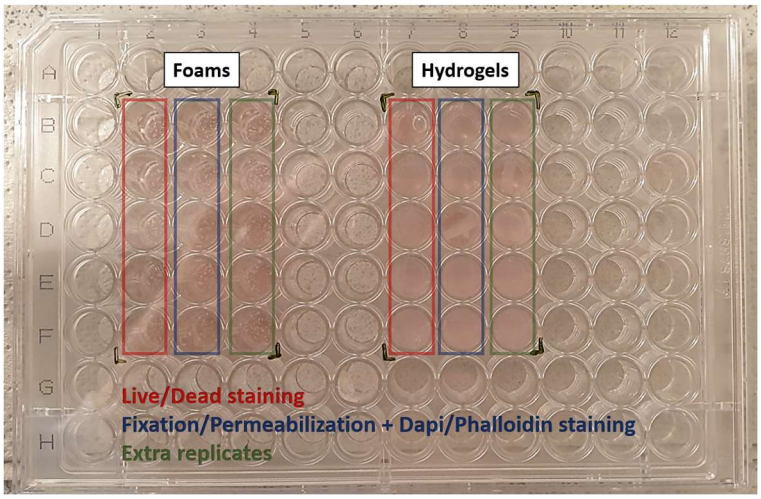

Figure 23: Example of a 96-well plate on D0. Foams and hydrogels were casted side by side on the same plate. The scaffolds have been added culture media (bright pink). The colored frames show replicates planned for analyses. Light microscopy and collection of media for LDH Cytotoxicity test could be conducted on any replicate. Some extra replicates (green) were always prepared in case required for the planned analyses or for any further analysis. The goal was at least three replicates for each analysis.

The hydrogels were washed after 30 min of incubation by removing old media and adding new (150 µL). Washing step was repeated once. The next day half of the media was removed (75 µL) and new was added for both foams and hydrogels. The plate was kept in incubator (5% CO_2 atmosphere, 37°C). Half of the media (75 µL) was changed every 2-3 days. To keep the scaffolds from drying, the wells always had around 150 µL media. The status of cells and the scaffolds was monitored by media colour and light microscopy. An overview of the casting is shown in Figure 24.

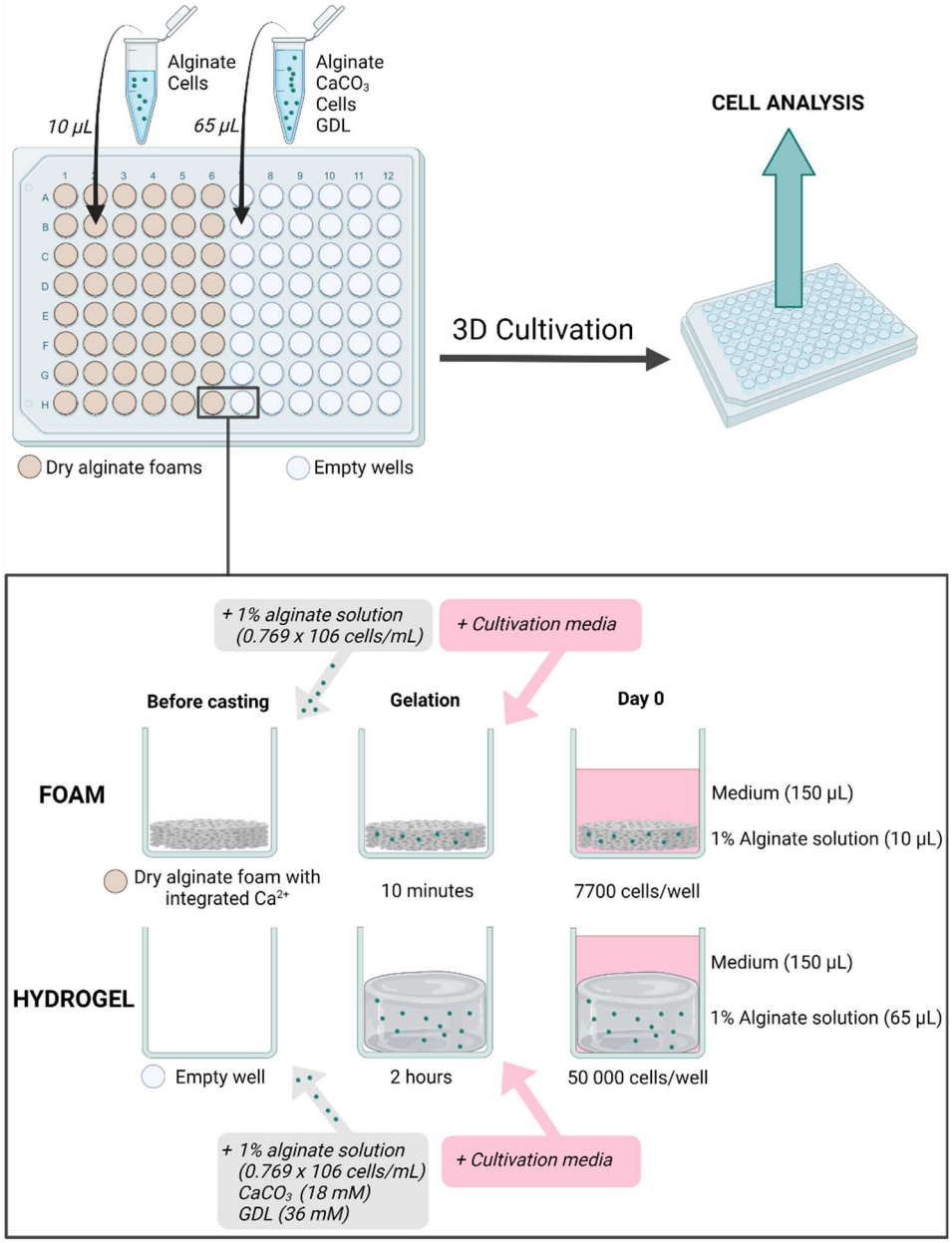

Figure 24: Detailed casting of foams and hydrogels in 96-well plates. The foams were seeded with 7700 cells/well, while the hydrogels were seeded with 50 000 cells/well. Both scaffolds were added 150 µL of cultivation media after gelation. The hydrogels were washed with 3DLife buffer prior to addition of cultivation media. Foams and hydrogels were always in the same plate. The cells were cultivated and analyzed, always remaining in the 96-well plate. Illustration created in BioRender.com.

2.4 Light microscopy

The light microscope allows to study the cells easily and quickly while they are alive without any staining or other preparation. As first assessment after casting, the light microscope was used to scroll through the layers of scaffolds to see how and if the cells had distributed well both vertically and horizontally. Cell shapes and structures of the scaffolds could be studied relatively clearly, and it was therefore an initial indication of cell behavior and distribution.

Bright field light microscopy was used throughout the main study and for additional smaller studies. It was used for imaging and for quickly checking cells and scaffolds when cultivating and passaging cells in T75 flasks, and for checking status of cells and scaffolds after casting the experiments. Light microscopy was also one of the tools of analysis and imaging at the analysis days (D1, D7 and D21). In addition, some samples of foams and hydrogels were imaged every time media was changed to monitor the experiments and to ensure the cells are healthy. The 96-well plates in which the foams and hydrogels were casted were studied under the light microscope with the lid on, always keeping the inside sterile.

Two different light microscopes were used for imaging, either Nikon Eclipse Ts100 or Nikon Eclipse Ts2, with cameras attached (Zyla ANDOR sCMOS). The latter was used for IMR-90 long term and all of HS-5, while the first was used for all of NHDF and the short term IMR-90. Images were taken were taken around the middle of the scaffolds, using 4x, 10x, 20x and 40x objectives. With the 4x, one could see a total image of the scaffold in the microscope, while 40x offers a close-up on single or few cells. For each imaging, 2-3 random, intact samples considered representative were imaged. The light microscope cameras were also used for imaging in the preliminary studies of cell distribution in foams and when comparing dry samples of the old and new batches of foams.

2.5 Cytotoxicity tests

To investigate if the scaffolds had a cytotoxic effect on the cells, a quantitative LDH Cytotoxicity test was performed, using the Cytotoxicity Detection Kit^{PLUS} (LDH) produced by Roche Diagnostics GmbH (Mannheim, Germany). Lactate dehydrogenase (LDH) is a cytosolic enzyme that is released if the cell membrane is ruptured [205], which indicates cell lysis or cell death. The LDH cytotoxicity test is a colorimetric assay based on using the amount of LDH released into the cultivation media from the cells as a measure of cytotoxicity. LDH was measured by absorbance in cell media at D1 and D7 for all the three cell types, NHDF, IMR-90 and HS-5. Three controls were used for each experiment: a positive control (dead cells) a

negative control (living cells), both cell specific, and a background control (only media). The positive control defines the maximum releasable LDH activity in the cells and the negative control shows LDH activity released from untreated cells [205]. The background control accounts for any inherent color changes in the media itself, and by that allows colorimetric determination of the LDH activity alone when subtracted from the measurements.

The controls were prepared in three separate 96-well plates (Tissue culture treated, Corning Incorporated, Costar®, USA). One plate contained negative controls (D1 and D7) and background control, one plate had D1 positive controls, and one plate had D7 positive controls. The negative and positive controls consisted of cells seeded on plastic in empty wells (without any alginate materials). Controls for the foam and hydrogel were seeded the same number of cells as the experimental wells with scaffolds, respectively 7 700 cells and 50 000 cells. For the released LDH to be comparable, the total liquid amount in the controls was kept the same as in the experimental samples. The foam control replicates consisted of 7 700 cells in 160 µL media, and the hydrogel control replicates of 50 000 cells in 215 µL media. 50 000 cells are too many for 2D cultivation in a single 96-well plate well, and therefore each of the three replicates for the hydrogel controls were divided into three wells. The background control replicates consisted of 150 µL cell specific media. Triton™ X-100 (Sigma-Aldrich®, Lot #MKBR0249V) was used to lyse the positive control cells. Triton X-100 (25%) was added to the D1 controls right after seeding (at D0), and to the D7 controls at D6, exposing the cells to 1% Triton X-100. Control plates were kept under same conditions as the experiment plates.

At D1 and D7, media (50 µL) from experimental wells and controls was collected in a new 96-well plate and kept on ice. The Cytotoxicity Detection Kit contains a Dye Solution (cat. #04744942001) and a Catalyst (cat. #04744926001). The dye solution consists of iodotetrazolium chloride (INT, 2-[4-iodophenyl]-3-[4-nitrophenyl]-5-phenyltetrazolium chloride) and sodium lactate and dyes the reaction mix. The catalyst contains diaphorase and NAD^+, and catalyzes the reaction mix [205]. The dye solution and the catalyst were stored in freezer before use. At first use, the dye solution was thawed overnight, and the lyophilizate catalyst was dissolved in 1mL distilled water (MQ water) for 10 minutes. Dye solution and dissolved catalyst were kept light protected in fridge for the following experiments.

The reaction mixture was made by mixing dye solution and dissolved catalyst in a 1:45 ratio. Because of light sensitivity, the mixture was kept covered as much as possible. 50 µL of reaction mixture was added and mixed carefully to each well with collected media in the 96-well plate. The plate was incubated (30 min, RT, light protected). The amount of released LDH was

determined by measuring the end-point absorbance of the media from the wells in a multi-mode microplate plate reader (SpectraMax®i3x, Molecular Devices) at wavelength 490 nm. No stop solution was used for stopping the LDH reaction. However, timing for absorbance reading was constant for all experiments (30 min).

Results were obtained using the computer software SoftMax Pro 6.5.1 and presented as relative percentage cytotoxicity, with standard deviations. The relative percentage cytotoxicity was calculated from average absorbance values of the media from experimental wells and their respective cell specific negative and positive controls, using the following equation:

Cytotoxicity (%) = ((exp. value – neg. control) / (positive control – negative control)) x 100

Average absorbance of the media controls was subtracted from all absorbance values to remove background disturbance. The procedure was adapted from the supplier's product protocol [205] to fit this experiment. The procedure was the same for all cell types. Significance of the cytotoxicity was calculated with unpaired t-tests (Section 2.9).

2.6 Confocal microscopy

The main method of analysis in this study was qualitative analysis by confocal laser scanning microscopy (CLSM), using a Leica DMi8 microscope (SP8) from Leica Microsystems GmbH. CLSM was used for assessing the distribution of alginate solution within the foams (described in Section 2.2.5) and for qualitatively investigating the viability and morphology of the cells in alginate hydrogels and foams. Distribution of alginate was visualized using the fluorescent alginate LF200S, and cell viability by staining cells with a LIVE/DEAD® Viability/Cytotoxicity Kit (Thermo Fisher, Invitrogen™). Cell morphology was studied by co-staining the cells nuclei and actin filaments with 4',6-diamidino-2-phenylindole dihydrochloride (DAPI) and Phalloidin, respectively (both from Invitrogen by Thermo Fisher Scientific).

All confocal images were taken using a dry lens (HP PL APO CS) with 10x objective and 0.40 numerical aperture. Other settings used were a DD Beam Splitter 488/552, in resolution format 1024x1024 pixels, speed 600Hz and Z-step size 3.5 µm. Image sizes were 1.55mm x 1.55mm with pixel size 1.52 µm x 1.52 µm, and optical section 7.23 µm. Line average was set to 2 and a digital zoom factor of 0.75 was applied to all images except the magnified DAPI/Phalloidin images which were taken with a digital zoom factor of 3.0 and line averaging of 3. Z-stacks were taken either from bottom up or top down, starting and ending where there were cells visible. For the foams, stacks would mostly cover the entire vertical plane of the scaffold in the particular spot that was imaged, including all the cells in that particular plane. The hydrogels

were significantly thicker than the foams and did not always allow for imaging the entire vertical plane, due to limitations posed by the focal distance of the lens itself. The maximum possible Z-stacks were 143 steps, which equals to 500 µm.

CLSM was also applied in some additional studies of the foam. These involved a comparison of foams with alginate solution made with cultivation media vs. 3DLife buffer, and a comparison of the different batches of foams that were used. LF200S was used to visualize the alginate in these additional studies, and the same microscope parameters were implemented as in the study of alginate distribution. Optimization of cell distribution and investigation of black aggregates in the foams were performed by running a short-term study (D1 and D7) with NHDF, applying the DAPI/Phalloidin staining and settings.

2.6.1 Distribution of alginate in foams

CLSM was used in the investigation of the alginate distribution within foams, which was described in Section 2.2.5. 24-well plate foams with 1% and 0.5% LF200S solution were imaged at three timepoints (15 min, 48 h and 7 days). The fluorescens of LF200S was due to its conjugation with fluoresceinamine, an amine derivate of the commonly used fluorescent label fluorescein. The amine group provides a binding site, allowing attachment to molecules [207]. The green fluorescence was excited by a 488 nm filter, and with emission filter of 493-560 nm. All images were captured full z-stacks of the foams. A bright field PMT Transmission channel was also used to be able to see visualize the foam structure and where the alginate accumulated. 3D renders were made to be able to see how the distribution in the foam was vertically as well, using the LAS X software. At 15 min, the foams were imaged as they were with no addition of liquid. The foams that were to be imaged at 48 h and 7 days rested in media (4°C) to prevent drying.

2.6.2 Live/Dead Viability Assay

To qualitatively assess cell survival and cell viability over time in the scaffolds, a LIVE/DEAD® Viability/Cytotoxicity Kit (Thermo Fisher Scientific, Invitrogen™ , Lot 2098892) for mammalian cells was applied. This is a two-color assay, where dead cells will appear red and living cells will appear green, which in this case was visualized with CLSM. The cells were stained simultaneously with the two dyes calcein-acetoxymethyl ester (calcein-AM), and ethidium homodimer-1 (EthD-1), respectively causing green fluorescence and red fluorescence [169, 174]. Both dyes are non-fluorescent until they react with the cells they are used for, which results in low background fluorescence [167]. Calcein-AM stains live cells green by indicating

intracellular esterase activity, EthD-1 stains dead cells red by indicating loss of plasma membrane integrity [167, 174].

In this study, NHDFs, IMR-90 and HS-5 cells that had been cultivated in hydrogel and foam were stained with EthD-1/calcein-AM and imaged with CLSM at D1, D7 and D21. The staining solution was made by thawing prepared aliquots of Calcein-AM and EthD-1 from the LIVE/DEAD® Viability/Cytotoxicity Kit (Thermo Fisher Scientific, Invitrogen™, Lot 2098892), and mixing calcein-AM, EthD-1 and serum-free media in a 1:4:2000 ratio (light protected and sterile). Media was removed from the wells, and staining solution was added to foams and hydrogels (150 µ/well, n=5). Cells were incubated for 45 minutes (5% CO_2 atmosphere, 37°C).

To visualize the green fluorescence, 488 nm excitation and 493-560 nm emission filters were used. For the red fluorescence, filters of wavelengths 638 nm and 643-790 nm, respectively for excitation and emission, were used. Bright field images were taken simultaneously to visualize the scaffolds. Images were taken of at least three stained samples that were considered most representative. When imaging the scaffolds, it was observed that foams often floated. To improve the quality of images, some staining solution, was removed before imaging from both the hydrogels and the foams, which made sense also regarding the use of a dry lens.

2.6.3 DAPI/Phalloidin Morphology Assay

Cell morphology was studied closer by co-staining with 4',6-diamidino-2-phenylindole dihydrochloride (DAPI) (2116138, 14.3 mM) and Phalloidin (2151755, Alexa Fluor™ 568 phalloidin). DAPI and Phalloidin are fluorescent dyes that respectively stain cell nuclei blue and actin filament red. Both stains were purchased from Invitrogen by Thermo Fisher Scientific and are commonly used fluorescent probes [158]. NHDF, IMR-90 and HS-5 cultivated in alginate foam and hydrogel were fixed and permeabilized at D1, D7 and D21, stained with a solution of DAPI and Phalloidin (mastermix) and visualized with CLSM.

Prior to staining with DAPI/Phalloidin, the cells were prepared by simultaneous fixation and permeabilization. This treatment permeabilizes and preserves the cells as they are at the particular timepoint. The solution used for this contained PFA (4%) and Triton™ X-100 (Sigma-Aldrich®, Lot #MKBR0249V). Formaldehyde fixates the cells, while Triton X-100 permeabilizes the cells [200]. These agents are some of the most common agents for these purposes [202]. Media was removed from all the wells and the scaffolds containing cells were washed briefly with a staining buffer (Table 9). The cells were fixed and permeabilized (100

µL/well) and incubated (1 h, RT). The solution was removed, the scaffolds were washed twice and then stored in staining buffer.

Staining buffer was prepared as outlined in Table 9. This buffer was used for washing and storage of all fixed/permeabilized and DAPI/Phalloidin stained cells. HEPES, calcium chloride ($CaCl_2$) and sodium chloride (NaCl) were mixed and dissolved in MQ water. pH was adjusted to 7.4 with sodium hydroxide (NaOH) (1M).

Table 9: Recipe for Staining buffer, used to wash cells before and after fixing/permeabilization and DAPI/Phalloidin staining. Table shows the ingredients with their chemical formula and concentration (mM) in 1x buffer.

Concentration in 1x buffer (mM)	Component	Manufacturer
10	HEPES	PanReach/AppliChem VWR® Chemicals
5	Calcium chloride	Merck
140	Sodium chloride	VWR AnalaR NORMAPUR

The mastermix was prepared under as light protected conditions as possible due to light sensitivity of the dyes. Aliquots of DAPI and Phalloidin were thawed, and then Staining buffer, DAPI and Phalloidin 568 were mixed in a 1000:1:2.5 ratio, respectively. Staining buffer was removed from the experimental wells, the cells were added mastermix (100 µL/well) and then incubated (2 h, RT, light protected). The cells were washed twice and stored in fridge (4°C, light protected).

To visualize the Phalloidin 568, filters for excitation and emission were respectively 638 nm and 643-710 nm. To visualize DAPI, excitation filter of 405 nm was used. Bright field images were taken simultaneously. The cells were studied and imaged bottom up, top down, in middle and on edge of the foams and hydrogels. Out of several samples of foam and hydrogel, images were taken of the ones intact, showing cells clearly and considered representative. At least 2-4 out of several samples were imaged with at least 4 images in each. The images were taken in spots of the scaffold considered representative for that sample and that showed cells clearly. In some cases, images were not taken in both magnifications (30x and 7.5x) or in both edge and middle.

2.7 Image processing

Included in this thesis are light microscope images and CLSM images. To be comparable, all light microscope images of the cells were adjusted for brightness and contrast. The images taken

with the Nikon Eclipse Ts100 were cropped with a factor of 1.75 to adjust for differences in zoom factor. Images taken with Nikon Eclipse Ts2 had colors and were therefore adjusted to grey scale to be comparable to the ones imaged with Nikon Eclipse Ts100. Scalebars were added manually. All adjustments on light microscope images were performed in PowerPoint (Microsoft, version 2107).

Confocal images included images of foams with fluorescent alginate, the Live/Dead assay and the DAPI/Phalloidin assay. These were all processed with the imaging software Leica Application Suite X (LAS X) 3.5.6.21594 and in the image processing program ImageJ/Fiji.

2.7.1 LAS X

LAS X is an imaging software platform that is used for life science imaging with Leica Microscopes. It was used here for imaging and for initial processing during and right after imaging. The main tool that was used was making maximum projections of Z-stacks, which is a merging of the steps in the stack, giving one image. This image represents the multiple layers of the scaffold, which is beneficial when studying a 3D material. LAS X was also used for cropping the Z-stacks when necessary. For the alginate distribution images, it was also used for 3D visualization of the Z-stacks, creating 3D renders and color depth mapping.

2.7.2 ImageJ/Fiji

For processing of CLSM images, Fiji was used. Fiji, an extension of ImageJ, is a Java-based software platform for processing and analysis of scientific and biological images [208]. It was used for merging and splitting channels and creating overlay images of these channels. It was also used for removing background in the images and adjusting differences in brightness and contrast. Another tool in Fiji that was used was the addition of scalebars.

2.8 Image analysis

The analysis of images in this master thesis study was based on qualitative comparison of the appearance of and differences between cells in the images taken. This applies to both the initial assessment with light microscopy where both cell distribution and cell shapes were assessed, the Live/Dead viability assessment where the difference in red and green staining was compared, and in the morphology study with DAPI/Phalloidin staining.

2.9 Statistical analysis – LDH values

For calculations and presentation of the relative percentage cytotoxicity values from the LDH cytotoxicity test in one diagram, Excel (Microsoft, version 2107) was used. Calculations include averages and standard deviations. For each cell type, the significance of the difference

between foam and hydrogel at each timepoint and between D1 and D7 in each scaffold was calculated. The background absorbance in media was subtracted from each all absorbances. Relative percentage cytotoxicity was calculated for each replicate using average control values and was compared in the t-test. The significance between experimental values and negative control values was also calculated.

The significances were calculated in terms of p-values in an unpaired Welch's t-test using SigmaPlot 14.0.

2.10 Additional tests

Additional small studies that were performed were,

1. Assessing of the volume of the foams
2. Comparison of alginate solution for foams based on either media or buffer
3. Assessing the effect of cell concentration on cell distribution and aggregates in foam
4. Comparison of the foam batches that were used throughout the study.

The approximate volume of a foam in 96-well plate was determined by weighing wet (saturated) and dry foam samples, checking if the difference would correspond to recommended casting volume (10 µL). Three replicates of each were used. The wet foams that were used were samples that had been used for optimization and practice of casting hydrogels with cells and imaging.

Differences between alginate dissolved in either media or buffer was evaluated. While the hydrogels had been optimized for 3DLife buffer, it was recommended by NovaMatrix® to dissolve the alginate for foams in culture media (serum free DMEM). To make the two scaffolds as similar as possible, it was investigated whether dissolving alginate solution for foams in 3DLife buffer would affect gelation within the foams. 2% LF200S stock solutions were prepared, one with media and one with buffer, and dissolved overnight (15 rpm, 4°C, light protected). 1% solutions were made from the stocks by further dilution with media and buffer. Solutions were added to a 96-well plate with foams (NovaMatrix®) (10 µL/well, dropwise). The gelled foams were imaged with CLSM at three timepoints (15 min, 48 h, 1 week). In addition, at 48 h, one foam of each of the groups were removed from its well and placed on a petri dish to check if the alginate had gelled, and if there were any immediate differences between media and buffer. The foams were also touched and squeezed flat between two fingers to also control if there were any noticeable differences in behavior when destroyed or in strength.

Test runs with cells in alginate foams (1% alginate) showed some black aggregates in the light microscope. Therefore, it was a desire to investigate whether these were affected by cell concentrations. In addition, there was a question if the cells would look significantly different with changing cell concentrations in the foams, which was necessary since they were going to be compared to the hydrogels which were larger an had more cells. To investigate these matters, an optimization study was run. Three different and relatively low concentrations of cells were seeded in the foams, and the foams were studied with light microscopy and CLSM. 5000, 2500 and 770 cells were seeded in 96-well plates with foams in a volume of 10 µL. The cells were analyzed with DAPI/Phalloidin and CLSM, and with light microscopy before fixing at both D1 and D7.

Lastly, differences in alginate distribution in the three different batches of foams were tested. This was investigated to evaluate differences in the foam appearances and color, and to consider for batch-to-batch variations. Differences between foam batches were investigated by comparing dry foams and foams casted with 1% LF200S. Light microscopy was used for imaging dry foams. CLSM was used for imaging foams with LF200S at different timepoints (48 h, 8 days). The foams were also qualitatively assessed for their appearance in both dry and wet conditions (with buffer).

3 RESULTS

The results are separated into sections as per the assay, with subsections for cell type or time point. Firstly, the distribution of alginate solution in foam is presented. Observations from light microscopy are presented in the next section, followed by Live/Dead CLSM images, results of the LDH-based cytotoxicity test, and CLSM images of the DAPI/Phalloidin morphology assay. In the end the findings in additional tests are summed up. Images from the additional tests are presented in Appendix F. For all results, foams and hydrogels were directly compared since the central focus of this thesis is to identify any differences linked to the structuring of these scaffolds.

3.1 Preliminary study - Distribution of alginate solution in foam

The distribution of alginate solution across foam and its pore structures was evaluated. The objective was to obtain an insight as to where the cells would be seeded in the foams. Foams with fluorescent LF200S were imaged at 15 min (Figure 25), 48 h (Figure 26) and 1 week with CLSM. At 15 min, the intensity of fluorescence across a foam pore was measured in addition, shown as an intensity graph (Figure 25b, 25d). At 48 h and 7 days, 3D renders were generated

from the Z-stacks (Figure 27). The 3D renders from day 7 are also presented with color depth mapping (Figure 28). Alginate distribution at the foam edge is shown in Figure 29.

Confocal images at 15 min (Figure 25a, 25c) shows the green-fluorescent LF200S distributed within the pores of the foam structure. The foam structure appears as dark, opaque, thin walls. All replicates seem to have bubbles within, appearing as black, oval or circular dots. The LF200S seems to fill and distribute uniformly within the pores, as in the image of the 0.5% LF200S (Figure 25a, left). The 1% LF200S (Figure 25c) is a little more unclear, due to physical obstructions that present as black shadows. However, foam walls and green LF200S are visible underneath the shadows, showing green coverage evenly distributed in the foam and close to foam walls. The images to the right in Figure 25a and 25c show the bright field channel on the same location. In 1% LF200S (Figure 25c), the bright field image shows a clear indication of bubbles that match the location of the shadows in the corresponding fluorescence image.

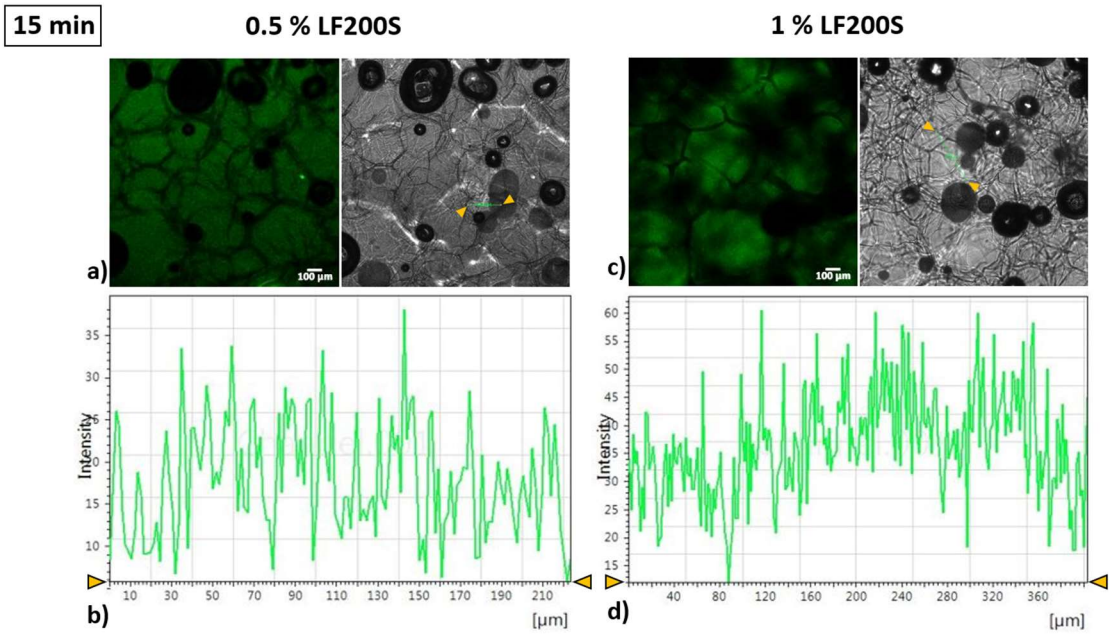

Figure 25: Alginate foams containing 0.5% LF200S (**a**) and 1% LF200S (**c**), imaged with CLSM after 15 minutes, with intensity graphs of fluorescence from one foam wall to another, respectively **b**) and **d**). The left image in **a**) and in **c**) show the foam structure with green fluorescence signal from LF200S, while the right images show the bright field channel, including where the signal intensity was measured, marked by a green line and yellow arrows at the ends. Graphs **b**) and **d**) show the fluorescence intensity, for 0.5% LF200S and 1% LF200S respectively. This was measured across a straight line from edge to edge in a foam pore. These images and graphs were processed by Aman S. Chahal, NTNU.

The fluorescence intensity was measured across a foam pore using the LAS X software and is shown in the graphs in Figure 25b and 25d. The measured locations are indicated by a green line between yellow arrows in the grey bright field images (Figure 25a, 25c). The graphs show shift in light intensity (nm) by position (µm) on the green line. Both ends of the green lines

(foam wall area) are low on intensity, and the middle part (pore centers) of the lines varies but has generally higher intensity. Overall, higher intensities were measured for the 1% LF200S than the 0.5% LF200S. The measured line in 0.5% LF200S was ≈ 224 µm long from strut to strut in a relatively small foam pore (Figure 25a), and the intensity graph shows a range in intensity from 6 nm to 38 nm (Figure 25b). The 1% LF200S line was ≈ 404 µm long (Figure 25c) with light intensity ranging from 12 nm to 60 nm (Figure 25d). The maximum value was around 0.6 times higher in the 1% LF200S than in 0.5% LF200S.

The foams were also imaged at 48 h (Figure 26). Figure 26 shows the fluorescence channel, bright field channel and a channel merge for 0.5% LF200S (top) and 1% LF200S (bottom). 3D renders generated from the Z-stacks are shown in Figure 27. At 48 h, bubbles are no longer present. However, there are some rounded shadows in the pores that look like holes, marked with yellow arrows in the fluorescence images (Figure 26, left). These holes were also observed at 7 days (Figure 27). Else, the distribution of LF200S at 48h and 7 days looks similar to at 15 min. In the channel merges (Figure 26, right), a mesh of foam structure can be seen as a layer above the pores filled with LF200S.

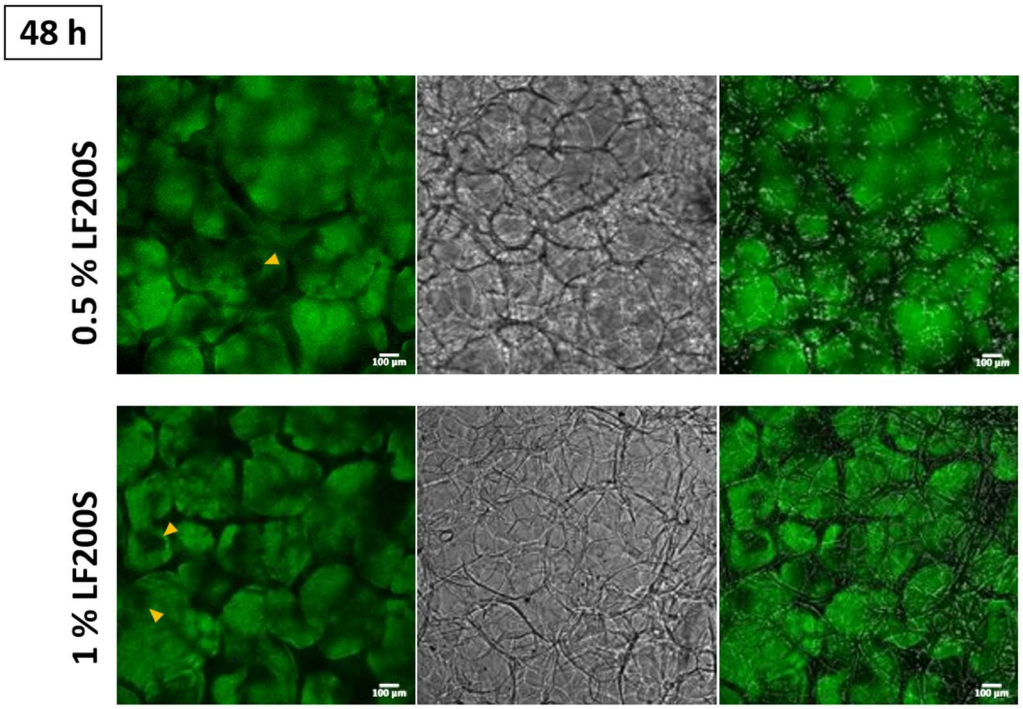

Figure 26: Alginate foams with 0.5% LF200S and 1% LF200S imaged at 48 h. The three images for both alginate concentrations show the green fluorescence of the alginate solution (left), the bright field channel (middle) and both channels merged (right). Scalebars are 100 µm. Yellow arrows point at examples of holes in the fluorescent alginate, which could remain from air bubbles seen at 15 min. Images were processed by Aman S. Chahal, NTNU.

3D renders at 48 h and 7 days were generated to visualize how the LF200S distributed vertically in the foams (Figure 27). At 48 h, the images from above (upper rows) show very much the same as in Figure 26. The 0.5% LF200S looks uniformly distributed across the foam, with dark foam walls and shadows. In the merged image to the right however, we see the top of the foam structure as opposed to in the projected image in Figure 26. In the channel merge seen from above, there is less green LF200S visible due to the foam structures. The 1% LF200S (48 h) is similar to 0.5% LF200S, but is brighter green. More LF200S is visible in the 1% channel merge than 0.5%, but as seen in the tilted 3D renders, the 1% LF200S stacks are also thinner in thickness. The foams look similar after 7 days. In the 1% LF200S, the foam walls appear more distinct and uniform in signal brightness. Opposite from at 48 h, a thicker Z-stack was made of 1% LF200S sample. Still more alginate is visible seen from above than in 0.5%.

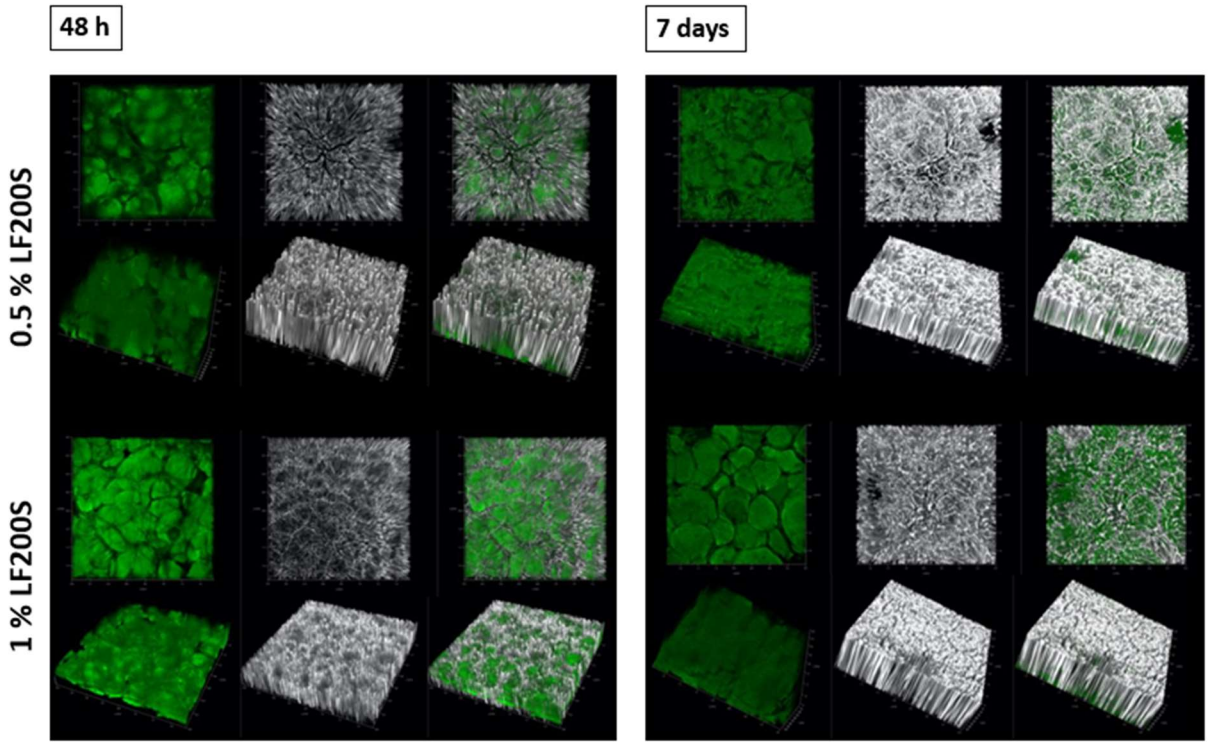

Figure 27: 3D-renders of 0.5% and 1% LF200S foams, made from Z-stacks taken at 48 h (left) and 7 days (right). Each of the four sets of images show the fluorescence channel (left) the bright field channel (middle), and a channel merge (right), both seen from above and a as tilted 3D representation. Images processed by Aman S. Chahal, NTNU.

At day 7, depth mapping with colors was performed on the 3D renders to demonstrate the alginate distribution on different depths, across different Z-planes, of the foams (Figure 28). The Z-plane depth is represented by a color scale of blue, green, yellow and red, respectively from bottom to top. The left images (Figure 28) show LF200S. Both 0.5% and 1% show coverage in all Z-plane colors. It could look like there is a little more 0.5% LF200S at the top

(red), than in the 1% LF200S, and some more at the bottom (blue) in 1% than in 0.5%. The bright field images (middle) of 0.5% have some darker areas, and these correspond to the red LF200S in left image. The bright field (middle) and the merged channel (right) images have more red than the images to the left where only LF200S is showing.

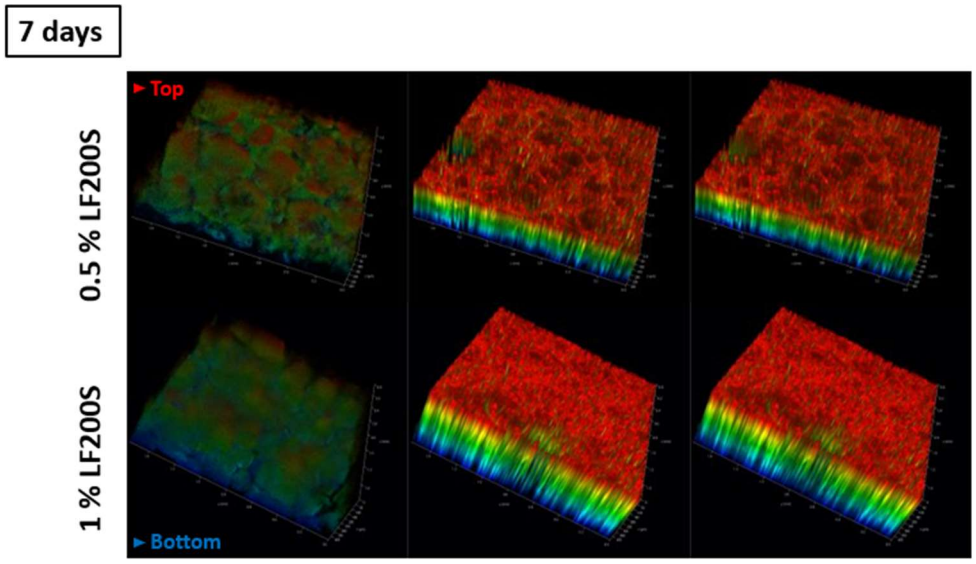

Figure 28: Color depth mapping of CLSM images of foams with 0.5% LF200S and 1% LF200S, taken after 7 days. Red represents top and blue represents bottom of the foam. Left image shows only LF200S, middle image shows only the bright field channel, and the right is a channel merge. Images processed by Aman S. Chahal, NTNU.

At day 7, foam edges were imaged to see how the alginate distributed out in the edge. Figure 29 shows an example of the edge of a 1% LF200S sample. The LF200S was not spread all the way out to the very edge. Some autofluorescence from the dry foam itself is seen as green silhouettes of the foam walls. The bright field image shows that the edge is not completely even, rather a little rough and thinner in the outermost parts.

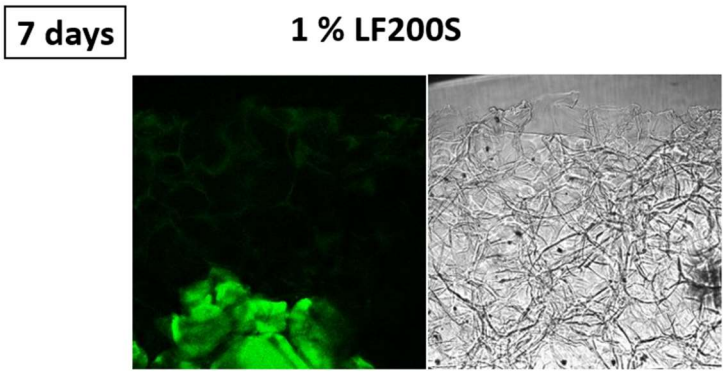

Figure 29: Foam edge with 1% LF200S, at day 7. Left image shows the fluorescence channel, with the bright green, fluorescent alginate at the bottom of the image, while the right picture shows the corresponding bright field channel, showing the foam structure and the edge of the foam. Top of the images is the edge of the foam. Images processed by Aman S. Chahal, NTNU.

3.2 Initial assessment and monitoring of live cells

The cells in the scaffolds were monitored and imaged with light microscopy along the way in each experiment. This was the initial assessment that was used, checking appearance of cells and scaffolds. Out of multiple pictures taken, the ones considered the most representative were chosen. The different magnifications (4x, 10x, 20x and 40x) are sometimes from the same sample, sometimes not. NHDF, IMR-90 and HS-5 imaged at D1, D7 and D21 are shown respectively in Figure 30, Figure 31 and Figure 32. Four light micrographs with increasing magnification from column a) to d), are presented for each timepoint. The red circles in column a) indicates the middle of the scaffold as seen from above. Blue squares in two different micrographs indicates a zoomed-in area. Yellow arrows and blue circles point out specific observations. Images of additional timepoints are included in Appendix A.

All intact foams and hydrogels were observed with cells distributed vertically and horizontally. There were also usually cells attached to the well bottom beneath the scaffold. An observation in foams was black aggregates, which were studied to see if had anything to do with the cell concentration (Section 3.6 and Appendix F). Over time, higher cell numbers were observed around the edge areas of the foams. Dark, spherical bubbles were observed in all foams at D1, and these were no longer present at D7. These corresponded to observations in the alginate distribution study (Section 3.1, Figure 25). Mostly the gelation of hydrogels made them transparent, but sometimes they remained cloudy, which could cause difficulty observing the cells. Cells at the well bottom could sometimes be seen in other layers of the hydrogel as a striped pattern. Over time, it was observed that there would often be fewer cells in the middle of the hydrogel.

3.2.1 NHDF

Images from D1, D7 and D21 are presented in Figure 30. Additional images from D3 and D13 (from same plate as D21) are commented here and presented in Appendix A. The first batch of alginate foams were used.

At D1, the cells observed in the foam were quite few. They were evenly distributed from the middle (●) to the edge (Figure 30a, Foam, D1). An example of a bubble is indicated with a yellow arrow (▽). The bubbles are several 100 µm in diameter. An example of the mentioned black aggregates seen in all foams is pointed out in bottom of Figure 30b, Foam, D1. The other arrow in Figure 30b (Foam, D1) points at a foam wall. The cells are mostly rounded, with some exceptions where the cells have branches or an elongated shape. Some cells look connected to

other cells. In Figure 30c (Foam, D1) an elongated cell, more than 50 µm long, is shown to the left. To the right, a rounded cell with a branch is pointed at. A completely rounded cell and a cell with two branches at one end is shown in Figure 30d (Foam, D1). Both cells have a black spot that almost looks like a hole. The cells were distributed well in the hydrogel as well, and a higher number of cells was observed. Most of the cells were rounded and some few droplet-shaped. The variety of shapes is shown in Figure 30b and 30c (Hydrogel, D1). Many cells had 1-5 branches, giving them a star shape, as the one indicated with the left yellow arrow in Figure 30d (Hydrogel, D1). The middle arrow shows an elongated cell, that seems to be connected to other cells with a thin branch. The right arrow points out a branch on a rounded cell. A check of the foams at D3 (Figure A1, Appendix A), showed that bubbles had disappeared, and the frequency of elongated cells was higher. Cells in the hydrogel were very similar to D1, also shown in Appendix A, Figure A1 (Gel, D3).

The foam samples **At D7**, appeared to have higher number of cells than the D1 samples, as can be seen in Figure 30a and 30b (Foam, D7). There were more large and elongated cells. The 200 µm long cell in the blue square in Figure 30d (Foam, D7) is an example such a large cell. It could also be that this example is a structure of several connected cells. Cells that seemed to line the foam were observed, indicated by three yellow arrows in Figure 30c (Foam, D7). In the hydrogels, more cells had branches and the branches were longer. A typical branched, spherical cell is pointed out in Figure 30b (Hydrogel, D7). Cell connections were observed, as in Figure 30c (Hydrogel, D7), where a cell seems to be connected to the branch of another cell. The size of the typical rounded cell with branch varies, but in Figure 30d (Hydrogel, D7) it looks like it is around 100 µm long in diameter, counting both cell body (30 µm) and branch. More examples of cells lining the foam pore walls were seen at D13, in addition to examples of cell connections, and is shown in Appendix A, Figure A1 (Foam, D13). In the hydrogels at D13, some very long and thin cells were observed, shown in Appendix A, Figure A1 (Gel, D13). The size difference between the long, large cells and small, round cells is quite significant.

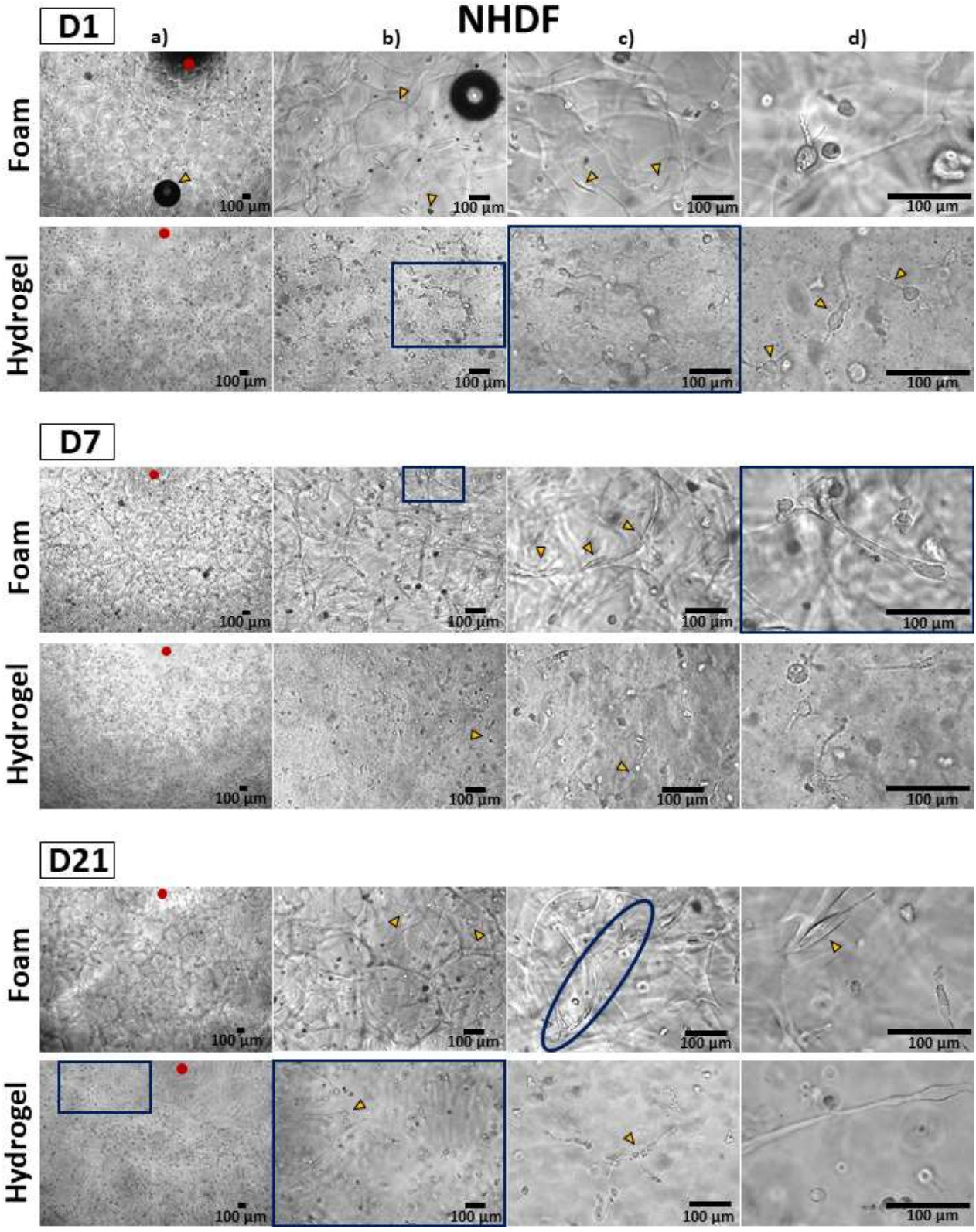

Figure 30: NHDFs cultivated in foams and hydrogels, imaged with light microscopy at D1, D7 and D21. For each timepoint, upper row represents samples of foam, while bottom row represents samples of hydrogel. Columns **a**), **b**), **c**) and **d**) show increasing magnification, respectively with objectives 4x, 10x, 20x and 40x. Scalebars represent 100 µm. Red circles (●) in **a**) indicates center of the scaffolds, as seen from above. Yellow arrows (▽) and the blue oval circle (⬭) point out observations. Small blue squares (▭) correspond to the larger blue squares (▭) with higher magnification.

Many of the cells in the foams were still rounded **at D21**, as pointed out to the right in Figure 30b (Foam, D21), but a relatively high number were elongated, as the cell pointed out to the left in Figure 30b (Foam, D21). However, the difference from D7 was little. Large cells were observed, as shown in Figure 30c (Foam, D21), which looked like a large structure of cells or a large cell, around 400 µm long. The typical NHDF in the foams was rounded or elongated, either droplet shaped or very long. An example of an elongated cell is pointed out in Figure 30d (Foam, D21), which is a large cell around 100 µm long, attaching to a foam wall. At D21 in the hydrogels, very long, thin elongations of cells were observed, often with several 100 µm long elongations. These cells can be seen in Figure 30a, 30b and 30d (Hydrogel, D21). The cell pointed out in Figure 30b (Hydrogel, D21) has a small, round body, with two very long "legs". The cell in Figure 30d (Hydrogel, D21) is too long for the image, and what is shown is more than 300 µm in length. However, there were still many small, rounded cells, as in the foams. Cell connections were observed, like as the clustered cells in Figure 30c (Hydrogel, D21).

3.2.2 IMR-90

For the short-term IMR-90 experiments, the new batches of alginate foams were used. A higher number of these foams folded when solutions were added, and they also had some appearance differences. Foam batch differences were explored (Section 3.6, Appendix F, Figure F1, F2 and F3). Light micrographs of IMR-90 at D1, D7 and D21 are presented in Figure 31, with the same set up as in Figure 30. Additional images from D3 and D12 are included in Appendix A (Figure A2). For D21, the microscope was switched to Nikon Eclipse Ts2. The foam structure of the new batches here differed somewhat to the first batch that was used with NHDF. Some of the pores were less visible, and some areas had less structuring, as shown in the circled area in Figure 31c (Foam, D1). This area also has fewer cells. There were quite many observable cells in the foams **at D1**, as seen in Figure 31a and 31b (Foam, D1). Cells were mostly rounded without elongations or branches. Compared to what was seen with NHDF (Figure 30, Foam, D1), there were fewer elongations. Many cells had grainy debris around them, and the surface of the cells often looked uneven, as the cell in top right in Figure 31c (Foam, D1) and top left in Figure 31d (Foam, D1). Cells with the shape of a ring were observed, as pointed out in two cases in Figure 31b (Foam, D1). There was a large size difference between cells, shown by the cells pointed out in Figure 31d (Foam, D1), where the largest cell is around 40 µm in diameter, while the smaller one is around 10 µm.

In the hydrogels at D1 (Figure 31), cells were also mostly rounded, as the cell pointed out in middle of Figure 31c (Hydrogel, D1). However, compared to the foam there were some more

with droplet shapes or hints of branches. The blue squared example in Figure 31c and 31d (Hydrogel, D1) shows connected cells in a structure of around 100 µm in length. The largest cell in the same image is around 30 µm long. There were many cells in the lower layers of the hydrogel, and these were seen as shadows in the layers above, as seen in the blue circle in Figure 31b (Hydrogel, D1). Some cells were grainy or had grains around them, as shown by the right yellow arrow in Figure 31b (Hydrogel, D1) and to the bottom left in Figure 31c (Hydrogel, D1). Ring-formed cells were seen, pointed out with left arrow in Figure 31b (Hydrogel, D1) and top left arrow in Figure 31c (Hydrogel, D1). In a check of cells in the foam at D3, more grains were observed, but not always around a defined cell. In the hydrogels, silhouettes of the cells at the well bottom were visible in the layers above. Grains alone and around cells were observed. D3 images are shown in Appendix A, Figure A2.

At D7, the cells in foam looked very much the same as at D1. Some of the grainy cells almost looked pulverized, as in left corner of Figure 31c (Foam, D7). Elongations in the foam were still very few and small, as the examples shown by top yellow arrow in Figure 31b (Foam, D7) and the yellow arrow in Figure 31d (Foam, D7). Clustering of cells was observed, as pointed out with yellow arrow to the right in in Figure 31c and 31b (Foam, D7). The blue circle in Figure 31b (Foam, D7) shows cells touching a foam wall. The blue circle in Figure 31d (Foam, D7) shows a cell, or cells, with a lot of grains around. The total length of the grainy cell in the blue circle is around 70 µm, while the cell body itself constitutes less than half of this length. In the hydrogels at D7, there were a lot of cells at the well bottom, seen as stripes in the layers above. Comparing the foam and hydrogel in Figure 31b (D7), the cells look smaller in hydrogel than in foam. The elongations in hydrogel at D7 were longer than at D1/D3, but still few. Examples of elongated cells are shown in left upper corner Figure 31b (Hydrogel, D7) and left bottom corner in Figure 31c (Hydrogel, D7). In Figure 31d (Hydrogel, D7) another example of an elongated cell is shown. It has an oval cell body and thin, long elongation, at least 100 µm long. The cells are grainy, but less than in foams. The cell pointed out to the right in Figure 31c (Hydrogel, D7) is rounded with grains. At D12 (Figure A2, Appendix A), the cells in foam had some more elongations than earlier, and some elongated cells were observed lining the foam walls. In addition, more cell clustering was seen. An observation in the hydrogels at D12 was that much fewer cells were observable, especially high up in the hydrogel. Some areas had more cells, as shown with the blue circles in Figure A2, Appendix A (4x, Gel, D12). Some dark areas (a spot and a curved line) not seen before were observed, and there was an increase in large, long cells.

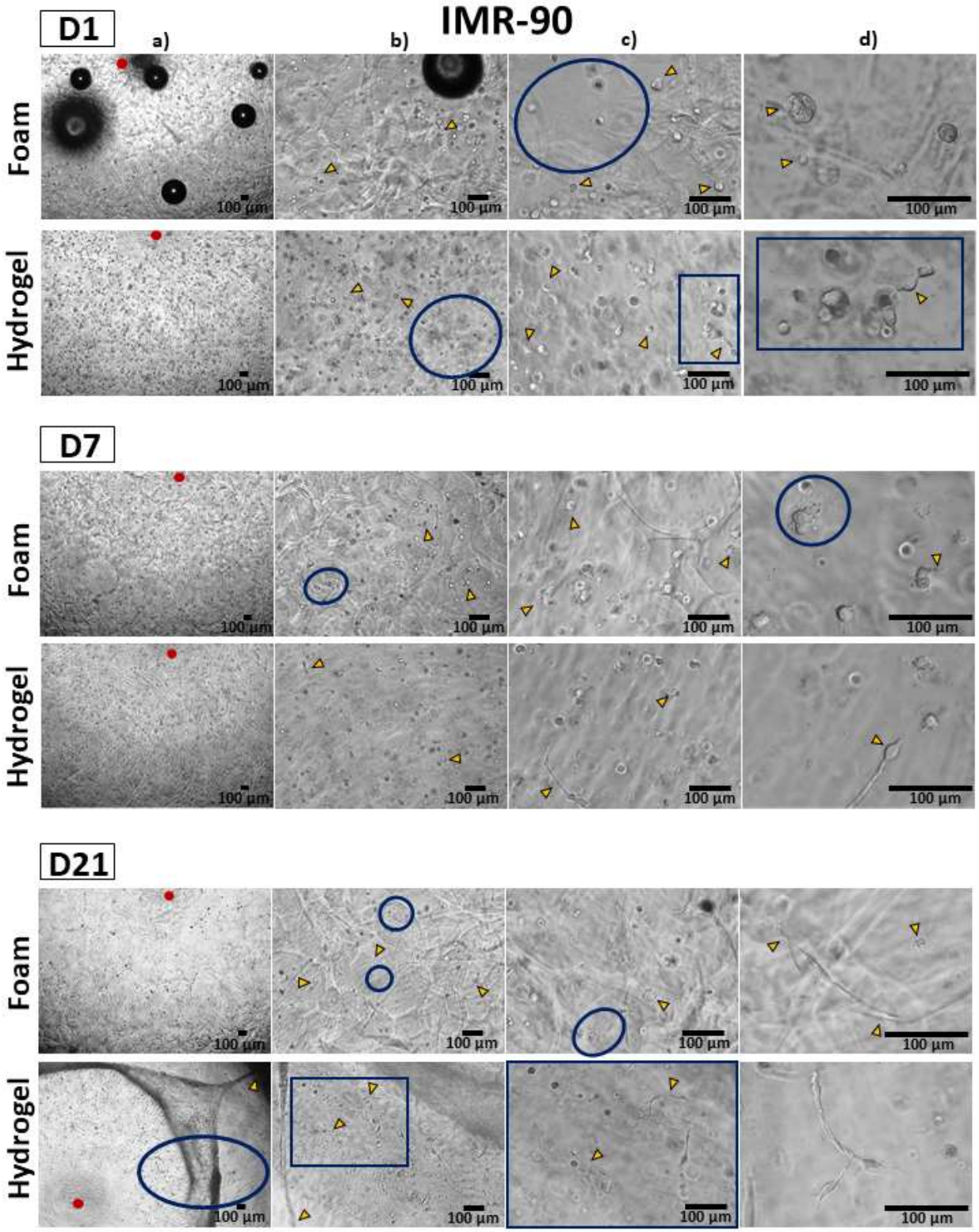

Figure 31: IMR-90s cultivated in foams and hydrogels, imaged with light microscopy at D1, D7 and D21. For each timepoint, upper row represents samples of foam, while bottom row represents samples of hydrogel. Columns **a**), **b**), **c**) and **d**) show increasing magnification, imaged with objectives 4x, 10x, 20x and 40x. Scalebars represents 100 µm. Red circles (●) in **a**) indicates the center of the scaffolds, as seen from above. Yellow arrows (▽) and blue circles (⬭) point out observations. Small blue squares (▭) correspond to the larger blue squares (▭) with higher magnification.

At D21, in the foam there were more elongated cells and more branching, but the typical cell was rounded and with grainy debris. Examples of cells with elongations are pointed out with yellow arrows in Figure 31b (Foam, D21), and the one to the right looks like it is lining a foam wall. Another example of attachment to a wall is shown by the large, elongated cell marked with yellow arrow in Figure 31d (Foam, D21). This image also shows a small, grainy cell is to the right. This small cell, around 7 µm long, is the most commonly seen morphology here. The elongated cell, around 180 µm long, looks smoother and is generally different from the common cell appearance. There were generally less elongations in IMR-90 foams than NHDF foams. Most cells had debris around them, and the blue circles in Figure 31b and 31c (Foam, D21) show large areas with grains. Ring-like cells were observed, as shown with the yellow arrow in Figure 31c (Foam, D21). These ring-formed cells were not observed in NHDF. The ring-formed cells were also observed in the hydrogels.

A new observation, not seen with NHDF or at any earlier timepoint with IMR-90, was made in the hydrogels at D21. Large cell structures had formed in just about every well, observable both with the naked eye and in the microscope (Appendix C, Figure C1 and C2). These structures appeared as large, dense rings of cells, or in some cases just dots or strings, in the well. They appeared to consist of a lot of cells. The structure was often attached to the plastic well walls with thin strings from the structure, like pointed at with yellow arrow in Figure 31a (Hydrogel, D21), and in and in the left bottom corner of Figure 31b (Hydrogel, D21). Scrolling through the scaffold from bottom to top gave the impression that the structure grew from the monolayer of cells at the well bottom, and up as large “walls” of cells. Figure 31a (Hydrogel, D21) shows an example of the dense cell structure, forming a ring-structure in the hydrogel. The blue circled area in Figure 31a (Hydrogel, D21) shows the edge of the hydrogel to the right, cell structure in the middle and the area inside the cell structure, to the left. The area to the left looks like intact hydrogel, is cell rich and shows both rounded cells and elongated cells. The area in the middle is much darker, while the area to the right looks almost empty, only with some few rounded cells. More details of the cell structures are shown in a collage in Appendix C, Figure C1. Elsewhere in the D21 hydrogel wells, single cells looked as they usually had at earlier timepoints. There were many rounded cells, but there had been an increase in elongations, branching and cell-cell connections, as shown in Figure 31a (Hydrogel, D21), where many elongated cells are visible around the middle (●). Other examples are in the blue square in Figure 31b and 31c (Hydrogel, D21). In Figure 31d (Hydrogel, D21) there is a detailed elongated cell or cell connection, around 200 µm long, almost looking like two cells intertwined.

3.2.3 HS-5

The HS-5 samples were imaged with Nikon Eclipse Ts2. Light micrographs from D1, D7 and D21 are presented in Figure 32. Images from D3 and D13 are shown in Appendix A, Figure A3. As with IMR-90, there were a lot of rounded HS-5 cells in the foams, especially at short term. The cells in foams were grainy, but not as much as IMR-90. Some elongated HS-5s could be observed in foams, and some were seemingly attaching to foam walls. In the hydrogels, some few rounded cells had thin elongations protruding, but cells were mostly rounded without branches. On the long term, both scaffolds became more difficult to examine, because of a lot of disturbance/cloudiness. The hydrogels became cloudier with time and cells were hard to distinguish and to study and image in detail. In addition, few cells were observable in the middle and upper layers of the hydrogel. Different from the other cell types, a much quicker yellowing of media was observed in these cells, especially in the last week of the long term plate. Yellowing of media is shown in Appendix D, Figure D1 and D2.

On D1 in the foams, almost all cells were rounded, with some few exceptions of elongated cells. The blue square in Figure 32b, magnified in 32c (Foam, D1) points out a typical rounded cell (left) and an elongated cell close to a foam wall (right). In Figure 32d (Foam, D1) a rounded cell, 23 µm in diameter, and a droplet shaped cell, 64 µm in long, are shown. The hydrogel also had mainly rounded cells, with some few with thin branches. Some examples of cells with branches are pointed out in Figure 32b and 32c (Hydrogel, D1). Cell sizes were varying a lot, exemplified in Figure 32d (Hydrogel, D1), where the largest cell has a diameter of 29 µm, and the thin branch is 21 µm long. At D3, there were some more elongations in the foams, and attachment to foam wall was observed (Appendix A, Figure A3). Small grains around and inside some cells were observed. The hydrogels at D3 had become cloudy but appeared clearer closer to the bottom. Some cells had thin branches, giving them a star shape. Cell connections were observed (Appendix A, Figure A3).

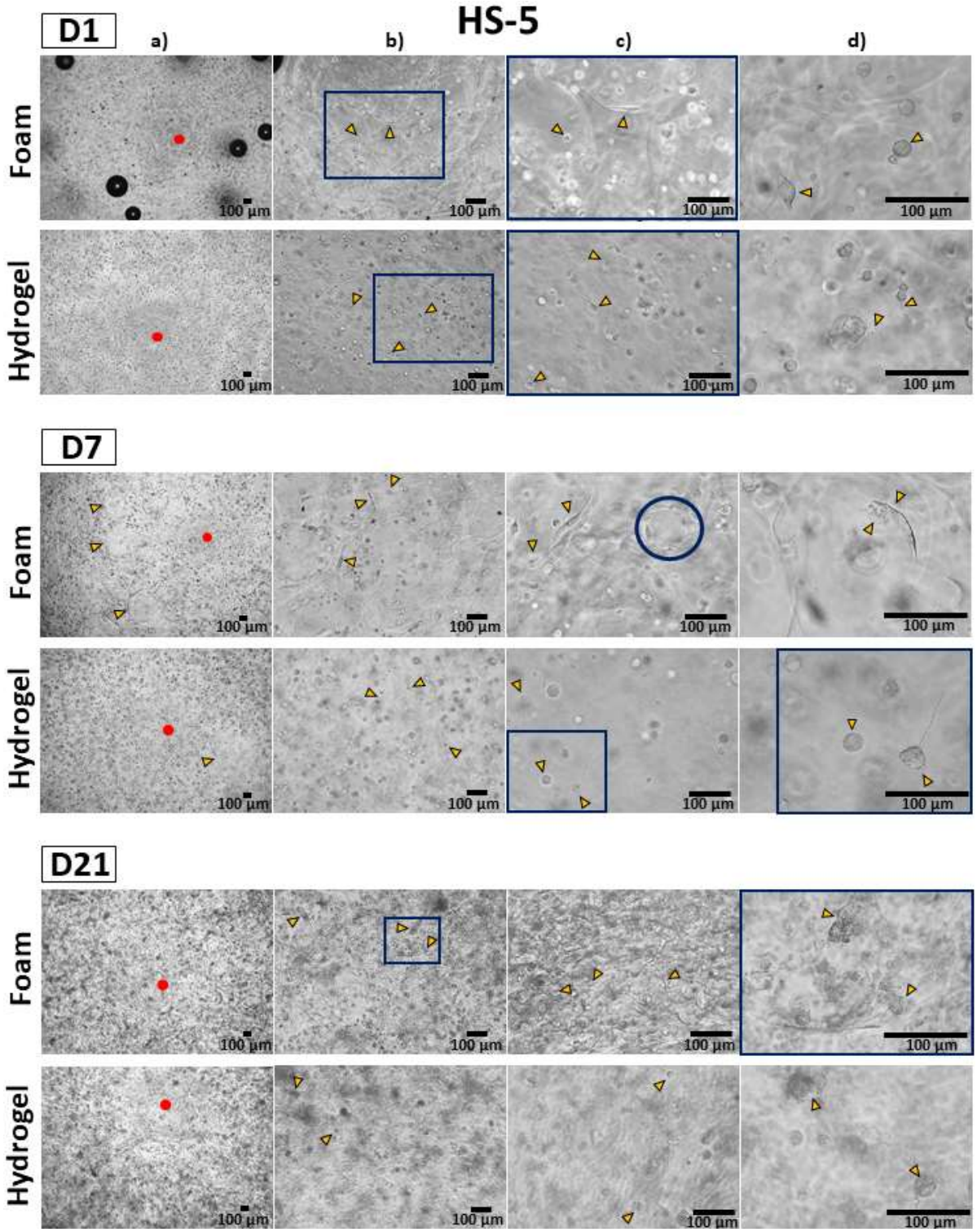

Figure 32: HS-5s cultivated in foams and hydrogels, imaged with light microscopy at D1, D7 and D21. For each timepoint, upper row represents samples of foam, while bottom row represents samples of hydrogel. Columns **a**), **b**), **c**) and **d**) show increasing magnification, imaged with objectives 4x, 10x, 20x and 40x. Scalebars represents 100 µm. Red circles (●) in **a**) indicates the center of the scaffolds, as seen from above. Yellow arrows (▽) and blue circles (⬭) point out commented observations. Small blue squares (▭) correspond to the larger blue squares (▭) with higher magnification.

At D7, there were more large and elongated cells in the foams, but rounded cells were the most typical. Examples of elongated cells and a rounded grainy cell are pointed out in Figure 32b (Foam, D7). The grains could be around or on/in the cell and were also seen with elongated cells. Another example of a grainy cell is shown to the left in Figure 32c (Foam, D7). The other yellow arrow in Figure 32c (Foam, D7) points out a large, elongated cell attached to the foam. In Figure 32d (Foam, D7) there is a grainy elongated cell lining the foam. This cell is around 100 µm from tip to tip, compared to the smaller rounded cell in the left corner which is around 20 µm. In Figure 32c (Foam, D7), encircled with a blue ring, is a circle of elongated cells that was observed. This tendency to form such structures was seen on several occasions in the HS-5. Many cells were observed in small cell clusters. Some areas of the foam had fewer cells, as pointed out by the three yellow arrows in Figure 32a (Foam, D7). The cells in hydrogels at D7 were mostly rounded, some with thin branches as pointed out in Figure 32b (Hydrogel, D7). Some had several branches, giving them a star shape. In Figure 32d (Hydrogel, D7) there are two rounded cells, one with no branching and one with several short branches and one long branch. The branches are thin and tree-branch like. The cell with branches is 30 µm in diameter and its longest branch is more than 70 µm. Some cells were grainy, but less than seen in foam.

There was a lot of cell clustering in the D7 hydrogels. In Figure 32a (Hydrogel, D7) an area with fewer cells is pointed out. Images from D13 (Appendix A, Figure A3) showed that the samples had changed a lot. There seemed to be a lot of cells, but also a lot of disturbance and cloudiness. The foams had a lot of large cell clusters. It almost looked like the cells were completely covering the foam structure. Cell clusters growing in ring shapes were seen, and there were grains around cells. In the hydrogels at D13, it was challenging to see the cells because of the cloudiness. Also here, large cell clusters were seen. **D21** was difficult to image because of cloudiness, in both foams and hydrogels. It looks like there are more cells compared to the other cell types, and neither NHDF nor IMR-90 became cloudy like this. In the foams the foam structure was almost not visible anymore. The cells that could be seen were rounded and small. Some few were elongated, as the one in the left corner of Figure 32b (Foam, D21). The blue square magnified in Figure 32d (Foam, D21), shows rounded cells, cell clustering and a long, elongated cell at the bottom. In Figure 32c (Foam, D21), more cell examples are pointed out, though hard to distinguish from the background: a rounded cell (left), a cluster (middle) and an elongated cell around 200 µm long (right). There is generally a big variation in cell sizes and shapes. The hydrogels were very cloudy, and therefore cells were hard to get in focus and to distinguish from the background. The cells were either rounded, large and bulky, or in

clusters. Figure 32b (Hydrogel, D21) shows an example of a cell cluster in the left corner. The other arrow in Figure 32b (Hydrogel, D21) points at a single rounded cell. Another bulky cell cluster is shown in the bottom of image Figure 32c (Hydrogel, D21), and on top there is a rounded cell. Figure 32d (Hydrogel, D21) shows a cluster (left) and a rounded cell with a small branch (right).

3.3 Viability of cells

The cell viability in foam and hydrogel was qualitatively assessed with a Live/Dead viability assay. This involved co-staining of live and dead cells, respectively with green-fluorescent calcein-AM and red-fluorescent EthD-1, and imaging with CLSM. The results are divided into sections with a comparison of the cell types at each timepoint (Figure 33, 34 and 35). All images are projections of Z-stacks. Additional Live/Dead images of large cell structures observed in the IMR-90 cells at D21 are presented in Appendix C, Figure C3. Generally, there were some green (live) cells in all cell types at all timepoints. In the long-term samples, the fluorescence signal tended to be lower, and both red and green cells looked smaller and fewer. NHDF seems to be the cell type with generally fewest red (dead) cells, while IMR-90 seems to be the one with the most red (dead). For NHDF and IMR-90, it seems that there are more cells in the hydrogel than in the foam, while the HS-5 samples for some reason had quite many cells in the foam as well, compared to the other cell types.

3.3.1 Day 1

At D1 (Figure 33), there were a lot of green cells in both foams and hydrogels with NHDF, IMR-90 and HS-5, and all have some red also. NHDF is the cell type with the least red cells, both in foam and hydrogel. Almost all the cells are green, and the red can even be counted with the naked eye. Around 7 red dots can be counted in the foam, while in the hydrogel around 60 can be counted, giving 8.5x more red cells in the hydrogel than in foam. There were 6.5x more cells in the total hydrogel than in the foam, for comparison. Compared to NHDF, The IMR-90 has more red cells in both the foams and the hydrogels. The green color is a little yellow, indicating some co-staining. Comparing the foam and the hydrogel by the bare eye, it looks as if both have around 50/50 red and green cells. The HS-5 sample seems to have much more cells in the foam than the two other cell types. The foams and hydrogels (HS-5) look quite similar regarding the distribution between red and green cells. There is some co-staining in the foam. Comparing in the hydrogel of IMR-90 and HS-5, these look similar, with around a 50/50 red-green ratio. To sum up, both IMR-90 and HS-5 seem to have around 50% red (dead) cells. They appear different in foam, in the way that HS-5 seems to have more cells.

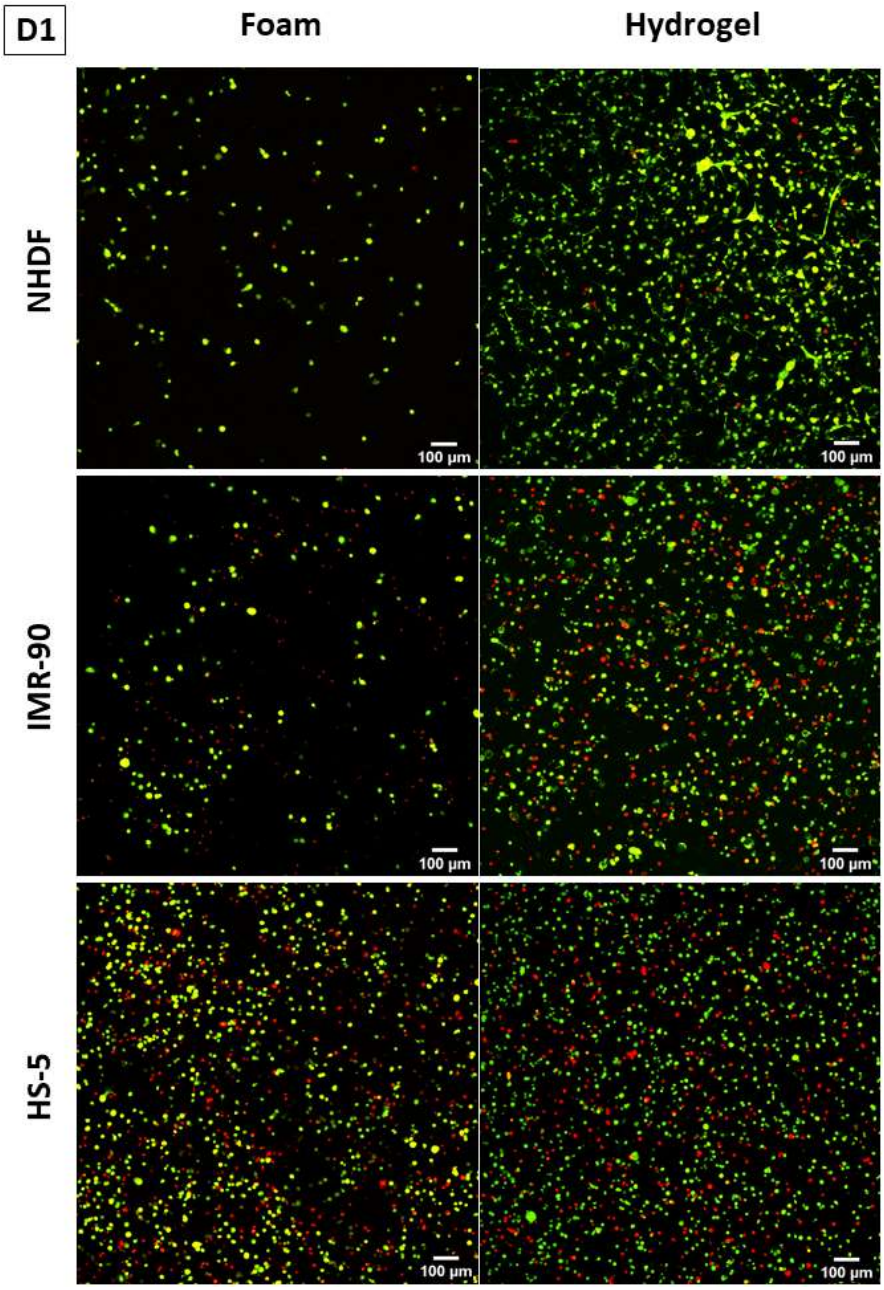

Figure 33: Live/Dead Viability assay of NHDF, IMR-90 and HS-5 in foam and hydrogel after one day of cultivation. Cells were stained with red-fluorescent EthD-1 and green-fluorescent calcein-AM, and visualized using CLSM. Red cells have loss of plasma membrane integrity, indicating dead cells, while green cells show presence of intracellular esterase activity, indicating living cells. Scalebar is 100 µm.

3.3.2 Day 7

At D7 (Figure 34), there were noticeable changes. NHDF looked very much the same, but there were more red cells in IMR-90 than at D1, and the HS-5 had an increase in green, large cells, especially in the foam. The NHDF foam had very few red cells, counted with the bare eye around 8. The NHDF hydrogel also had few red cells, counted around 53. This gives a 6.6x difference between foam and hydrogel, which is a lower difference than at D1 (8.5x). The number however was very similar to the total seeded cell number difference (6.5x). IMR-90

had an increase in the percentage of red cells from D1 to D7 in both foam and hydrogel. The foam sample at D7 seems to have more cells generally (both red and green) than at D1, and there seems to be more red cells than green cells. The number of red cells look similar in hydrogel and foam, but there seems to be slightly more green cells in hydrogel. Comparing the D7 hydrogel with the D1 hydrogel there is a clear increase in red cells, however. From bare eye assessment of the IMR-90 D7 images, the foam appears to have more red cells than the hydrogel does.

The first thing to notice with HS-5 at D7 is the very bright green fluorescence in foam. Compared to D1, the green cells appear more numerous, larger, and brighter, and the number of red cells looks lower than at D1. The red-green ratio in hydrogel and foam looks almost the same, but the green cells may be slightly fewer in hydrogel. Comparing the D7 hydrogel to the D1 hydrogel, the ratio appears very similar between red and green cells, around 50/50. Between foam and hydrogel, the ratio between red and green cells looks not so different, but the hydrogel appears to have somewhat more red cells.

The three cell types look more different from each other after seven days than after one day. The NHDF has again the most green cells in both foam and hydrogel, while IMR-90 in foam seems to be the one with the highest percentage of red cells. HS-5 has red cells in foam, but a lot of green cells as well. IMR-90 seems to be the cell type with the most red cells in both foam and hydrogel, but HS-5 also has quite a lot of red cells - closer to 50/50 between red and green.

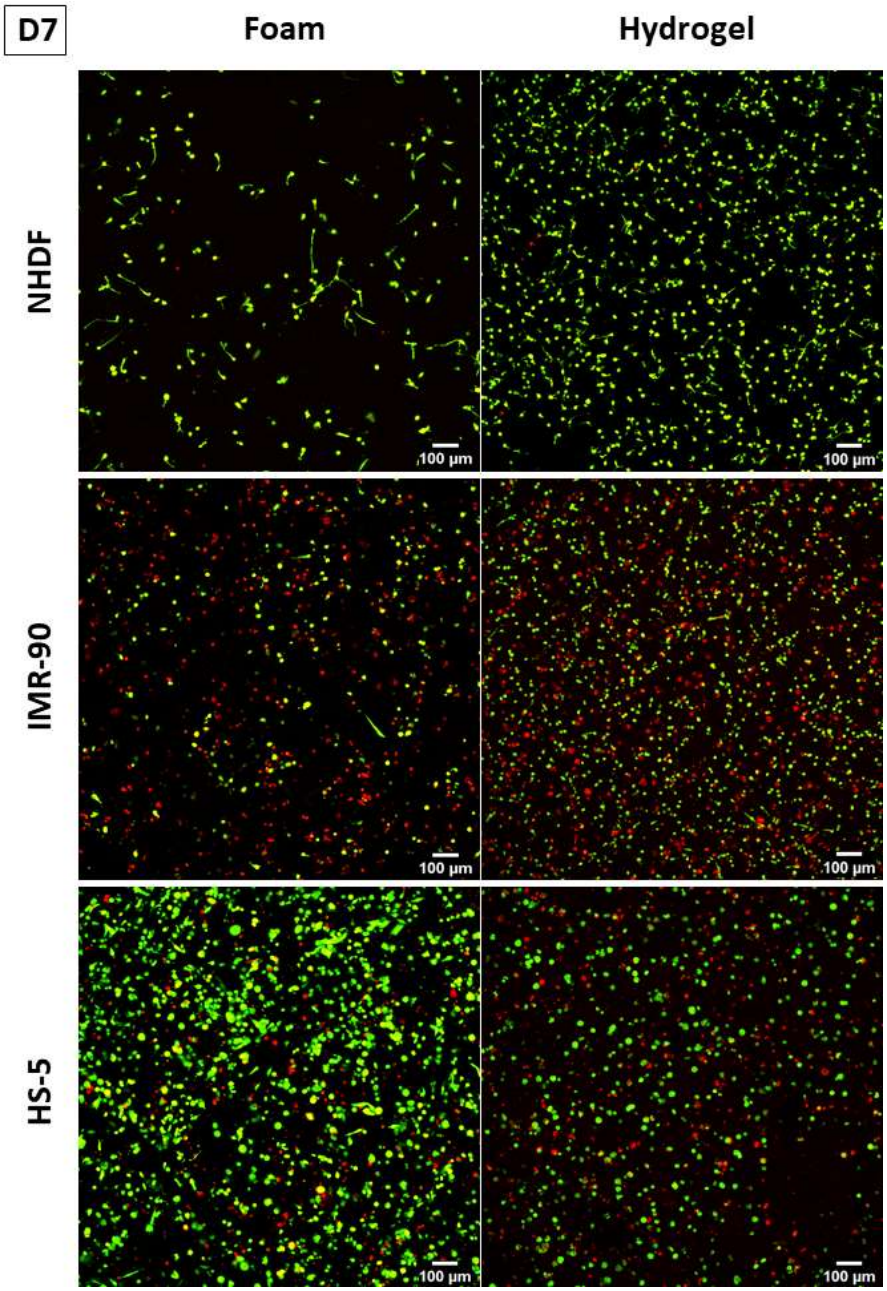

Figure 34: Live/Dead Viability assay of NHDF, IMR-90 and HS-5 in foam and hydrogel after one week of cultivation. Cells were stained with red-fluorescent EthD-1 and green-fluorescent calcein-AM, and visualized using CLSM. Red cells have loss of plasma membrane integrity, indicating dead cells, while green cells show presence of intracellular esterase activity, indicating living cells. Scalebar is 100 µm.

3.3.3 Day 21

At D21 (Figure 35), the overview of the images gives the impression that there are fewer cells and less bright signaling, generally. NHDF still appear very similar - with green cells dominating. The IMR-90 does not have the same overweight of red cells as seen in the D7 sample. Regarding HS-5, cell distribution and cell shapes look different, and the ratio between red and green appears to lean more to dominance of green cells, especially in the hydrogel.

NHDF still after 21 days looked quite similar to D7 and D1. Counted with the bare eye, NHDF foam image at D21 has only about 10 red cells. The hydrogel also had few red cells, counted around 32, which is 3.2x more than in the foam. This number was 8.5x at D1 and 6.6x at D7, compared to the total cell number difference when seeding which was 6.5x. There seems to have been a shift from the hydrogel having more red, to the foam having more red.

IMR-90 in foam has very few cells in general, the majority being red. Compared to the samples representing D1 and D7, which themselves look very different from each other, cells look fewer and smaller at D21. Comparing foam and hydrogel IMR-90s at D21, the ratio between red and green looks quite similar – different from at D7. The foam has more co-staining than hydrogel. The foam seems to be the one with most red cells, although this is hard to say. Almost all IMR-90 samples had some large and dense cell structures with a lot of cells at D21. Live/Dead images of areas with those structures can be found in Appendix C (Figure C3) - the cells in Figure 35 are those that were elsewhere in the IMR-90 hydrogel.

The HS-5 foams had a lot of large, green cells and many small, red cells. The shape of the green cells in the foam indicate that they have grown in a microstructured material, demonstrated by the circular shapes. From first sight, it looks as if the green cells dominate in both foam and hydrogel. The hydrogel at D21 is not so different from D7, but there are more clustering of green cells and fewer red cells are visible. Comparing HS-5 in foam and hydrogel at D21, it seems as if the foam has relatively more red cells than the hydrogel. However, there are generally more cells (or larger cells) in the foam than hydrogel. The green-red ratio looks almost the same in the two scaffolds, but there may be some more red in foam if not thinking about the very bright, large green cells.

Among all cell types at D21, NHDF again had the lowest numbers of red cells in both scaffolds. The highest number of red cells is again seen in IMR-90, and next after that in the HS-5 foam.

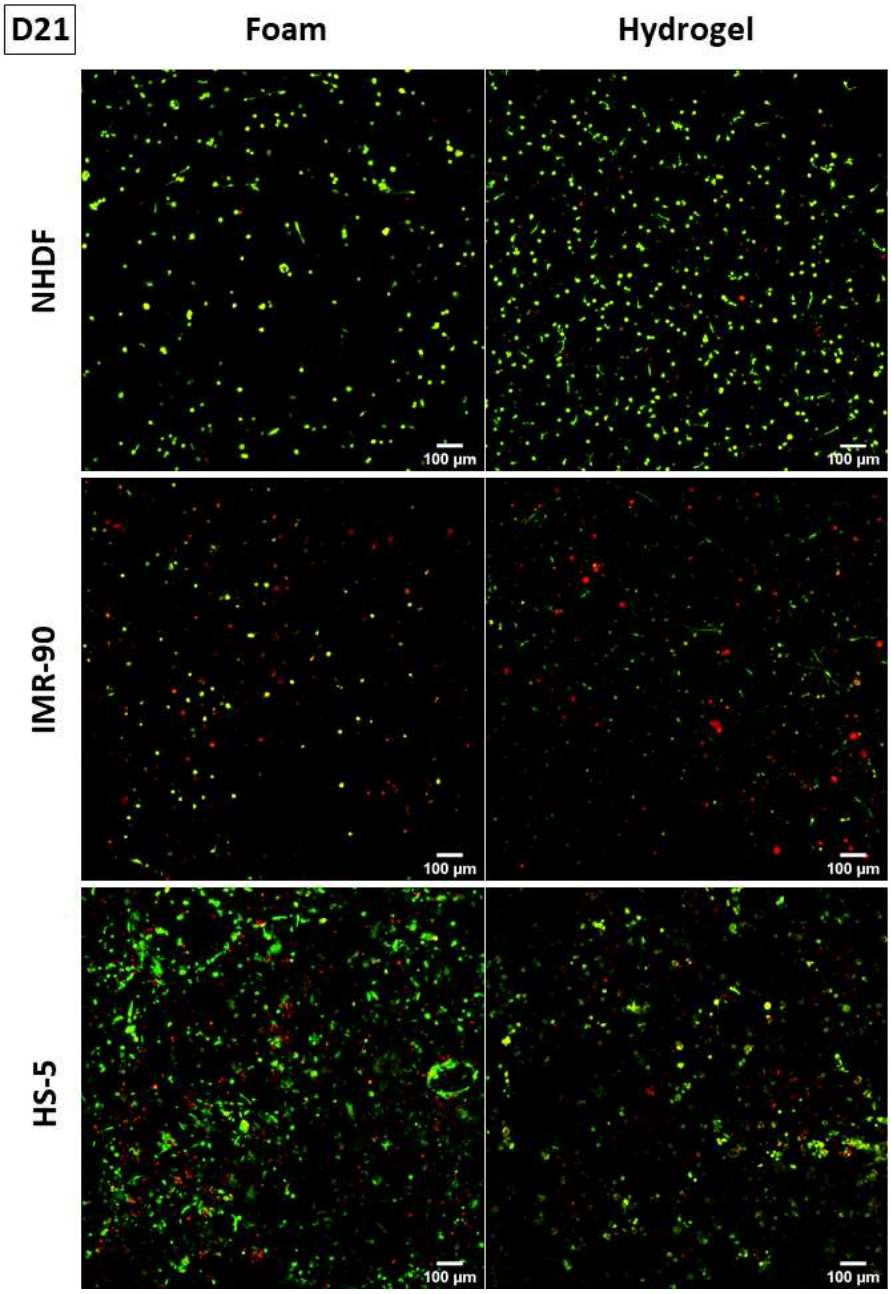

Figure 35: Live/Dead Viability assay of NHDF, IMR-90 and HS-5 in foam and hydrogel at 21 days of cultivation. Cells were stained with red-fluorescent ethidiumhomodimer-1 and green-fluorescent calcein-AM, and visualized using CLSM. Red cells have loss of plasma membrane integrity, indicating dead cells, while green cells show presence of intracellular esterase activity, indicating living cells. Scalebar is 100 µm.

To give an overall summary of the viability of NHDF, IMR-90 and HS-5, NHDF had the least red cells at all timepoints in both scaffolds, and from the counting of red cells, there was a change from hydrogels having more red cells at D1 to foams having more red cells at D21. IMR-90 was probably the cell type with the most red cells compared to number of green cells, and more were dead at D7 than D1. At D21, there were generally few IMR-90 cells. IMR-90 had large cell structures at D21, and the viability of the cells in these will be commented further

in the next paragraph. HS-5 had around 50/50 red and green cells most of the time, but actually appeared to have fever red cells over time. If this is due to cells or signaling, and where the red cells go will be discussed later. HS-5 looked very different from earlier timepoints and from other cells at D21, by having shapes of structuring in foams, and in hydrogels a lot of clustering.

Regarding the IMR-90 cell structures, four images are presented in Appendix C, Figure C3 of an example of this. The bottom of the cell structure had a lot of red cells compared to elsewhere in that same slice. Most of the cells in the structure was red, but on the outer sides of the structure as well as a thin layer underneath, there are some green cells. The cells assumingly in hydrogel around the cell structures showed a distribution between red and green cells similar to the image for IMR-90 hydrogel in Figure 35.

3.4 Cytotoxicity of scaffolds

Supplementing the Live/Dead imaging, a quantitative cytotoxicity assay was run. The cytotoxicity was measured in terms of relative amounts of lactate dehydrogenase (LDH) in collected media from the culturing wells. Media was collected on D1 and D7 and treated with the Cytotoxicity Kit before absorbance was measured. Averages of optical density (OD) raw data is found in Appendix E (Table E1). Results for D1 and D7 are presented as relative percentage cytotoxicity in Figure 36. Green bars represent NHDF, orange represents IMR-90 and yellow represents HS-5. Standard deviations are shown for each value with a line on each bar.

Almost all the percentages were negative values, with exceptions of **IMR-90** on D7, in both foam and hydrogel, which respectively were 0.1% and 7.3%. These are the cases where the relative LDH-production was highest among all the cases, and it was highest in the hydrogel. Looking at IMR-90 at D1 however, the percentage is highest for the foam. The cytotoxicity percentage in the hydrogel (-81.1%) is the lowest measured cytotoxicity among all samples, while in the foam it is in the middle (-14.5%) between the two other cell types. The D1 in hydrogel for NHDF was -6.01%, and -24.3% for HS-5. The cytotoxic percentage of IMR-90 in hydrogel at D1 (-81.1%), is a clear outlier among the rest of the values.

At D1, **NHDF** had less relative LDH in hydrogel (-9.02%) than in foam (-6.01%), and it was the cell type with the highest percentage cytotoxicity in both scaffolds. At D7, the values for NHDF in foam and hydrogel were respectively -1.7% and -1.1%, meaning that both had increased in amount of LDH. The values had decreased in difference, and now the hydrogel was slightly higher than foam instead of lower. Compared to IMR-90 and HS-5, it was in the

middle of these in percentage value, with IMR-90 over and HS-5 under in both foam and hydrogel. **HS-5** was the cell type with the most stable values in this test, when comparing the very equal D1 and D7. At D1, the hydrogel was higher than the foam in percentage cytotoxicity, respectively -17.4% and -24.3%. This is different from the two other cell types which both had higher values of LDH in the foam than hydrogel on D1. The D1 HS-5 foam value (-24.3%) is also the lowest among the other cell types at D1. At D7, the case was the same with higher cytotoxic percentage in the hydrogel (-19.7%) than in the foam (-23.4%). For HS-5, the foam value was slightly higher at D7, -24.3% compared to -23.4%, while the hydrogel value slightly lower, -17.4% compared to -19.7%. Something very noticeable about HS-5 is the very large standard deviation of the foam value at D1, which is a bigger deviation than the other values had, which all are based on average absorbance values. Generally, it seems that the standard deviations were larger for the measurements from D1 than from D7. IMR-90 in hydrogel at D7 on the other side has a standard deviation equal to 0.

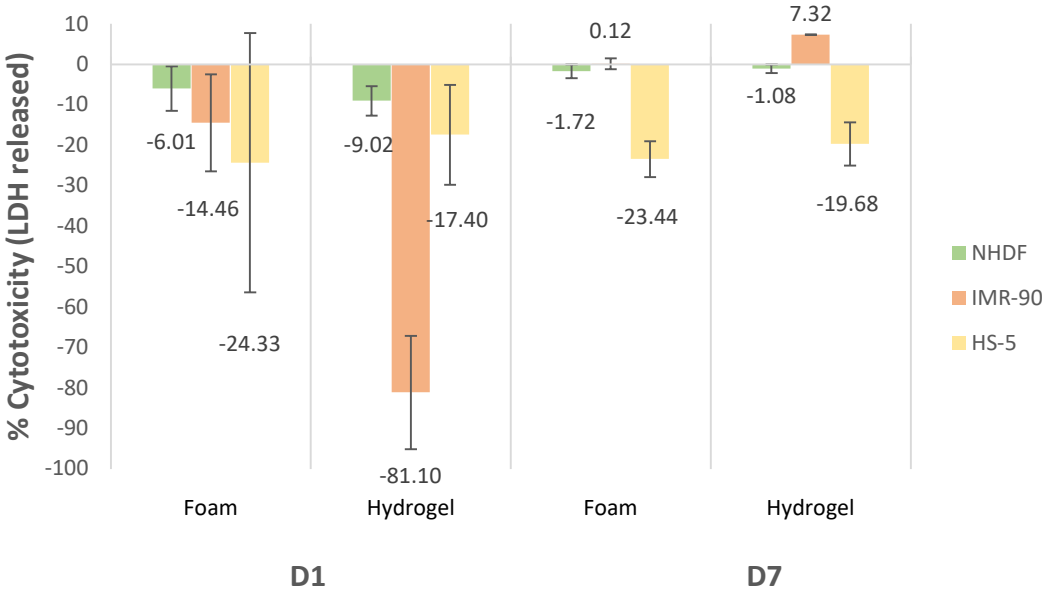

Figure 36: Percentage cytotoxicity in foams and hydrogels for NHDF, IMR-90 and HS-5, based on LDH release. LDH content was measured after one day (D1) and after one week (D7) with a colorimetric assay, using the Cytotoxicity Detection Kit^{PLUS} (LDH) from Roche. Absorbances of experimental samples and control samples were read with a plate reader (490 nm) and used for calculation of percentage cytotoxicity for each cell type.

To sum up, comparing foam and hydrogel, the samples which had highest cytotoxic percentage in foams were NHDF and IMR-90 at D1, while the rest were highest in hydrogel. The samples highest for the cell types on D1 were NHDF foam and IMR-90 foam and HS-5 hydrogel, while the samples highest on D7 were NHDF hydrogel, IMR-90 hydrogel and HS-5 hydrogel. The

highest percentage in foam at D1 was NHDF, while the lowest was HS-5. The highest in hydrogel at D1 was also NHDF, while the lowest was IMR-90. Over to D7, the highest in foam was IMR-90, and the lowest was HS-5, while in hydrogel the highest and lowest were respectively IMR-90 and HS-5. HS-5 was the lowest value in three out of four cases, whereof the last case, the lowest value was the outlier value of IMR-90 in hydrogel D1 (-81.1%). IMR-90 went from being middle and lowest in foam and hydrogel at D1, to at D7 being highest in both. NHDF were the highest in both scaffolds at D1, but in middle at D7, because of the increasing IMR-90 cytotoxic percentage. Looking only at D1 separately, there is no immediate pattern in difference between released LDH in the two different scaffolds. NHDF and IMR-90 is highest in foam, while HS-5 is highest in hydrogel. Looking at D7 separately doesn't either show any immediate pattern in difference between foam and hydrogel visible to the bare eye here either. Here, NHDF and IMR-90 is highest in hydrogel, so this has turned around from D1. HS-5 is higher in hydrogel than in foam, both at D1 and D7.

Unpaired Welch's t-tests were run to assess the significance of the differences between LDH release in foams and hydrogels and D1 and D7 for each cell type (Table 10). In the t-tests, all comparisons passed the Normality test (Shapiro-Wilk). All comparisons passed the Equal variance test (Brown-Forsythe), except Foam IMR-90 and Hydrogel NHDF. The significance of the difference between experimental values and negative control values was also calculated (Table 11).

Table 10: Unpaired Welch's t-tests were run to find the significance for difference between scaffolds and over time for each cell type. Two-tailed P-values are presented. P values lower than 0.05 are considered significant (green font). Performed with SigmaPlot 14.0.

Hydrogel and foam			**D1 and D7**		
D1	NHDF	P = 0.391	**Foam**	NHDF	P = 0.192
	IMR-90	P = <0.001		IMR-90	P = 0.071
	HS-5	P = 0.690		HS-5	P = 0.959
D7	NHDF	P = 0.133	**Hydrogel**	NHDF	P = 0.012
	IMR-90	P = 0.043		IMR-90	P = <0.001
	HS-5	P = 0.313		HS-5	P = 0.536

Table 11: Two-tailed P-values from unpaired Welch's t-tests comparing experimental values to the negative control values. P values lower than 0.05 are considered significant (green font). Performed in SigmaPlot 14.0.

Cell type			
NHDF	D1	Foam	P = 0.101
		Hydrogel	P = <0.001
	D7	Foam	P = <0.001
		Hydrogel	P = 0.267
IMR-90	D1	Foam	P = 0.097
		Hydrogel	P = <0.001
	D7	Foam	P = 0.926
		Hydrogel	P = 0.042
HS-5	D1	Foam	P = 0.247
		Hydrogel	P = 0.016
	D7	Foam	P = 0.097
		Hydrogel	P = 0.015

3.5 Morphology of cells

Cell morphology was qualitatively studied using a DAPI/Phalloidin co-staining assay. This assay involved fixing and permeabilization of the cells at D1, D7 and D21, followed by staining of cell nuclei and actin filament with blue-fluorescent DAPI and red-fluorescent Phalloidin 568. The cells were imaged with CLSM and the resulting images are presented here by cell type, respectively NHDF (Figure 37, 38 and 39), IMR-90 (Figure 40, 41 and 42) and HS-5 (Figure 43, 44 and 45). For each cell type and timepoint, one image with magnification 7.5x (objective 10x and zoom factor 0.75) and one with 30x (objective 10x, zoom factor 3.0) from both the edge and middle of the scaffold are presented. The presented images are those considered best regarding representativeness and image quality. In some cases, images were not taken in both 30x and 7.5x, or in both edge and middle. In these cases, an empty black square is placed in the figures. All images presented are maximum projections made from the Z-stacks. Additional images with bright field channel merge are included in Appendix B.

3.5.1 NHDF

At D1 (Figure 37), the NHDFs in the foam were mostly rounded. Some few cells were droplet shaped or more elongated. In the 30x image of the edge, there is an example of an elongated cell among rounded cells. In the 7.5x images of both middle and the edge, there are both

rounded and elongated cells. Some cells seem to be mostly blue with little actin filament. The cells look similar on the edge and in the middle. Some cells appear to be in clusters or to have several nuclei, as shown in the 30x foam middle. All images have grains of red. There is a difference in cell sizes, and some cells are relatively large. The diameter of a rounded cell in the foam middle is 28 µm, while the length of the elongated cell on the edge image is 176 µm.

It looks like the hydrogel images had more cells than in foam, which makes sense, as the foams were seeded 7700/well and hydrogels 50 000/well. The cells in the hydrogel look different from the foams in the way that they seem to have more elongations, in the form of long branches on rounded cells, giving them a star shape. The hydrogel also seemed to have more cell-cell connections. The 30x images in both middle and edge show many cells with elongations and some cells with little actin filament. The main difference between the foam and hydrogel seems to be that the foams have more large, elongated cells, while the hydrogel has rounded cells with long, thin branches. Both cell types have a lot of rounded cells, with red actin filament circled around the nucleus. However, the rounded cells in hydrogel often have branches. The cells look smaller in the hydrogel than in the foam.

At D7 (Figure 38), the NHDFs look smaller and with lower red fluorescence. Compared to D1, the cells in foam have changed more than in hydrogel. The foam had increased in large, elongated cells. Sometimes these long cells were attached together, almost forming rings, like in the middle of the 7.5x image of the foam-middle (magnified in the 30x image under). Else, there were still many small and rounded cells. The cells in the hydrogel were similar to D1. They were mostly rounded with several thin branches. Regarding the number of cells being lower (7700/well) in the foams, there seems to be more incidents of elongations in foam than in the hydrogel. The actin filament in foam looks more even, while more scattered in the hydrogel. Sometimes, the shape of elongated cells in foam would correlate with the foam structure when merging the fluorescence channels with the bright field channels. An example is shown in Appendix B (Figure B1a), showing a cell lining the wall of the foam. Also in Appendix B, in Figure B1b, there is a 7.5x zoom example of how the cells were distributed in the foam.

After 21 days in the scaffolds (Figure 39), the NHDFs in both foam and hydrogel had changed. In the foam, there was a lot of variation in morphologies, as shown in the 30x foam middle. Some were rounded, in clusters, long or droplet shaped. Some cells were connected by actin filament. Some cells were very large, as shown in the bottom of the 7.5x foam edge image.

This cell structure looks like it is composed of multiple cells. It has at least more than 10 blue nuclei and is around 500µm long. In the foam-middle, it looks as if there are fewer cells and elongations than at D7. The 7.5x edge images show a higher number of elongated cells.

In the hydrogels, there were more and longer elongations than earlier. Some cells were very long and thin, and these were often observed far up in the gel. Examples of these cells are shown in the 7.5x and 30x hydrogel middle. They have rounded main bodies with nuclei and long, thin branches of actin filament. The cell in 30x is at least 400µm long, with a middle cell body (30 µm) and a middle branch (175 µm long) connecting two cells. However, small, rounded cells were still very common. There were often fewer cells in the middle of the scaffold, as can be seen in the 7.5x image of the hydrogel middle. Comparing the two bottommost 30x edge images of foam and hydrogel, the cell morphologies are quite different from each other.

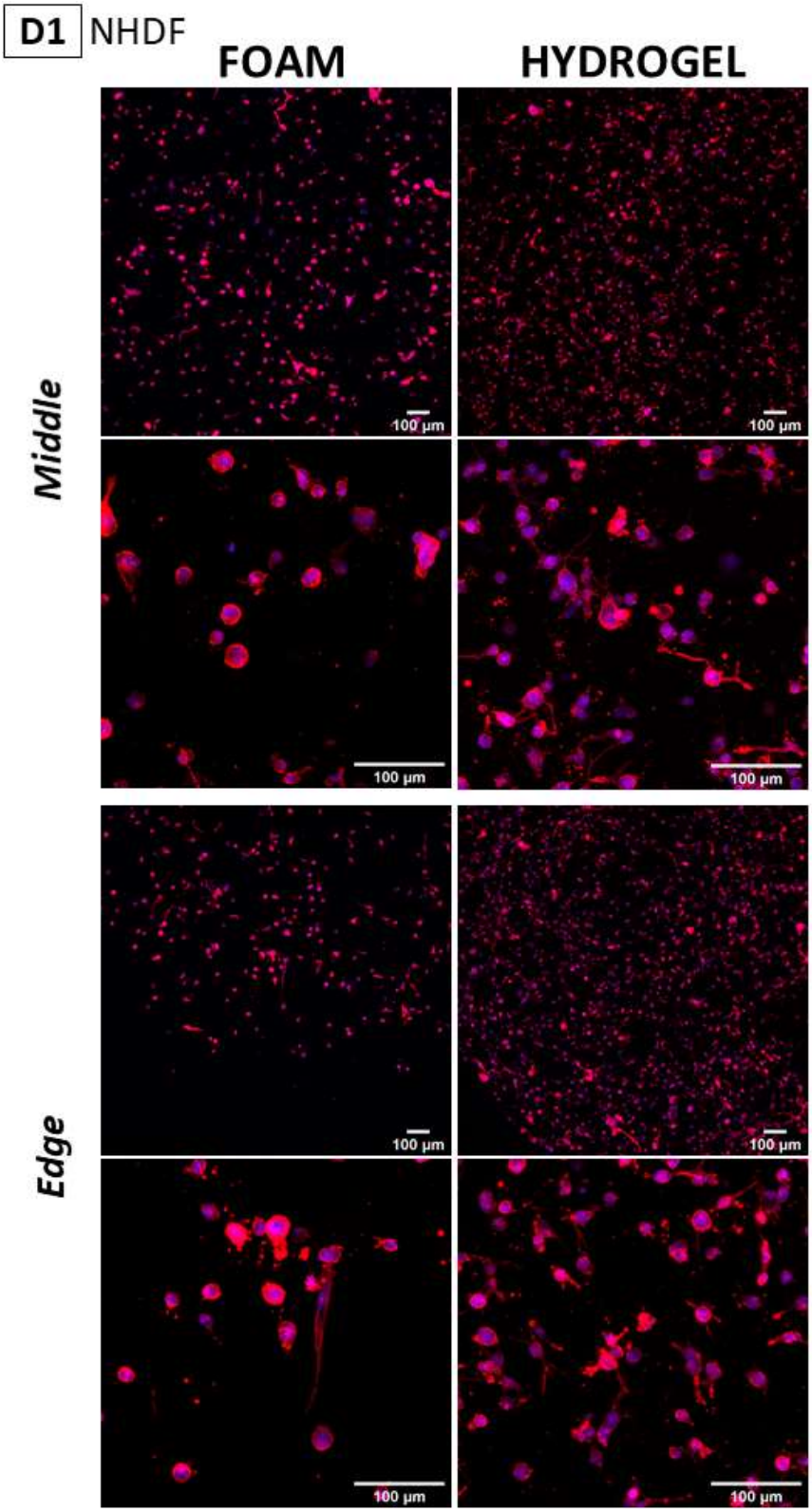

Figure 37: Primary cells of Normal human dermal fibroblasts cultivated in alginate foam and alginate hydrogel. The cells were fixed after 1 day in the scaffolds, then stained with DAPI (blue) and Phalloidin 568 (red), imaged with CLSM and are presented as projections of Z-stacks. Left column shows cells in foam, and the right one shows cells in hydrogel. The four upper images show a spot in the middle of the scaffolds, the four bottom images show cells at the edge. Each location in scaffold is represented by magnification 7.5x and 30x. Scalebars are 100µm.

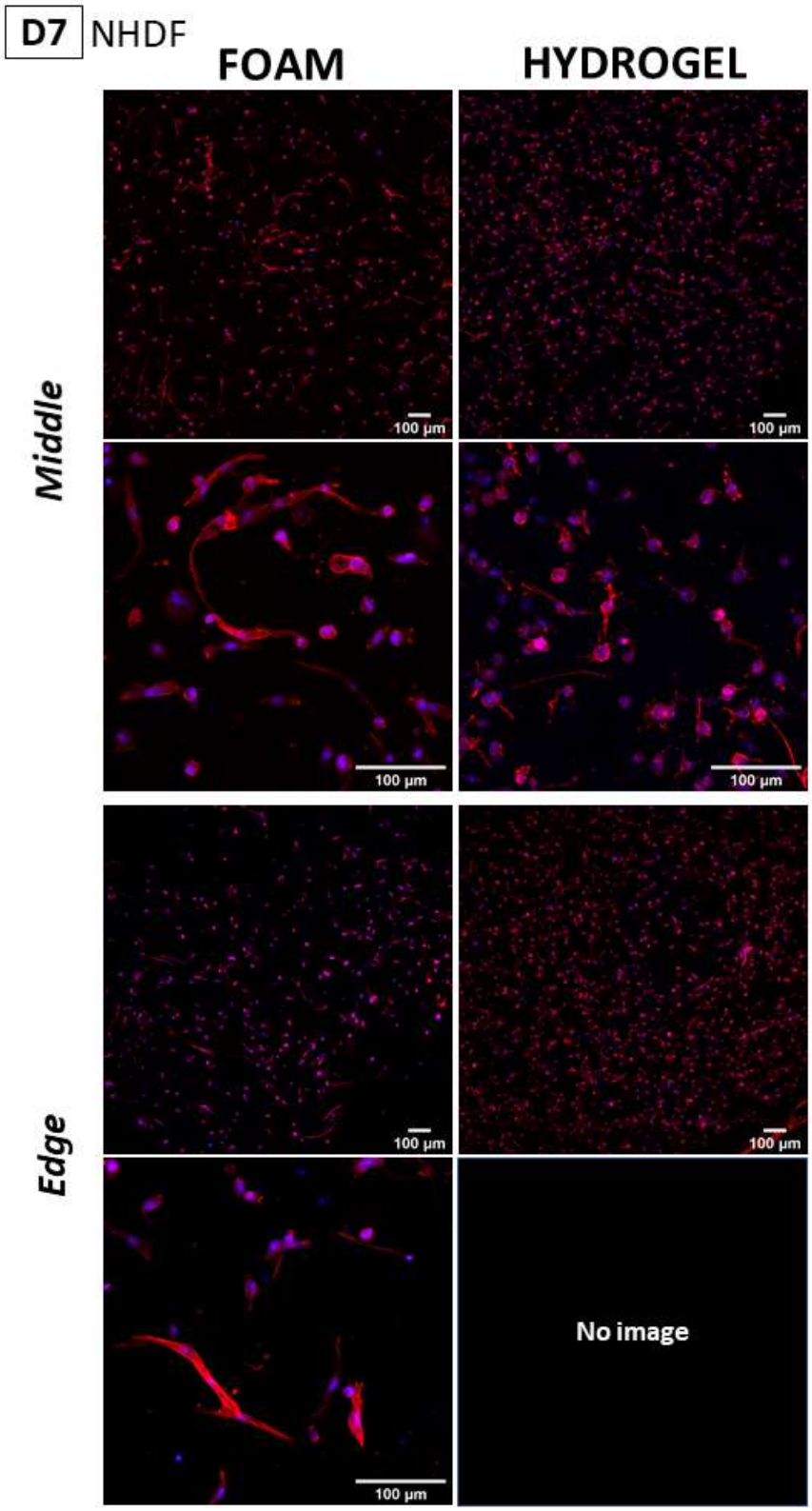

Figure 38: Primary cells of NHDFs cultivated in alginate foam and alginate hydrogel. The cells were fixed after 7 days, stained with DAPI (blue) and Phalloidin 568 (red) and imaged with CLSM, and presented as projections of Z-stacks. Left column shows cells in foam, and the right one shows cells in hydrogel. The four upper images show a spot in the middle of the scaffolds, the four bottom images show cells at the edge. Each location in scaffold is represented by magnification 7.5x and 30x. Scalebars are 100µm. 30x magnification of the edge of hydrogel was not imaged, and image is therefore lacking.

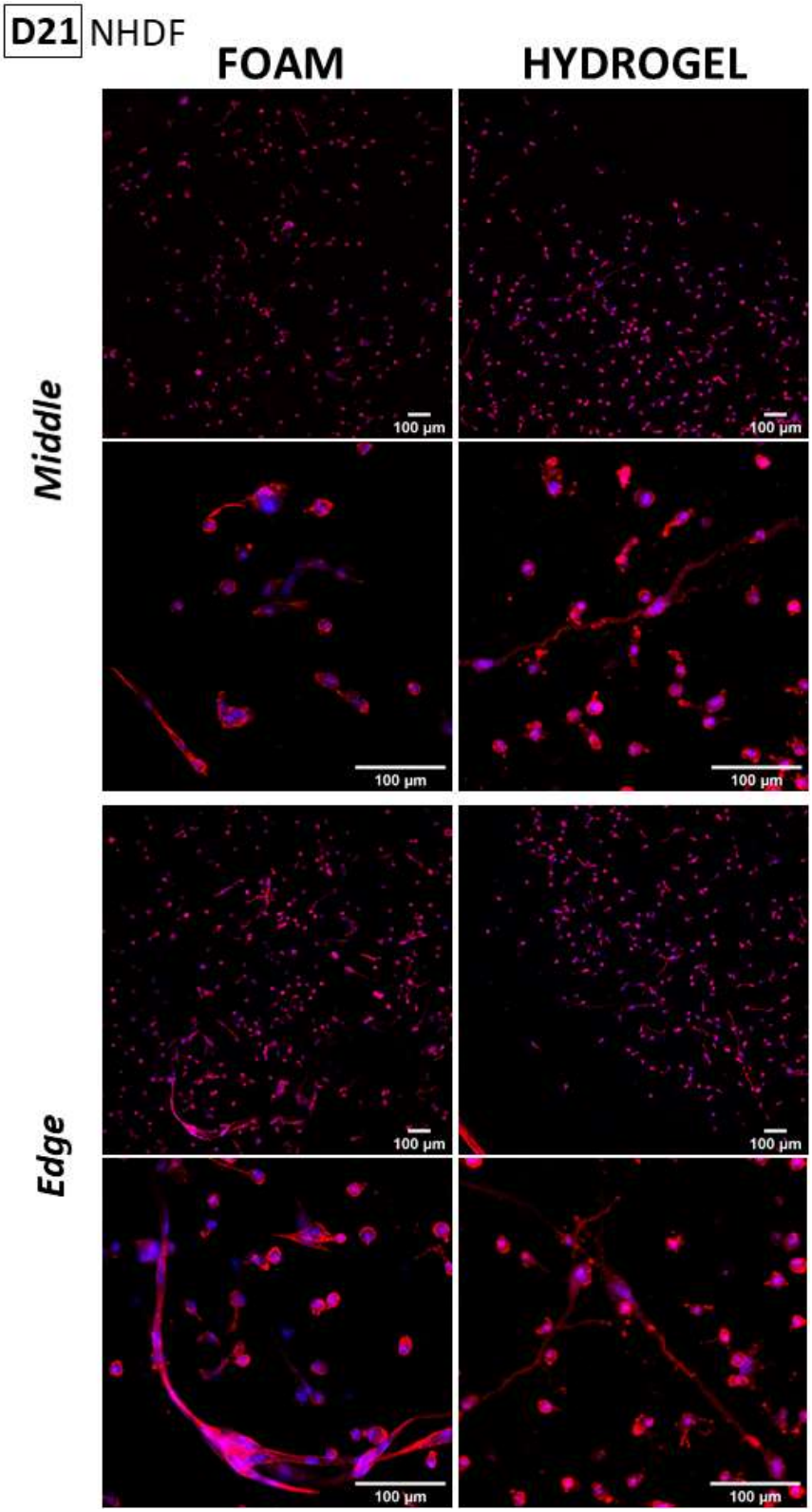

Figure 39: Primary NHDFs cultivated in alginate foam and alginate hydrogel. The cells were fixed at day 21, stained with DAPI (blue) and Phalloidin 568 (red) and imaged with CLSM, and are presented as projections of Z-stacks. Left column shows cells in foam, and the right one shows cells in hydrogel. The four upper images show a spot in the middle of the scaffolds, the four bottom images show cells at the edge. Each location in scaffold is represented by magnification 7.5x and 30x. Scalebars are 100µm.

3.5.2 IMR-90

Generally, IMR-90 (Figures 40, 41 and 42) had less elongations than NHDF, especially in foams. Not observed in any other cell types were the large cell structures that formed in the IMR-90 scaffolds at D21. These will be commented here and further presented with images in Appendix C, in foam (Figure C4) and in hydrogel (Figure C5).

At D1 (Figure 40), the IMR-90 were almost exclusively rounded in both foam and hydrogel, with little or no elongations. Some cells were oblong or in clusters, as seen in the 30x and 7.5x foam edge. The cells in the foams varied in cell sizes, from very small to larger cells. Some cells were only blue dots without actin filament, seen in both the 7.5x and 30x image. The cells in the hydrogel were also rounded, but not as spherical as in foam. There was also a generally a weaker red signal in hydrogels than in foams. However, almost all cells had some actin filament around them, compared to the foam which had many cells appearing as blue dots. Generally, the cells looked smaller in hydrogel. Looking closely at the 7.5x hydrogel middle, there are some few hints of elongations. Grains of actin filament not attached to the cell can be observed in the 30x image and this was less common in foams. As with NHDF, the red actin filament looks more even in the foams than in hydrogels. Comparing the 30x images of both scaffolds, the cells in foam look larger and more spherical than in hydrogel.

At D7 (Figure 41), the cells in the foam looked smaller than at D1, and red signaling was lower. The cells were rounded, and sometimes the red actin filament looked like it had shrunk, close around the blue nuclei. A cell to the top left in the 30x foam middle image, has a halo of actin filament around, and looks very different from other cells observed. The actin filament in this particular cell looks more thread-like, like a network. Very few cells were elongated, but some examples can be spotted in the 7.5x foam edge image. An example of how the IMR-90 cells were dispersed in the foam is shown with bright field images in Appendix B, Figure B2, where the 30x image is the same as in Figure 41. In the hydrogel, the actin filament looked very grainy. The cells were mostly rounded and small. Different from the foam, the cells in the hydrogel had more elongations and some cell-cell connections. This was not observed at D1. Cell-cell connections and elongated cells are shown in the 30x hydrogel middle image.

At D21 (Figure 42), there were observed larger, more elongated, and connected cells - predominantly in the hydrogels, but also some in the foams. However, in both foam and hydrogel, there seemed to be a decrease in cell numbers and red signaling intensity. The number of cells with actin filament looks almost equal in the two scaffolds, which indicates a decrease

in actin filament, especially in the more cell rich hydrogels. In the foam, most cells still appeared rounded and very many are just blue dots. A few have elongations or droplet shapes, like the examples in the 30x images. This was almost non-existent at D1 and few at D7. More of this was seen in the 7.5x edge image. In the bottom right corner of the 7.5x edge image, an example of the large IMR-90 cell structuring attaching to well wall can be observed. In the foam, these structures appeared as a layer under the foam that stretched out under the foam and up in the well on the sides of the foam to touch the walls of the plastic well (Appendix C, Figure C4).

In the hydrogel at D21 a lot of cells were only blue dots. In the 7.5x hydrogel middle image, more than half of the cells are without actin filament. Large cell structures were observed in all the hydrogel samples, which also, unlike in foams, were observable in the wells with the bare eye. Images of these structures are included in Appendix C (Figure C5). Images in Figure 42 were chosen to show cells in what seems to be intact hydrogel, for the cells to be the comparable with the other cell types. The cells else in the wells, apart from the ones in the large cell structures, were rounded and many with elongations, especially far up in the hydrogel. There were fewer single cells in the hydrogel than earlier, and there were areas without cells in the middle of the hydrogel. Studying the 7.5x middle image of hydrogel, one can see that most cells are blue dots, most of those with actin filament are large, elongated cells. Examples of elongated cells are shown in the 30x hydrogel images.

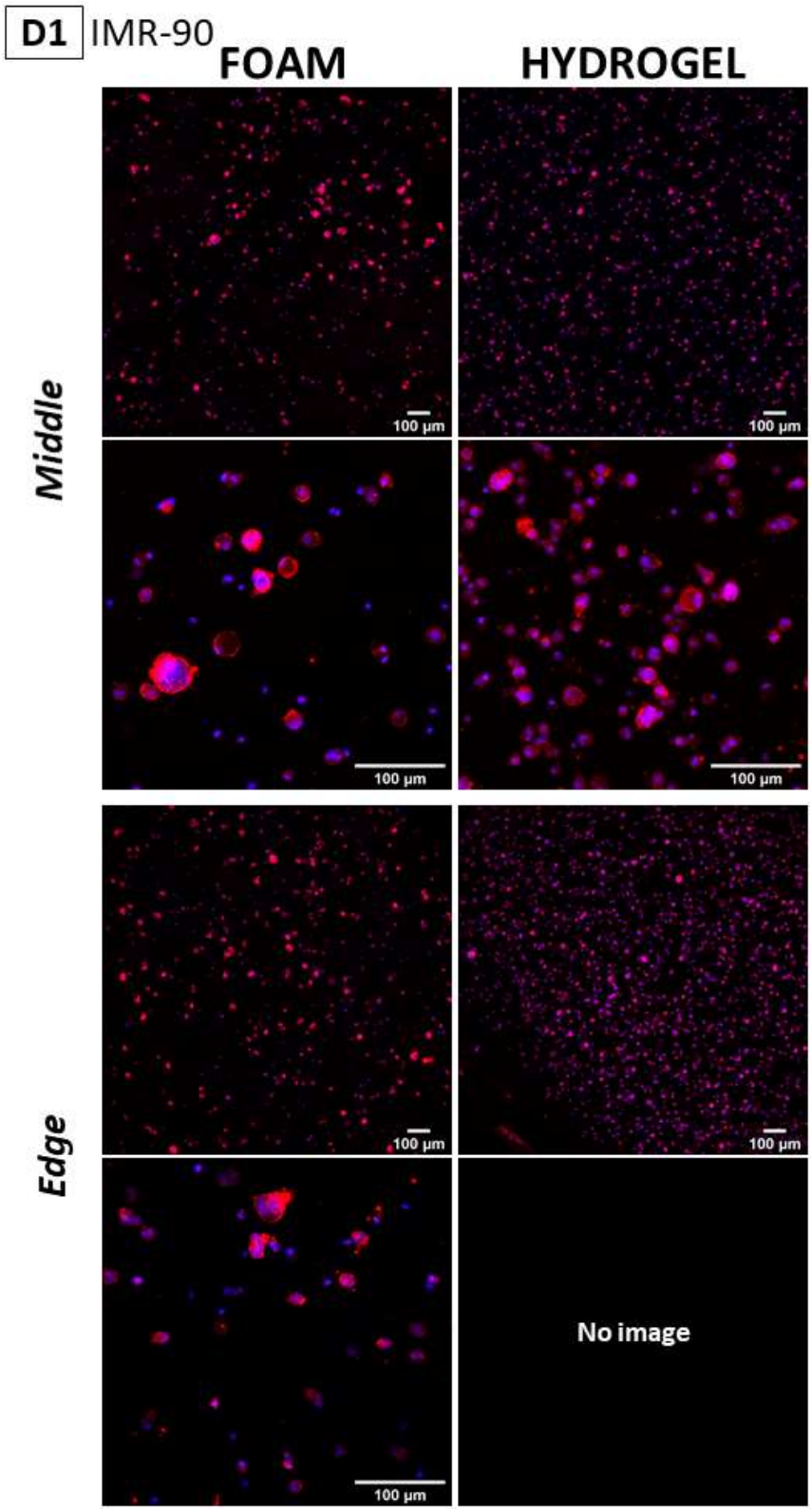

Figure 40: Cell line IMR-90 cultivated in foams and hydrogels. The cells were fixed after 1 day in the scaffolds, stained with DAPI (blue) and Phalloidin 568 (red) and imaged with CLSM, and images are presented as projections of Z-stacks. Left column shows cells in foam, and the right one shows cells in hydrogel. The four upper images show a spot in the middle of the scaffolds, the four bottom images show cells at the edge. Each location in scaffold is represented by magnification 7.5x and 30x. Scalebars are 100µm. 30x magnification of the edge of hydrogel was not imaged, and image is therefore lacking.

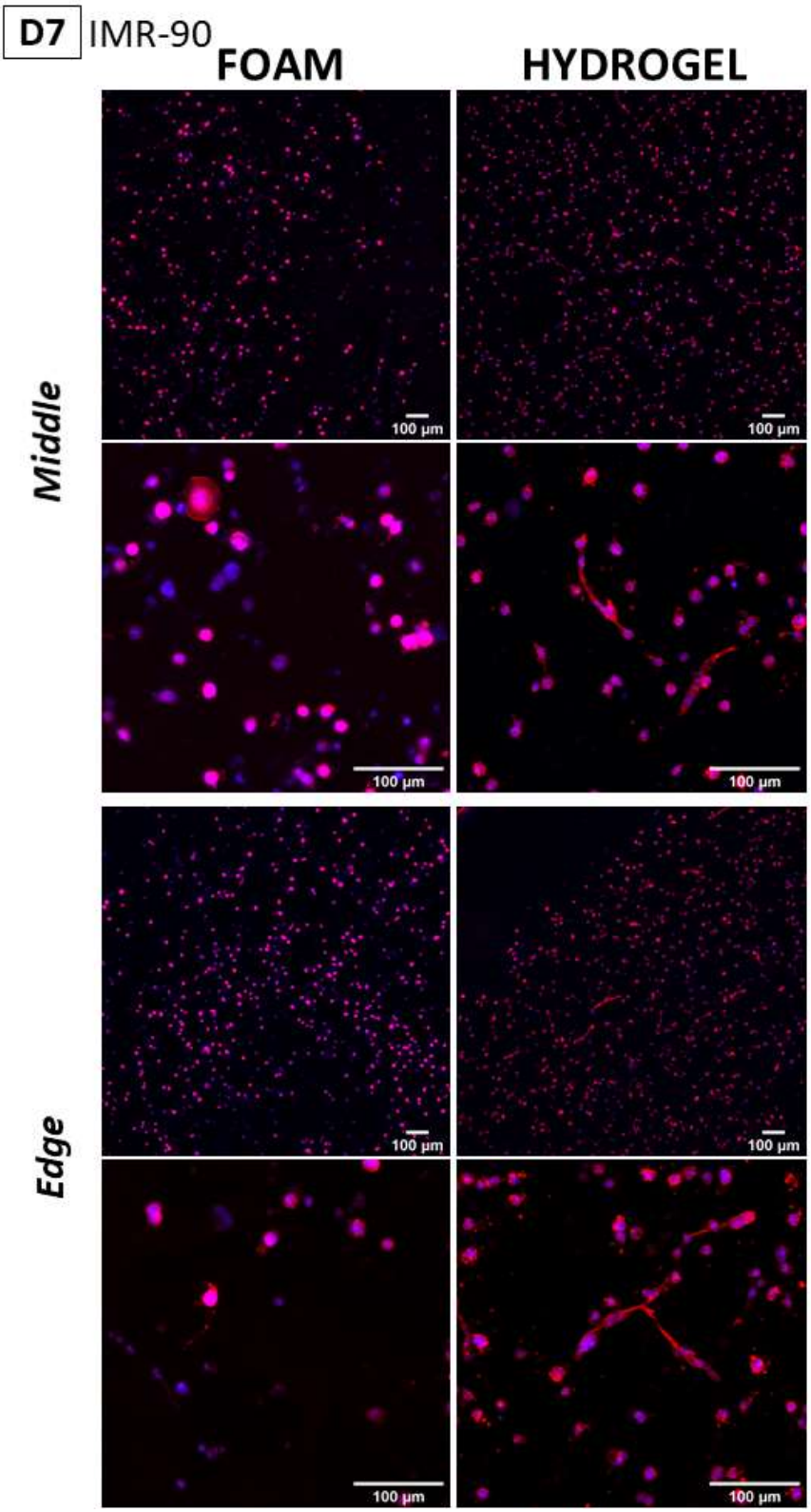

Figure 41: Cell line IMR-90 cultivated in foams and hydrogels. The cells were fixed after 7 days in the scaffolds, stained with DAPI (blue) and Phalloidin 568 (red), imaged with CLSM and are presented in projections of Z-stacks. Left column shows cells in foam, and the right one shows cells in hydrogel. The four upper images show a spot in the middle of the scaffolds, the four bottom images show cells at the edge. Each location in scaffold is represented by magnification 7.5x and 30x. Scalebars are 100µm.

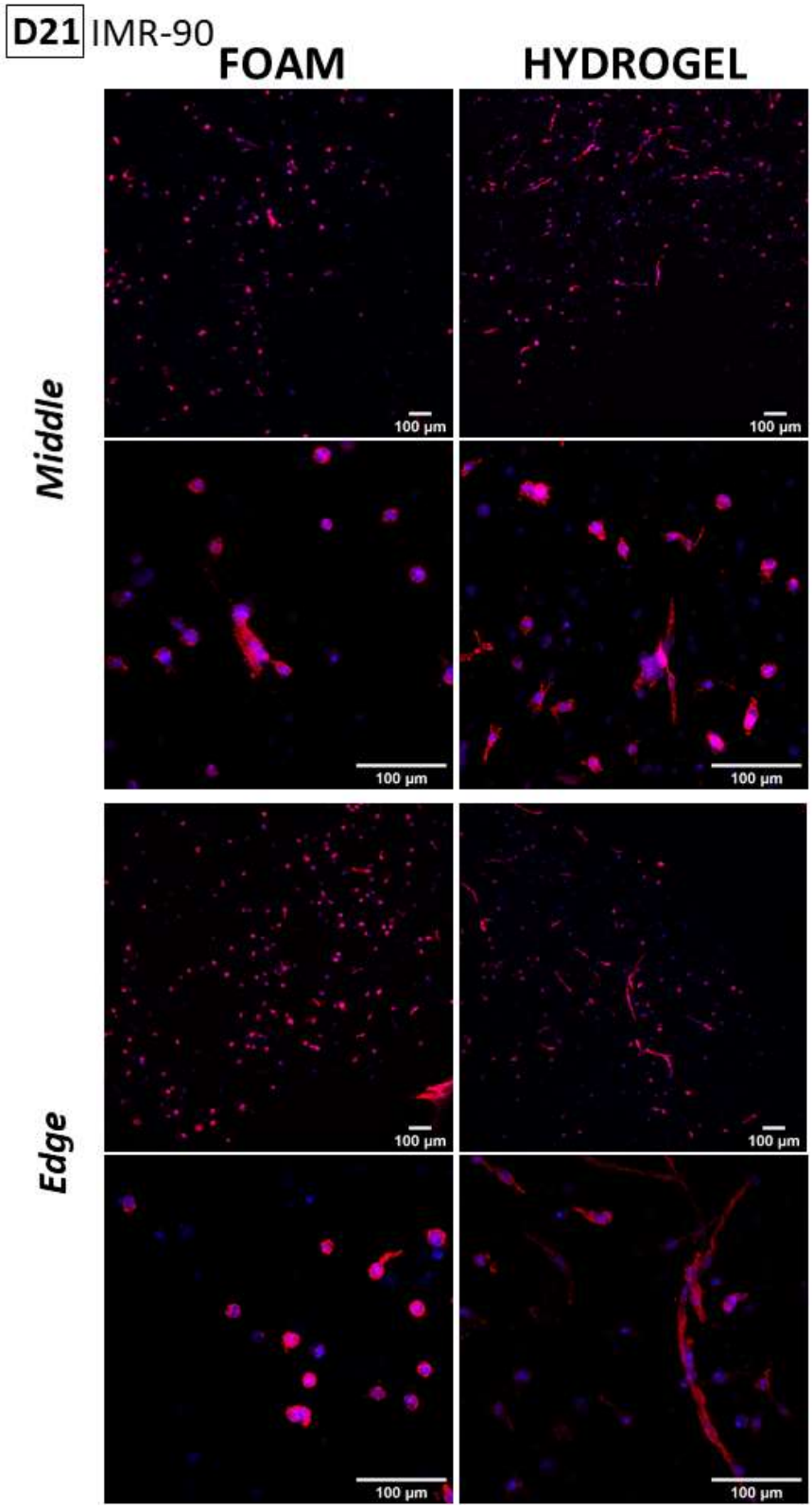

Figure 42: Cell line IMR-90 cultivated in foams and hydrogels. The cells were fixed after 21 days in the scaffolds, then stained with DAPI (blue) and Phalloidin 568 (red). CLSM images are presented as projections of Z-stacks. Left column shows cells in foam, and the right one shows cells in hydrogel. The four upper images show a spot in the middle of the scaffolds, the four bottom images show cells at the edge. Each location in scaffold is represented by magnification 7.5x and 30x. Scalebars are 100µm.

3.5.3 HS-5

At D1 (Figure 43) the cells looked similar in foams and hydrogels. The cells were rounded, with spherical actin filament. However, the red fluorescence was stronger in the hydrogel than in foam. Some few elongated cells were seen in both the foam and hydrogel. In foams, these were elongated cells, while in hydrogel, rounded cells with branches. In both scaffolds, there are some blue nuclei without red actin filament. A problem when imaging the cells **at D7** (Figure 44) was that the blue DAPI was very low on fluorescence. There had been a small increase in elongations (almost none at D1) in foams. An example is the short, elongated cell in the bottom of the 30x foam middle image, which is flat on one side. In the foam middle 7.5x image, there is a long cell right under the scalebar, more than 100 μm long. Clusters were seen, like in the right upper corner of the 30x foam middle. Some cells were much larger than the others, like in the upper right part of the 7.5x edge image. Elongated cells were often large and seemingly in clusters. Elongated cells lining the walls of the foam structure were also observed, as the elongated cell shown in Appendix B (Figure B3). The red fluorescence was particularly weak in the hydrogel, making it harder to see the cells, and requiring high laser power for visualization. The cells in the hydrogel were smaller and less elongated than the cells in the foam. They were typically rounded (as seen in the 7.5x images) and sometimes with a branch. Branches can be seen in the 7.5x foam edge image and the 30x middle image. There was no 30x image taken of any of the edges.

At D21 (Figure 44), the HS-5 looked quite different compared to earlier timepoints and the other cell types. Both scaffolds were dominated by cell clustering. In foam there were many large cell clusters, shown in the 7.5x middle image. The actin filament in the clusters is not as strongly fluorescent as around single cells, and the DAPI shows no clear single nuclei - just a large dot of blue surrounded by some actin filament. The clusters often have rounded shapes, forming a sickle or half a ring. There are more examples of this in the edge image, showing cells forming rounded structures. Apart from these, there are some few single rounded and elongated cells. In the merge with the bright field channel (Appendix B, Figure B9), the clustered areas appear as black holes in the foam – almost like the “hole” in the bright field image of the D21 IMR-90 hydrogel (Appendix C, Figure C5) where the cell structure was located. In the HS-5 hydrogel at D21, the cells tended to grow circularly or in clusters. The DAPI fluorescence was weak, which can be seen by the dominating red color. There are some elongations in the form of branches or elongated cells. However, the typical cell is rounded or in cluster, as the cluster seen in the 30x edge image, in the left bottom corner.

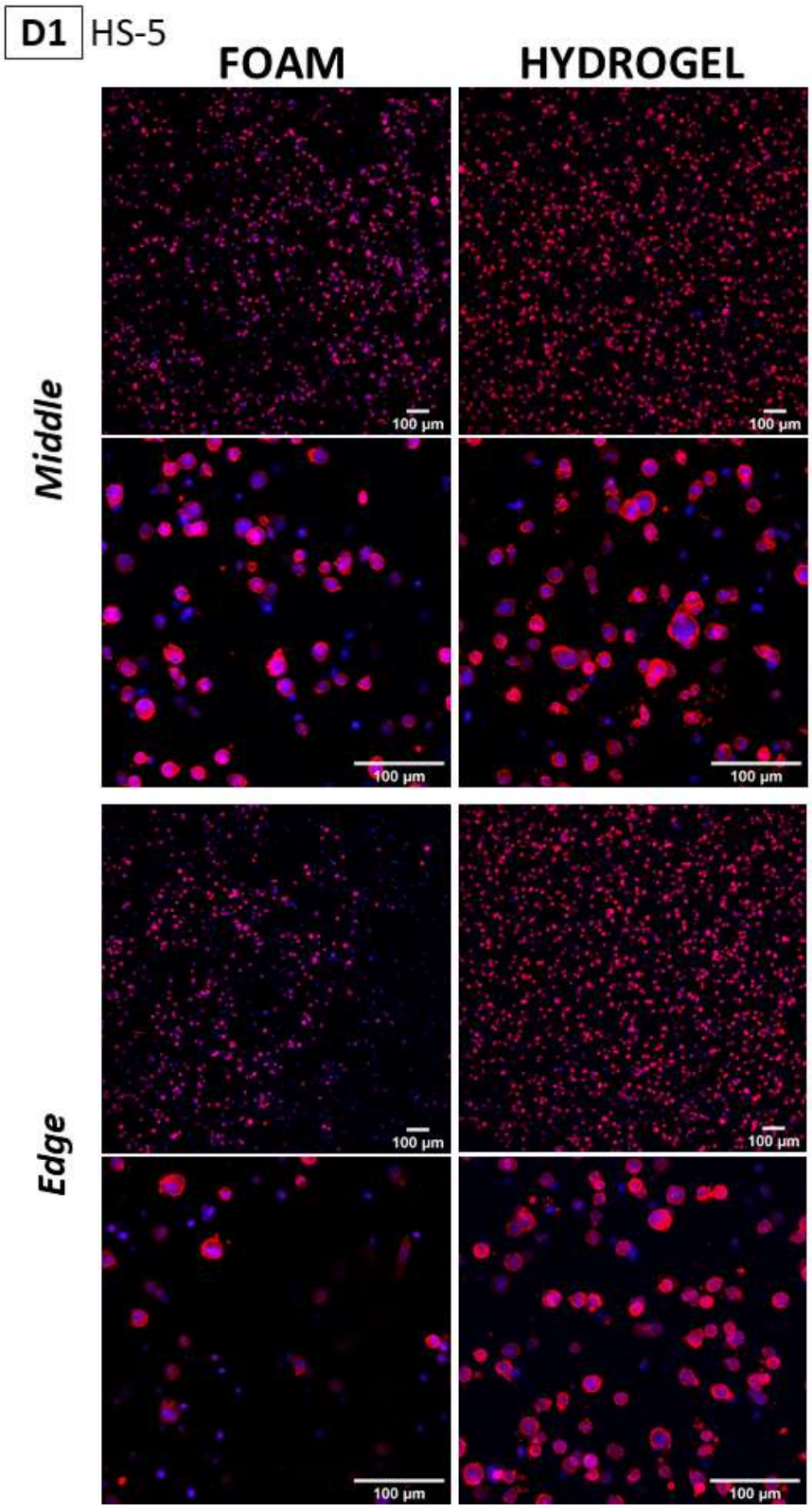

Figure 43: Cell line HS-5 cultivated in foams and hydrogels. The cells were fixed after 1 day in the scaffolds, then stained with DAPI (blue) and Phalloidin 568 (red), imaged with CLSM and are presented in projections of Z-stacks. Left column shows cells in foam, and the right one shows cells in hydrogel. The four upper images show a spot in the middle of the scaffolds, the four bottom images show cells at the edge. Each location in scaffold is represented by magnification 7.5x and 30x. Scalebars are 100µm.

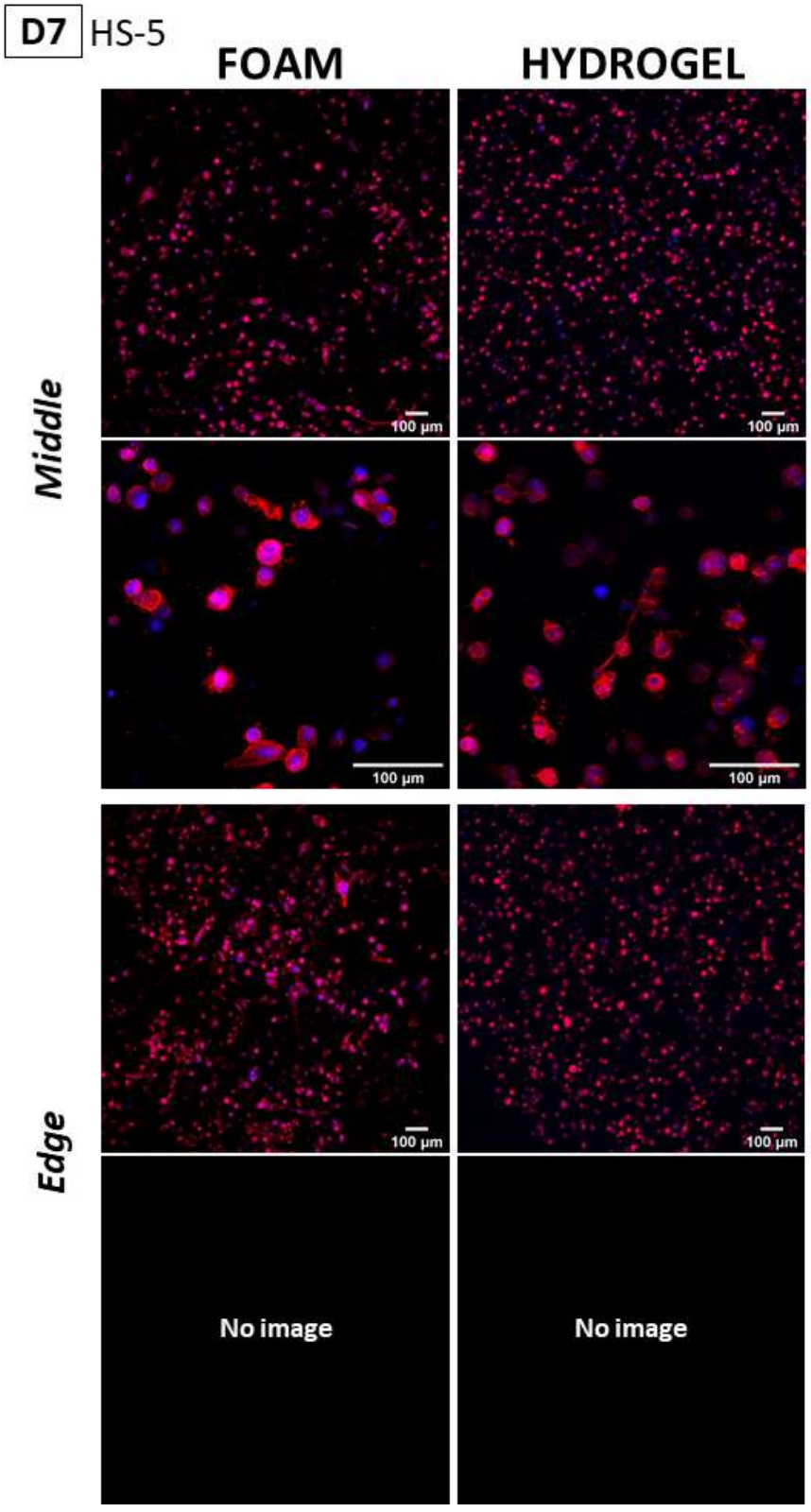

Figure 44: Cell line IMR-90s cultivated in foams and hydrogels. The cells were fixed after 7 days in the scaffolds, then stained with DAPI (blue) and Phalloidin 568 (red) and imaged with CLSM and are presented in projections of Z-stacks. Left column shows cells in foam, and the right one shows cells in hydrogel. The four upper images show a spot in the middle of the scaffolds, the four bottom images show cells at the edge. Each location in scaffold is represented by magnification 7.5x and 30x. Scalebars are 100µm. 30x magnification of the edge of both foam and hydrogel was not imaged, and images are therefore lacking.

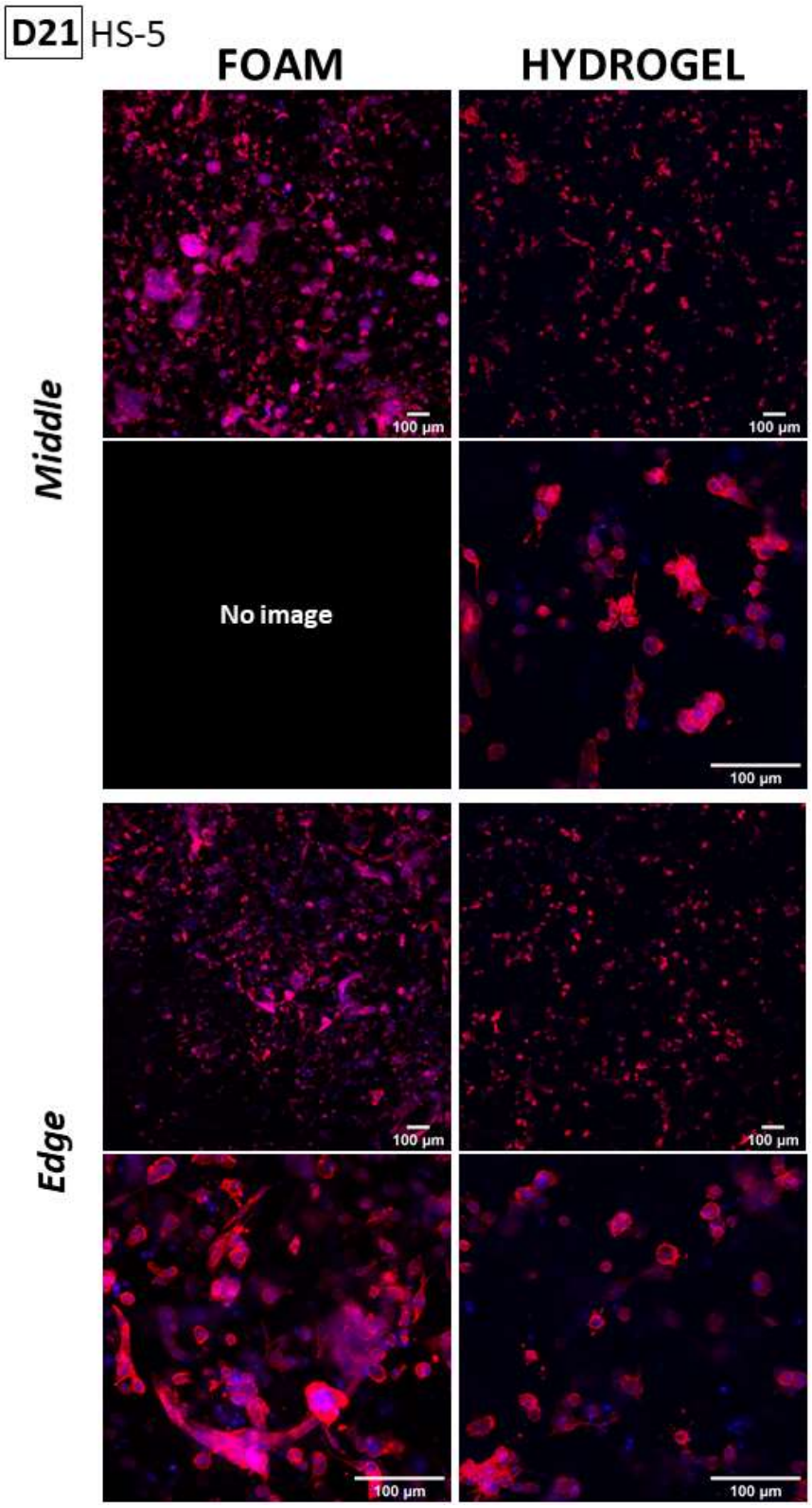

Figure 45: Cell line IMR-90s cultivated in foams and hydrogels. The cells were fixed after 21 days in the scaffolds, then stained with DAPI (blue) and Phalloidin 568 (red) and imaged with CLSM and are presented in projections of Z-stacks. Left column shows cells in foam, and the right one shows cells in hydrogel. The four upper images show a spot in the middle of the scaffolds, the four bottom images show cells at the edge. Each location in scaffold is represented by magnification 7.5x and 30x. Scalebars are 100µm. 30x magnification of the middle of foam was not imaged, and image is therefore lacking.

3.6 Additional tests and observations

In addition to the main study, some small tests were run. These were an assessment of foam volumes, a comparison of media or buffer in foam alginate, optimization of cell concentration in foams, and assessment of foam batch differences. Observations during the experiments that should be taken into consideration in discussion of the results were also explored. The results are commented here and shown in Appendix F.

Assessment of foam volume:

The volume of the foam was assessed and was determined to be 10 µL by weighing both dry and wet, saturated foams, three replicates of each. The average weight of dry foams was 1.3 mg, while the average weight of wet foams was 10.4 mg, which gives a difference of 9.1 mg. This result indicates that adding 10 µL will result in a filled foam, because 1 mg corresponds to 1 µL. That the weight was a little lower than 10 mg might just be that the foams already had lost some liquid when being removed from its well or that some had evaporated when being without media or buffer.

Comparison of alginate dissolved in media or buffer for foams:

It was investigated whether gelation in foams was different when using buffer instead of cultivation media to dissolve the alginate. After 48 h, foams casted with buffer-based alginate solution and media-based alginate solution were investigated with the bare eye (Appendix F, Figure F1) and controlled manually by feeling the foams and squeezing them between two fingers. There were no significant differences that were observed or felt, and both foams had gelated. The alginate that was used was 1% LF200S, allowing visualization of the alginate distribution in the foam with CLSM as well. The results are shown as 3D renders of the green fluorescence channel, bright field channel, an overlay of these, and in addition color depth mapping of the alginate (Appendix F, Figure F2 and Figure F3). These images are from D7, and both the alginate with media and with buffer seemed to distribute well across the foam both vertically and horizontally. In both cases it covers all layers of the foam. There were found no significant differences between foam with alginate dissolved in buffer or in media.

Optimization of cell distribution and investigation of aggregates in foams:

To investigate if cell concentration influenced cell distribution and black aggregates in foams, an optimization study was run on this. The cells were analyzed light microscopy before fixing at D1 and D7, and with DAPI/Phalloidin staining and CLSM at both D1 and D7. The aggregates

seemed equal at both timepoints. The question was if anything would change with changing cell densities, regarding cell distribution, morphology, and black aggregates. Light microscopy images of the concentrations on D1 and D7, and CLSM images with DAPI/Phalloidin staining, are shown in Appendix F, Figure F4. Observations in light microscopy were that there were fewer bubbles and more elongated cells and cell connections at D7. Aggregates did not seem to change with time or changing cell concentrations, but there were decreasing cell numbers and elongations/connections with lower cell concentrations. The aggregates/dark dots were visible as dark particles, either as small grains or big lumps. Some looked defined with smooth surface, other looked more like a fuzzy squiggle or like a ball of hair, and they were present in different sizes and shapes. The aggregates did not show in DAPI/Phalloidin assay. The aggregates were not present in hydrogels. After this assessment, it was decided to go for the same cell density in foams and hydrogels, which means a higher concentration than those tested in this study (7700 cells in foam, 50000 in hydrogel). Conclusion was to use the same concentration of cells in foams and hydrogels, and that the aggregates were not cell clusters, because there was an equal amount no matter the cell concentrations. Later it was seen that these also were observable in foams without cells, and therefore were probably rather a feature of the alginate foam themselves.

Assessing foam batch differences:

During the experiments, the first batch of foams ran out, and it was noticed with the new batches that they had a somewhat different appearance. They were more yellow than white in color, were more electrostatic and therefore harder to handle when seeding cells, and also looked in some cases a little different in the microscope. A small comparison study was performed to look at the differences between the old and new batches. Foams batches were studied and the results are shown in Appendix F, including by the bare eye, dry and with added buffer (10µl) (Figure F5), dry in light microscope (Figure F6), with FL-alginate using CLSM at 48 h (Figure F7) and 8 days (Figure F8). The new batch of foams were observed to be more yellow, while the old was white, in addition the new batch had some darker spots on the corner and had some uneven pigmentation also when added liquid. The new batch looked darker and more cloudy when dry in the light microscope. The pores were visible as in old batch, but less roundedness of the pores maybe. In the light microscope the LF200S spread a little differently. The rounded pores were not as visible, and there was a more uneven spread of the alginate, seen by the signaling strength varying more. It could also be caused by a somewhat maybe different structuring inside the foam. However, when studying the bright field channel images taken

simultaneously as the green fluorescence images, there is no significant difference between the batches observable with the naked eye.

Observations of large cell structures in IMR-90:

Some observations that diverged from the norm during the experiments were the changes in IMR-90 and HS-5 on the long term. The IMR-90 assembled into larger cell structures in both scaffolds, and in the hydrogels especially much, where it even was observable with the naked eye in the wells (Appendix C, Figure C2). It was also noticed when treating these hydrogels before the assays at the last day that they were very fragile and easily destroyed, much more than usual where the hydrogels kept relatively firm all the time. It was almost as if these hydrogels had started to dissolve or fall apart, and this was not noticed with any of the other cell types at D21. Several of them were sucked up without even noticing in the pipette, which usually was very easily noticed when happening.

Observations of yellow media and overgrowth in in HS-5:

In the HS-5, it was noticed generally that these cells multiplied very quickly and always were in high cell numbers when confluent in the flasks, compared to the other cell types. It was also noticed a quicker yellowing of media in the T75 flasks, which was not seen at all in the other cell types (Appendix D). On the long term, it was observed an increasing rate of yellowing of the pink media in the experimental wells. It started in the hydrogels, but over time this was seen also in more and more foams. Also noticed in the long term of these cell was that there were a lot of disturbances, debris and cloudiness in the scaffolds. There were a lot of debris around the cells, and in the light microscope it almost seemed that these particles were moving. But this could of course be due to liquid moving. If all of this were due to high cell growth or other properties of this cell type, or if there could have been some sort of infection can be discussed.

4 DISCUSSION

The intention of this study was to assess the effects of microstructures within 3D alginate culturing scaffolds on the viability and morphology of encapsulated cells. This was performed by qualitative analysis with CLSM and light microscopy, in addition to a quantitative cytotoxicity test. NHDF primary cells, and the cell lines IMR-90 and HS-5, were cultivated in porous alginate foams and homogeneous alginate hydrogels and assessed after 1, 7 and 21 days. Prior to this, the distribution of alginate was assessed to obtain insight of how the alginate solution spreads across the foam and its pores. In this section of the thesis, the findings of this

study will be discussed and evaluated. Firstly, the alginate distribution will be addressed, followed by an evaluation of cell distribution in the scaffolds. Next, the main results on cell viability and morphology are discussed in perspective of the methods employed an the literature in the field. The foams, hydrogels and all cell types were treated under the same conditions for both short term (D1, D7) and long term (D21) studies.

4.1 An overview of the scaffolds

To know where the cells were seeded across the foams and how the resulting porosity of foams would be, it was necessary to evaluate how the alginate distributes within foams. The alginate solution appeared to fill the pores of the foam structures quite uniformly, not just covering the structures with a layer of gel, but rather filling it. This probably leads to a lower degree of porosity across the scaffold. However, bubbles were observed in all foams after adding of solution. These were most likely to be bubbles of air, which were trapped in the foam structure and was held in place by the alginate upon casting. The bubbles disappeared over time and were not observed after 48 h (Figure 26). Perhaps the gel collapsed into these pores after a while, but this is not very likely considering that the gelation is completed within only 10 minutes. As the bubbles disappeared, holes remained in the hydrogel (Figure 26). There is therefore a possibility that these bubbles had a permanent effect on the structure of the foams, by adding porosity, which could involve higher diffusion, more access to nutrients and air, and also removing the barrier that the hydrogels can be for cells to spread in these particular areas. However, specific effects of the holes left by the bubbles would not be easy to observe when not using fluorescent alginate in the viability and morphology cell studies.

Although the pores looked quite uniformly green, the graphs over shift in fluorescence intensity across a foam pore showed some variations in the intensity (Figure 25). However, this could be caused by the foam structure itself not being even, and that the images are based on projections of several layers of foam. The intensity was slightly higher in the middle of the pore compared to the edges, where the foam walls are, suggesting that LF200S was abundant at the center of the pores, compared to the pore walls. The foam walls appeared dark and not fluorescent, indicating that the alginate solution did not go into these denser parts of the alginate foam. It is likely that even though the alginate foams become hydrated and gel-like, these walls consists of relatively permanently denser alginate structures. The fluorescence intensity seemed a little higher in the 1% LF200S, which can be linked to the fact that it has a higher concentration of alginate, making it more both more viscous and higher in fluorescence. The 1% LF200S also

seems to have a more distinct border between the foam wall and the alginate solution, which also could be an affect of the higher concentration of fluorescence. Apart from that, 1% and 0.5% LF200S appeared mostly similar. At 15 min, the 1% LF200S image has some dark shadows, instead of distinct black air bubbles as seen in 0.5%. This could simply be due to the fact that the images are projections, and multiple planes are presented in one image. It could also be that the bubbles just are out of focus, as the shadows seem to correspond to the location of bubbles in the bright field image. Nonetheless, it does not seem like the alginate concentration affected the distribution of solution significantly, as far as can be seen by qualitatively assessment.

Regarding the vertical distribution, the depth color mapping (Figure 28) showed that alginate was present in multiple layers across z-plane of foam structure. From the depth mapping it could seem like there were some more alginate in the bottom of the 1% LF200S and in the top of 0.5% LF200S, but this could also be due to random sample differences or differences in the foam structure. The 3D renders (Figure 27) indicate that both 1% and 0.5% alginate solutions "sinks to the bottom" of the foam. Despite this observation, the distribution across the foam structure appears sufficient and homogeneous. However, the outer edges of the foams were inadequately filled (Figure 29). This could potentially have given cells in these areas other conditions than cells in the middle of the foam for example.

Regarding the cell distribution, generally, all intact foams and hydrogels contained cells that were distributed throughout the whole of the scaffold. Over time however, higher numbers of cells were often observed closer to the edge. In certain replicates of the hydrogels, at the center of the scaffold, very few or no cells were observed. This could be random, as the distribution of the cells couldn't be completely controlled even though the cell-alginate solution was mixed before casting. Another theory is that this could be due to the edges being closer to cultivation media, air, and the stiff wall of the plastic well, giving better living conditions for cells in this area. The hydrogel volumes used ensured that the entire base of the well was covered with gel. However, the gels detach after gelation and media is added, so media was probably on the sides of both foams and hydrogels. In almost all wells, a growing layer of cells formed at the plastic bottom beneath the scaffold, indicating that cells were not completely trapped in the hydrogel and maybe preferred the stiffness at the bottom. As the hydrogel should function as a barrier for the cells to move out, it is likely that the layer was formed from cells that accidently sedimented before the gelation had occurred.

The fact that cells in foams (7700/well) were much fewer compared to hydrogels (50 000/well), meant that the foams also contained fewer cells than hydrogels. While the number of cells loaded into each scaffold was meticulously calculated, the number of cells that ended up in each scaffold varied. This could be due varying degrees of sedimentation prior to complete gelation. However, cells in foams were often easier to spot because the gel in foams was more consequently clear. In certain occasions, the hydrogel would not become transparent after gelation, remaining white and cloudy. When adding solution of $CaCO_3$ particles to the alginate solution, it becomes white. However, when the particles dissolve upon addition of acid, and calcium ions attach to alginate, the solution becomes transparent. The solution remaining cloudy can indicate that there still are undissolved $CaCO_3$ particles in the solution. Over time, experience showed that delaying the hydrogel casting as close as possible to 15 minutes after addition of GDL could promote transparency. This indicates that the cloudiness could be due to a need for more mixing and time for the solution to react before it was added to the well plate where no more mixing would happen. An important question is whether the gel properties were significantly affected by this. It could be that a lower degree of crosslinking would be the case, as not all the calcium ions would have reacted. According to Ingar Draget et al. (1990), high viscosity and a prolonged time for GDL to react with $CaCO_3$ before it sediments, gives better homogeneity, and in can be caused by sedimentation of $CaCO_3$ during gelation [51]. This supports that prolonged mixing could prevent $CaCO_3$ from sedimentation, and therefore give GDL and $CaCO_3$ longer time to react. $CaCO_3$-GDL systems have shown to produce uniform and transparent alginate gels, which leads to consistent mechanical properties throughout the gel [209]. In addition to the challenge in observing cells under the light microscope, unreacted $CaCO_3$ in the gel might give different mechanical properties.

An observation in the foams was a difference between the batches (Appendix F, Figure F1). The newer batches were more yellow in color, more electrostatic and had some differences in the foam structures when observed under the light microscope. These foams were used for HS-5 and the IMR-90 short term, but it was not observed that they had any significant effects on the viability or morphology of cells. Alginate color can vary from white to yellow to brown, and can among other things be affected by the degree of oxidation or the chemical composition and pigments in the alginate source [210]. It can be controlled by bleaching or by priorly soaking the seaweed in formalin [211].

4.3 Cell viability and cytotoxicity in the scaffolds

To be able to extrapolate observations towards cell responses, it is first and foremost necessary to know whether the cells inside the foams and hydrogels viable. The very first signs of viability were seen with the initial assessing with a light microscope, in the form of cells obtaining shapes other than the roundness they adapt when detached. However, to have more reliable signs of viability or death, a Live/Dead staining assay was used, as well as a cytotoxicity test. According to the Live/Dead assay used here, there were living cells of all three cell types at both D1, D7 and D21 in both scaffolds. This indicates that the cultivation conditions were sufficient for sustaining the cells with diffusion necessary nutrients and other factors, as well as providing anchoring. The used stains were EthD-1 (red), which enters damaged membranes and labels nucleic acids, and Calcein-AM (green), which permeates un-damaged membranes and becomes fluorescent if there is enzymatic esterase activity. The former indicates a dead cell and the latter a living cell. Generally, the NHDFs seemed to be the most viable cell type, both on the short-term and long-term, while IMR-90 was the least viable.

The IMR-90 and HS-5 both seemed to have around 50/50 dead and live cells in both the foams and hydrogels at D1. After one week, the NHDFs were still very viable with little difference between foam and hydrogel. The IMR-90 however, had an increased number of dead cells, seemingly making up more than 50% in both foam and hydrogel. The HS-5 at D7 is quite similar to D1, with around 50/50 dead and live in both scaffolds. NHDF was still very viable, with a slightly higher number of dead cells in foam than in hydrogel. However, neither the NHDF-viability over time nor difference between the scaffolds is considerably large. The IMR-90 cells at D21 seems to have around 50/50 living and dead cells, maybe with some more dead in foam than in hydrogel. There were generally fewer IMR-90 cells in these images than earlier, which may be related to the appearance of large tissue-like cell structures in the IMR-90 samples at this point. These structures seemed to have assembled a lot of cells, which were mainly dead, with some few living cells spread and in a thin outer layer of the structure. Assuming that these were IMR-90 cells that had assembled, one can speculate why they did this and why there are so many dead cells there. Possibilities are that they either for some reason underwent apoptosis, or they maybe did not get the nutrients or other factors needed when packed in this dense formation of cells. It is also possible that this happened due to cell type effects, or that they simply preferred to attach to each other rather than the material. IMR-90 was after all the cell type that seemed to thrive the least according to this assay. The HS-5 cells did not cha were similar to earlier timepoints, estimated to have more than 50% livings cells,

and with some more dead cells in foam than in hydrogel. However, the live HS-5 cells are very large, which could cause in illusion. As a tool for the discussion, the evaluations of viability in the two scaffolds are organized in Table 12, stating which scaffold that seemed to give highest viability for each cell type at the different timepoints.

Table 12: Qualitative assessment, based on the CLSM viability imaging, of which the two scaffolds that could seem to give the highest viability for NHDF, IMR-90 and HS-5 at after 1, 7 and 21 days of cultivation, according to Live/Dead staining with EthD-1 and Calcein-AM. No difference is indicated with (-). This is based on bare eye evaluation of the ratio of live and dead in each single image and is therefore simply a tool for better overview.

Cell type	D1	D7	D21
NHDF	foam	-	hydrogel
IMR-90	-	hydrogel	hydrogel
HS-5	-	foam	hydrogel

Primary cells are sensitive and known for exhibiting their native characteristics in high degree. Therefore, it is likely that the properties of the alginate scaffolds perhaps had similarities with the origin of NHFDs, which is adult, normal human dermis. Dermis is of dense connective tissue, and it could be that the alginate used for scaffolds here matched its stiffness, and perhaps porosity and degree of attachment possibilities as well. There was generally more viability in hydrogels for all cell types. However, NHDF had high viability also in foams, even at D1. If, as assumed, the foams have higher stiffness than hydrogels, it might be that this could be a reason for NHDF to have high viability also in foams – that it is a stiffness that is appropriate for NHDFs. Another explanation is that cultivation in 3D might be extra favorable for a primary cell, as it comes directly from tissue and "life in 3D", and is better adapted for this, as opposed to cell line cells.

IMR-90 are embryonic lung fibroblasts, which means that they were taken from a developing lung. This means that the cell is not that specific as if it were from adult tissue. This could indicate that it has some stem cell properties, and the ability to differentiate and perhaps adapt. However, IMR-90 was the cell with lowest viability in both the hydrogels and foams, and it seemed to do a little better in hydrogel. If hydrogel is softer than foam, it might be that this was due to this, as there are no other obvious reasons for the hydrogel to be a better fit. There were around 50 % dead cells, which is a quite large number, but cells were still viable at D21, which may indicate that some of the cells were able to adapt to this material. IMR-90 cells have been seen to be have smoot-muscle-like characteristics, and therefore by some classified as myofibroblasts. This would again give another perspective, as these cells are known to be stiffer

and more contractile. IMR-90 has shown to have longitudinal, periodical attachment sites along the surface of the cell, and to be more contractile than other fibroblasts, with the capacity to generate force like SMCs [212]. It can be speculated if this establishes a higher requirement for a material that can be pushed and pulled, regarding stiffness and perhaps a higher degree of attachment ligands such as RGD. Contrary to the argumentation that they prefer soft gels, it may be that soft gels can be difficult for them to function in due to these reasons. It is not known don't know the exact origin of IMR-90 in lung, if they are from smooth muscle or from contractile interstitium [212]. Smooth muscle exists throughout the body, and is important in contractile functions in for example lungs, airways, digestion, blood pressure, allowing the important uncontrolled contraction of these systems [213].

However, the large tissue-like structures that were formed could be an indication that the cells rather attach to each other than the material, which is another indication that these cells might not were very fit for the material. On the other hand, some trait in IMR-90, which the other cell types do not have, caused it to form these structures. The most important known differences are that IMR-90 is from lung, and that it is embryonic. Maybe the tissue-like structures were a sign of repulsion against the foam, or maybe it was a sign of cell differentiation, or maybe they tried to make a supportive connective tissue.

The viability of HS-5 was quite similar to that of IMR-90, with around 50/50 live and dead cells, however somewhat more viable on the long-term than IMR-90. These are both cell lines, but HS-5 is immortalized, which IMR-90 is not, and originates from adult bone marrow. Bone marrow is also a soft tissue, so this is something in common for IMR-90 and HS-5. Perhaps the scaffolds were too stiff for these cells. The HS-5 were seen to have a lot of clustering at D21, but still viability. However, it was noticed during cultivation of these cells in the long term, that the cultivation media turned yellow increasingly quicker. This indicates, by the use of phenol red, a lowered pH, which could indicate that something was wrong. This could be due to overgrowth, or even an infection. It was noticed that the media generally was turning yellow quicker for these cells, also in TC75 flasks, but as this increased in rate in the 96-well plates, it could indicate that something was wrong.

The tissue origin might still be important cues in understanding why the cell types differ. The fact that they are cell lines means that they have been suited for 2D cell culturing. This might cause them to have lower viability when put in a 3D environment, at least it will need them to differentiate. There could be many possible reasons for the lower viability in IMR-90 and HS-5, probably due to them not being able to exhibit their inherent functions in the material they

were placed in, and they might become apoptotic due to this. This could be reasons such as stiffness as mentioned, they not being able to attach sufficiently to the RGD, or the fact that the gels are not modified for enzymatic degradation, and therefore functioning as a barrier, if this is important for their viability. Hadden and Henke (2002) showed that primary human lung fibroblasts became apoptotic when adhesion receptors on the cells were blocked by soluble FN peptides, inhibition adhesion to a substratum [40], indicating the importance of adhesion.

However, the fact that there still was viability at D21 indicates that the scaffolds could sustain all the cell types, but primary NHDF in a higher degree. Other factors such as cultivation media can also be a source of effects, as it is part of the conditions. However, the media used should be optimized for keeping the pertaining cell type healthy.

Alginate foams have shown to be able to sustain viability and proliferation of MSCs added in suspension [216] and in human carcinoma NHIK 3025 cells and mouse NIH:3T3 [31], where in the latter study the presence of alginate increased cell seeding efficiency significantly. High concentrations of alginate have shown to result in more dead cells after seeding, while lower concentrations has shown to increase proliferation and formation rate of spheroids. Low cell seeding density decreased proliferation rate [217]. IMR-90 has been found to have more than 95% viability in 1% alginate beads for expression of VEGF (vascular endothelial growth factor) and they were also found to self-aggregate after one day, in the same study. This indicates that IMR-90 can have high viability. However, that was in beads and without RGD, and seemingly only short-term and based on cell aggregation instead of attachment to material [218]. It might be that the proximity of cell to the next cell is important for the survival of IMR-90.

It is important to remember that the Live/Dead assay is a qualitative assessment, and factors such as varying cells numbers, strength of fluorescence and cell sizes can function as illusions when considering the ratio between red and green stained cells. However, it is the ratio between dead (red) and live (green) cells that matters, not the size or shape. In addition, the images are projections of Z-stacks, meaning that some cells potentially could be covered by another cell if they have the exact same position. This could also be a cause of some of the co-staining that is seen in some images, for example in the IMR-90 at D21. Regarding this, however, the staining is quite reliable, as a cell only turns green if there is enzymatic activity, which is only in the living cells. Likewise, a cell will only turn red if the membrane is ruptured. At D21 the fluorescence signal appeared lower, which could be caused by a lower activity in the cells, or the cells being smaller and or fewer, and therefore giving that impression. It could also be simply due to differences in the staining strength, use of laser power or exposure to light,

because the dyes are light sensitive. None of the images are from the same samples, and therefore random sample differences can occur as well, even though the most representative samples and images were chosen. The total number of cells seems to vary, as seen with the HS-5 which seemed to have same number in both foam and hydrogel, even though foams were intended to have 7700 cells compared to 50 000 in hydrogel. The cell numbers were sometimes different in different spots of the sample and sometimes different from sample to sample, as the distribution cannot be controlled completely by the procedure used in this study. However, it was noticed with HS-5 that grew very quickly in 2D cell culture and could obtain very high cell numbers. Things like these mentioned can make the qualitative assessment more challenging and affects its reliability.

Colorimetric cytotoxicity tests were performed based on release of LDH from the cells into the media, and results were presented as relative percentage cytotoxicity. The results do not indicate that the cultivation conditions, in neither foams nor hydrogels, were significantly toxic to any of the cell types. However, to compare the scaffolds, hydrogel gave the lowest cytotoxicity at D1 to 2/3 cell types, while at D7 all cell types had lowest cytotoxicity in foam (Table 13).

Table 13: The scaffold giving the lowest relative percentage cytotoxicity for each of the cell types on D1 and D7.

Cell type	D1	D7
NHDF	hydrogel	foam
IMR-90	hydrogel	foam
HS-5	foam	foam

In the presentation of the results, where maximum LDH release in positive controls was defined as 100%, and minimum release from negative controls was 0%, nearly all the experimental values turned out to be negative percentages. This means that the media from the cells in hydrogel and foam actually had lower absorbances than the negative controls that were used. Potentially, this could be due to color differences in the media, but at it is a relatively clear trend, it is likely to believe that there was less LDH in the experimental media. However, what can have caused this is hard to say. It could of course be that there actually was less cell death in the scaffolds than in the negative controls on tissue culture plastic. Reasons for this could be that the adherent cells proliferate faster on flat tissue culture plastic, and thereby there are more cells in total which would lead to more release in LDH. It could also be that the scaffolds in some way reduced the diffusion of LDH out in the media, functioning like a barrier between cells and media. Negative relative percentage cytotoxicity values have been seen in other

cytotoxicity studies, for example in human gingival fibroblasts [219] and in mouse osteoblastic cell line MC3T3-E1 [220].

Even though the cytotoxicity mostly was low, there were still some variations between the cell types and scaffolds that can be discussed. Of all the 12 tested conditions, two had positive percentages. These were IMR-90 in foam and in hydrogel at D7, with respectively 0.12% and 7.32% relative cytotoxicity, which means that the hydrogel could seem to give some negative effects on the viability. IMR-90 was also the cell type that exhibited the lowest viability in the Live/Dead fluorescence staining assay, so these findings correspond quite well. However, at D1 the cytotoxicity in IMR-90 was lower. Lower values were also seen in NHDF at D1 compared to D7. This indicates that being seeded in the scaffolds had low immediate effect on the cells, but that eventual effects appeared with time. For IMR-90 this was also seen in the Live/Dead assay – the viability was reduced from D1 to D7. Which scaffold that was best for the viability seems to vary between the Live/Dead assay and the cytotoxicity tests, which makes sense regarding that the differences are so small that it is likely they are not significant. The IMR-90 in hydrogel D1 is an outlier (-81%), and probably not very reliable. In that particular reading, the absorbance reading of LDH the media alone (background control) was higher than the absorbance of the media IMR-90 cells in hydrogel and in foam (Table E1, Appendix E). It's hard to say what caused this, but it is likely that it was caused by some significant color change in the media.

Of all the cell types, NHDF had the highest cytotoxicity at D1. Between the scaffolds, it had lowest cytotoxicity in hydrogel at D1, and almost similar in foam and hydrogel at D7. Both increased a little however over time. HS-5 had lowest cytotoxicity in foam at both timepoints, and the cytotoxicity changed very little from D1 to D7. However, the standard deviation for the HS-5 value in foam at D1 is very large, which reduces the reliability of this particular value. Comparing NHDF and HS-5 to the Live/Dead staining, NHDF was the least viable of these both at D1 and D7 when comparing the released LDH. However, in the Live/Dead assay, this was opposite – the NHDF being the most viable. This could be just random, as these cytotoxicity's are so low they are not considered signs of cytotoxicity, and it could also be due to differences characteristics of the cells themselves, which also could include different amounts of LDH in the cell.

From the overview in Table 13, it seems that the foams gave the most LDH release at D1, while the hydrogels gave the most at D7. In addition, the only difference between foam hydrogels that was considered significant was the IMR-90 at D7, where the highest of all values was measured

in the hydrogel (7.32%). As not even this is a very high level of LDH, there still was a difference between foam and hydrogel. This could be caused by characteristics of the IMR-90 cell type that was not suitable for life in hydrogel. In addition the hydrogel is assumed to be softer than foam, while also perhaps being less porous and larger.

The significance of this quantitative cytotoxicity test was measured using unpaired t-tests, where p-values lower than 0.05 were considered significant (Table 10, Table 11). This showed that very few of the differences were significant. The difference between untreated cells (negative controls) and their pertaining experimental cells was significant for all hydrogel samples, except NHDF at D7. However, the NHDF in foam at D7 was significantly different from its negative control. This could indicate that the foam generally did not affect the cytotoxicity of cells significantly. No significant difference was found between scaffolds or timepoints for the HS-5. This was also the case for NHDF, where the only significant difference was the increased cytotoxicity in hydrogel from D1 to D7. For IMR-90, on the other hand, the difference between hydrogel and foam was significant at D1 (probably due to outlier) and at D7. The increasing cytotoxicity from D1 to D7 in both scaffolds was also significant according to the t-test. This means that the only cell type that showed significant difference between the cytotoxicity in foam and hydrogel was IMR-90 at D7, which had a significantly higher cytotoxicity in hydrogels than in foams. This could not be qualitatively seen in the Live/Dead images, which were considered the D7 foam to be least viable for IMR-90. But again, this can be due to random sample variations. However, from this, one can say that IMR-90 was the cell type that was significantly affected regarding its viability, which also was seen in the Live/Dead assay. In addition, HS-5 looks a more viable from this assay than the Live/Dead assay. However, the two assays use different measures for cell death. Both are based on damaged membranes, but the cytotoxicity measures the amount of enzymatic activity, while the Live/Dead assay will stain the cell red if it is dead. The latter therefore sounds more reliable, because it might be that levels of enzymatic activity varies between cell types, but again, the latter is also a qualitative measure, while the cytotoxicity test is quantitative. Both tests have their pros and cons, and it is exactly because of such things as this that is important to use more than just one measure.

The LDH cytotoxicity test offers some challenges, such as the sometimes varying or high background levels in media. In addition, according to the protocol [205], pyruvate can be an inhibitor of the LDH reaction, and it is therefore not recommended to use media with pyruvate for this test. Pyruvate is a component in both the media for IMR-90 and HS-5, which means

that it can potentially have affected the results here. However, this was not pursued to be investigated due to time restraints. It is also recommended to use low serum concentrations as serum can have high background. The NHDF media has around 2% FBS, while the media for IMR-90 and HS-5 have 10% FBS, indicating that this also could have affected the readings of the media for these two last cells with relatively high serum level. It can also be debated how the controls would be best suited. It was decided that the best solution was to seed the negative and positive controls without scaffolds, but priorly it was also considered to use controls with scaffolds, and this was also tested. However, then the negative control (living cells) would be completely similar to the experimental conditions, and it would not be known what was the mactual maximum potential of LDH release of the cells in case the scaffold functioned as a barrier. It was therefore considered to be the best to have the controls on tissue culture plastic. It could also be that the diffusion is different through foam and through hydrogel, and the foam is also considerably smaller than the hydrogel.

As mentioned, cells usually also grew at the bottom of the wells. If these cells were many, this can of course have affected the results, perhaps making it more similar to the controls. For later tests it would probably be wise to try reducing the sedimentation of cells until gelation is complete, to prevent formation of cell monolayer at the well bottoms. These monolayers were also seen by Andersen et al. (2014), who removed the foam into a new well in those cases [31].

It was also recommended in the protocol to determine optimum cell concentrations for the study, which is the concentration that gives the highest and lowest maximum and minimum values for controls. This was recommended because of the fact that different cell types may contain different amounts of LDH. However, this was not done here, as the goal was the compare the differences in the cell types.

Be that as it may, the test was performed to the best of our ability to investigate the cytotoxicity in the cells in the foams and hydrogels, given the time restraints for the study. However, using the Live/Dead viability assay and this cytotoxicity test together, supplementing each other, the reliability of the results is considered to be highly improved anyway.

4.4 Morphology

As opposed to the viability, the difference in cell morphology between effects of foams and hydrogels in the cells was more noticeable. There were also differences between NHDF, IMR-90 and HS-5. Upon seeding in the scaffolds, the suspended cells are initially rounded. Variations from rounded morphology was noticed for all cell types when cultivated in the 3D

alginate scaffolds, and the morphologies changed over time. This indicates that the cells were able to interact with the material, which here was provided through RGD-grafting in the 1% alginate, allowing change in cell morphology by anchoring, traction forces and cellular cytoskeletal movements.

The most common morphology for cells was generally rounded, however over time, degree of elongations and branching increased. There was a high variation in shapes - some cells were completely rounded, some rounded with branches, some droplet shaped and some very long. These morphologies show how the cell morphology is different when cultivated in 3D, as seen also seen for example by Bott et al. (2019) where human dermal fibroblasts (HDFs) attained native-like spindle shapes in gels with RGD and MMP-degradability [2]. When growing in a 2D monolayer, fibroblastic cells like NHDF, IMR-90 and HS-5 are relatively large, elongated, adhering to and stretching out on the TCP surface. Their appearance in 2D during cultivation prior to experiments is shown in Section 2.1 (Figure 19). The observed increase in elongations over time makes sense, as the cells need time to grow, and this process has seen to be slower in 3D gels compared to in 2D, as the cells cannot move as freely as in media on a flat surface, as seen for example with human carcinoma cells from cervix (NHIK 3025) in *in situ* crosslinked alginate in alginate foams by Andersen et al. (2014) [31]. In this study, the cells don't have the ability to enzymatically degrade the gels, and the gel can therefore function as a barrier to a higher degree. It has been shown that fibroblasts in gels that were not modified with enzymatic degradability had less spreading. However, that study used 2% alginate, as opposed to 1% here, and stiffness can also be a barrier for the cells to spread [2]. The alginate used here was oxidized, which increases its degradability some. Theoretically the cells could change the gel by mechanical forces if they exert a lot of traction.

There were some general differences observed between the cells in the foams and hydrogels that was seen in all cell types. Cell elongations in the foams were usually in the form of large, thick, elongated cells, while the more common observation in hydrogels was rounded cells with many spike-like, thin branches, giving them a star shape, or they could be really long and thin, usually with a rounded cell body. However, both types of elongation were also seen in each scaffold to some degree. It is likely to think that this difference was due to exactly the presence of the microstructures in foams, which may increase both porosity and stiffness. However, the latter is more relevant here, as it was seen that the pores were mostly filled with alginate solution. The difference between cells foams and hydrogels indicates that there were differences in the microenvironment that could be sensed by the cells, and that affected their morphology.

The elongated cells in foams were sometimes seen lining the surface of the foam structure, and this was also observed in all cell types. Examples are provided in Appendix B. Over time there could be observed almost rings of cells that lines the wall of pores. This clearly indicates an effect of the presence of these structures. However, the dry alginate foam did not have RGD-grafting, so this means that its presence can have affected the cells purely by changing the mechanical properties of the scaffold – most likely increasing rigidity, and by that increasing attachment in proximity to the foam structure. However, the presence of RGD in the alginate solution was probably of importance for the cells to sense their surroundings. In addition, it did not look like cells necessarily were more attracted towards the stiffer surfaces that were offered by the foam.

Macroporous scaffolds can potentially increase porosity, stiffness and in addition provide an environment of multiple relatively rigid surfaces, and be especially suitable for some types of cells, especially promising for bone cell growth [30, 31, 44]. Prior to experiments, it was therefore expected that the presence of foam possibly would affect the morphology of cells – which it seemingly did. What causes this difference in morphology can be a combination of different factors. Opposed to 3D scaffolds that are seeded with cells in suspension [4, 79], the foams in this study were added an alginate solution with cells that gelled in when it was absorbed. This method was shown by Andersen et al. (2014) using human cervical carcinoma cells and mouse fibroblasts, and allows spatial distribution without the need for e.g. centrifugation during gelation. In the study by Andersen et al. (2014), cultivation of the human cervical carcinoma cells using 0.5% alginate in foams resulted in formation of cell aggregates, both spheroid and non-spheroid. Compared to this study, they did not use grafting for adhesion, they used 0.5% alginate, and they used carcinoma cell with spheroid-formation tendency. The gelated foams had elastic modulus around 2700 Pa [31], which is softer than that of stromal tissue [150]. The fact that there is gel inside the pores makes it different from scaffolds where the cells are directly seeded onto the scaffold. Such scaffolds are often considered 2.5D instead of 3D, but the foam used here is actually not so different from the homogeneous hydrogel, and the cells can theoretically attach to the stiffer surfaces or to RGD else in the pores. However, the large, elongated cells in foam resemble cells on TCP in higher degree than the cells in hydrogel.

A question is, what is actually different for the cells in the foams and the hydrogels? It is likely that the foams appear stiffer due to the alginate structures inside. However, it does not seem like the cells are attracted especially against the foam walls, because there are just as many cells

that apparently are in the middle of pores. But, the cells that have obtained large elongated shapes are often seen touching or lining the foam structures. This could be just due to the cell randomly being located there after seeding, and therefore it was able to sense more stiffness in its proximity when exerting force on the surrounding material. If the cells were moving towards the foam structures, it is likely that more cells would have ended up there, as stiffer surfaces induce stronger binding mechanisms in cells. But again, the binding is dependent on the presence of RGD as well. So, the effect of the presence of foam also depends on how far the cell can be from the foam structures and sense the stiffness. Here, it looks quite random, but this could also be due to other factors preventing the cells from moving, such as gel degradability, gel stiffness and number of binding sites. The cells in foams also generally look larger, and it is likely that this is due to the stiffness, but also if the case is that there is more porosity, it could be that the cells have more nutrients. The foams were also smaller than hydrogels, which might also could have increased the diffusion of nutrients and other factors. These are both small scaffolds, but a common problem with 3D scaffolds when they become to big is exactly how to allow adequate diffusion throughout its whole. In addition, foams have more media than gels compared to the cell density, however, it is unlikely that this was important, as new media was added every 2nd day. Another difference is the way of gelation, where the foam takes only 10 minutes to gel, the hydrogel takes 2 h.

Regarding the viability test, it is hard to say which scaffold is most suitable for the cells. However, the goal with these studies is to better understand the cell-matrix connections, but also to improve the biological relevance of the cell responses. However, it is also hard to say whether the foam or hydrogel is the most similar to the natural cellular environment, and this will also depend on the different cell types in a large degree. It was not reflected in the viability assays that foams liked this or that better, but one can still discuss which allows the cells to exhibit their native characteristics more, because even though they did not seem to affect the viability, they induced different cell shapes.

In the 3D alginate scaffolds here, there were generally a lot of rounded cells dominating. The NHDF was the cell type that had the most elongations, both on the short-term and long term. It was also the one to in highest degree seem to interact with the foam structures when it comes to lining the foam. The IMR-90 were mostly rounded all the way, and on the long-long term formed large cell-formations that even were visible by the naked eye. The HS-6 were also mostly rounded, and over time developed a lot of clustering in both foams and hydrogels,

especially much in foam. So clearly, even though all the cells are fibroblastic, their inherent differences seems to have affected they morphological responses to the scaffolds.

NHDF had elongations in both foam and hydrogels at D1. In hydrogels, there was a lot of thin and long branches, filopodia from rounded cells. The cells in foam were rounded, droplet shaped or stretched. At D7 there was a large increase in elongations in the foams, and there were cells forming circular shapes clearly shaped by the foam structures and lining the pores. Star-shaped cells were seen in the hydrogel, and the branches were longer. At D21, large cells were observed in both hydrogels and foams, in the former in the shape of rounded cell bodies with very long and thin branched filopodia, and in the latter in the form of large, long cells and multicellular structures or cell-cell connections. Overall, NHDF was the cell type with the most elongations in both. The elongated cells in foams are larger, by the way that they seem to have more actin filament organization and stress fibers. This is a usually a response to stiffer materials in fibroblasts, but some cells, both fibroblasts, epithelial cells and cardiomyocytes, seem to prefer cell-cell contact when placed in soft gels [24].

However, the cells in that are elongated in foams could be said to have spindle-like shapes, which is the native description of fibroblasts. In the hydrogel, the actin filament is more densely packed around the nuclei, and the protrusions are in the form of thin filopodia or spikes that grows almost like a tree branch. However, the protrusion in both scaffolds indicates that the cells are able to interact with the material and attach to RGD. The cells that stay rounded however have for some reason not been activated. This could be due to not having sensed any RGD for adhesion, or that it is too far from other cells for example. However, why there is less thin branches in the foams is a question, because the hydrogel is the same concentration. This indicates that the stiffness of the foam causes an effect all over the gel in the pores. It could actually also be due to something with the gelation and amount of Ca^{2+}, which also affects the properties of the gel. Some cells have many nuclei, which could indicate cell division [221]. In comparison with IMR-90 and HS-5, spreading/elongating more in the materials at all timepoints, and it NHDF stayed stable up to 21 days. It does seem like the actin filament reaction was strongest in foam, and the actin filament there looks straighter and smoother. This indicates that the foam is sensed as stiffer. It could also seem like the cells in foam had spindle-shapes. NHDF being primary cells could be a reason for them to easily and quickly be adapted to interact in 3D. It could also be that human dermis matches some of the properties of the foam and scaffold. Human dermis is of dense connective tissue, and it could be that the foam better offers this stiffness than purely the soft hydrogel. HDFs were also used by Bott et al. (2019),

however in that study, there was a large difference between MMP-sensitive gels and not. Possibly, if the gels used here were more degradable, more cellular networks could have been observed – and maybe even cells moving towards the stiffer foam walls. Cells were larger in foams as well, so there are several things indicating that the foams were more stimulating for the NHDFs. This growth of NHDF also matches its high viability. It is also possible that NHDF as a primary cell will stay stable because it is from a specific tissue and is differentiated and will have these characteristics.

The cell lines cells, IMR-90 and HS-5 were both dominated of rounded cells at D1. As they are cell line, they have been adapted to life in 2D, so it might be that they needed some time to differentiate and adapt to the 3D environment. However, their slow and low reaction could also be due to other things not being suitable, such as type of or amount of RGD or stiffness of gel. In IMR-90 there were many cells without actin filament, and only the blue nuclei. It is possible that those cells were not very viable or at least active – this staining method does not separate between live and dead cells. There were large variation in cell sizes. Some elongations had appeared at D7 in hydrogel, but these were few. They were different from the thin branches seen in NHDF, more thicker and long cells. The cells in the foam seemed to have shrunk, as if the actin filament were closely packed round the nuclei. At D21 however, there were some very few droplet shapes in foam, and some more elongations and cell-cell connections in the hydrogel. It could almost seem like the cells adapted over time. Using the light microscope, there was observed a lot of grains and shattering around many of the IMR-90 cells. This was also seen in the HS-5 cells, but not at all in NHDF. Some cells in IMR-90 appeared as rings with a hole in the middle, or with several holes. It is possible that these observations were dead cells, as it could resemble cells undergoing apoptosis, being shattered into cell debris. This could correspond to the lowered viability of these cells, seen in the viability assays. Fragmentation of both nuclei and the whole cell is a sign of cell death by apoptosis [40, 222-224]. Some cells will undergo die when they are no longer needed, such as myofibroblasts after wound healing [41, 225]. If the case in IMR-90 is that the cells underwent apoptosis, it could be an explanation if it, as a myofibroblast, sensed conditions similar to one where it does not have a role. IMR-90 had generally a uneven cell surface, which is seen to be a characteristic with these cells having short microvilli and blebs on the surface, giving an irregular appearance [226]. However, these grains were not as visible when using the confocal microscope as the light microscope, although the actin filament did look more uneven in both HS-5 and IMR-90 compared to NHDF.

On the long term large, dense cell structures formed in IMR-90, especially in hydrogel, but also some in foam. In the hydrogels these were even were observable with the bare eye (Appendix C). In dialog with the group, Daria Zaytseva-Zotova (NTNU) reported that she also had seen the IMR-90s form these structures in her work, so it seems to not be just a coincidence with these particular samples in this study. The cells inside these structures looked small and rounded, and they were densely packed. However, it could seem like these structures were separated from the hydrogels. The structures often could seem to be growing from the monolayer at the well bottom and attaching with strings to the sites of the well, almost lifting the hydrogel upwards. It could also seem like the structures that seemingly was inside the gel, rather had "cut through it". When these hydrogels were handled in fixing and staining procedures, they were very easily destroyed, significantly softer than had been observed with the gels before. It could be that these cell-formations caused mechanical pressure on the hydrogels, so that they started falling apart. A theory with the large cell structures is that the cells assembled together instead of interacting with the material – that they really were not compatible with the material.

In the foam study by Andersen et al. (2019), it was found that the cells created multicellular aggregates and spheroids in 0.5% gels without RGD. It could be that cells prefer to attach to each other when there are low possibilities for interaction with materials. This makes also the cell density important for both viability and morphology of the cells. Cell density was not optimized for each cell type here, but that can be an important factor for different cellular behaviours, such as proliferation, viability, secretion of ECM an differentiation [31].

Reasons for the cells to prefer to attach to each other could be the absence of RGD for example as in that study, or maybe it also could be that the grafting is not sufficient or that the ligand for some other reason is not suitable for the cell. Attachment is crucial for adherent cells such as fibroblasts. As IMR-90 resembles a myofibroblast, which are highly contractile and have regular sites for matrix attachment, it could be that the RGD provided in these scaffolds were insufficient. Since IMR-90 also had low viability, it is likely that something was up with the attachment. IMR-90 is an adherent cell, but it did not seem to be able to interact a lot with neither foam nor hydrogel here, according to the low degree of actin filament elongations. It was especially low on cytoskeleton activity in the foams, which could indicate that this assumingly increase in stiffness did not affect the IMR-90 like it affected the NHDF. However, long elongated cells were seen in the hydrogel together with the large cell-structures. It could be that some of the cells over time adapted to the conditions that were. In addition, the hydrogels

had become much softer at this point. It seems that the IMR-90 is active in softer material, which does not match with them being highly contractile.

HS-5 was similar to the IMR-90, mostly rounded and grainy, but the shrinking of cells in foam did not happen. At D7, there were some few hints of elongations and cell-cell interaction. At D21 however, the HS-5 is characterized by a lot of clustering, especially in foam, where there are a lot of something that looks like large multicellular aggregates. Morphologies could almost not be observed with the light microscope at this point due to either overgrowth or some other disturbance that dominated and clouded the samples. However, these are easier studied in the fluorescence CLSM. Both the cell lines, IMR-90 and HS-5, seem to have a tendency to aggregate more than NHDF. It seems that they might prefer cell-cell contact in much higher degree than the primary NHDF. Maybe those cells are more dependent on cell-cell contact. The cells that Andersen et al. (2019) saw to cluster in the foams could resemble the growth of the HS-5, but these were cancerous cells [31]. However, cancer cells have some resembles with immortalized cell lines, by being infinite cells. The system they used resembles soft tissues, similar to the soft gels here.

Comparing the cells in foams and in hydrogel, it seems that the cells in hydrogel in the long term HS-5 were very low in DAPI, for some reason. It could be that the actin filament was very dense. It also seems as though the cells are very small, and not as aggregated as in foam. The foam also showed higher viability. Just like IMR-90, HS-5 had low assembly of actin filament elongation all the way, but the formation of these aggregates was unique for HS-5. It seems as if the aggregates formed on the foam structure, and the foam structure was completely hidden by the cell structures when studying them in the light microscope. It is also possible to see that the aggregates have rounded shapes, that could be caused by the foam pores. This indicates that the cells have attached to the structure some way, and that the foam structure allowed support for the cells to form these structures. HS-5 has shown to have the capacity to form irregular and granular spheroids. In addition, HS-5 cells don't retain contact inhibition, which can be a reason for their possible overgrowth. This has also limited their use for long-term culturing [227-229]. The media for the HS-5 wells became yellow on the long term, and the scaffolds themselves appeared cloudy in the microscope – especially hydrogels. It could be that the media turned yellow due to all the cellular structures, that an overgrowth of cells. It could also be an infection, but this did not seem to affect the viability of the cells significantly. The media did not turn turbid, however. If there is an overgrowth, it could indicate that these cells proliferate, and proliferate even more when the material is stiffer or has structures as the foam. The Bott et al.

(2019) study showed a decrease in DNA content over time, which indicates low proliferation [2], however, Andersen et al. (2014) saw proliferation in their foams [31]. Some moving particles were observed around the HS-5 in the microscope. These could potentially be infectious particles, but there is a possibility that it also was just moving cellular debris due to random Brownian motions [230] of suspended particles. A lot of cellular debris was usually seen around some of the HS-5 cells, which was suspected to be apoptotic. The fact that the media did not turn turbid or smell, however, makes the theory that this was cellular, debris more likely.

On the long term, the primary NHDFs and the cell line HS-5 seemed to react the most on the foam, while IMR-90 reacted very little to foam. However, both HS-5 and IMR-90 were mostly rounded, and IMR-90 showed some signs of repulsion towards the hydrogel. It's hard to say what was best, because that depends really on what is desired to study or use the model for. If the desire is to create a *in vivo*-like for the cell, for it to express, secrete and behave as its origin, the way to go would be to simulate the environment of the desired cell as much as possible. However, this is not as relevant when using cell lines, which have differentiated away from their origin. Or perhaps it could be used to differentiate them back? One can conclude that the presence of foam gave the scaffold changed mechanical properties when compared to the same 1% alginate hydrogel without the rigid alginate microstructures. This quite clear effect is a good example of the importance of also mechanical properties and microstructuring when designing 3D scaffolds.

4.5 Outlook and future studies

Qualitative measurements, like applied here, are important and can provide a good overview. However, to get reliable results, they should be supplemented by quantitative analysis as well. The study here could be further improved by applying quantitative analysis to the Live/Dead images and by for instance quantifying cell morphologies by image analysis. Also, looking at the cells themselves in 3D renders would be very interesting to see the vertical growth as well, but was not performed here due to time restrictions. Here only some few variables were applied, regarding material properties. Further studies should look deeper into possibilities for optimizations of factors such as RGD- functionality, different stiffnesses, material degradability, structuring, and surfaces available to the cells in the culturing scaffold. It could for example be interesting to apply a rigid structure, such as the foam used here, with modifications for adhesion, and see if that would affect seeded cells differently than when the

RGD is in the carrier solution. In addition, more factors in the 3D-cultured cells should be looked into, such as the immune responses, cell secretomics, proteomics and genomics. Studying gene expression data can be an important tool and a reliable source to information on the cells health and behavior [5]. Also, variations and optimizations in the effects of cell densities should also be looked further into, regarding the different requirements of different cells. In this current study, the two scaffolds were different in size, due to product availabilities and optimization. However, limiting such differences can be of importance to get more reliable results. It was seen here that primary cells and cell line cells might be differently adapted to 3D culturing, and this is also something to take notice of and could be studied further.

5 CONCLUSION

To investigate the effects of microstructuring, human fibroblasts (NHDF, IMR-90 and HS-5) were cultivated in soft RGD-functionalized 1% Ca^{2+}-alginate, being a porous alginate foam with gel within the structures and a homogenous gel, and analyzed with light microscopy, CLSM and a cytotoxicity test. There were viable cells at all timepoints (1, 7 and 21 days) within all cell types and in both scaffolds. NHDFs stood out with high and consistent viability > 90%. The viability of IMR-90 and HS-5 was around 50% at D1. At D7, the viability of IMR-90 had decreased, while HS-5 was stable. There were slight differences in viability between foams and hydrogels, but not significant. LDH-release showed no significant cytotoxicity. All the relative cytotoxicity percentages were lower than 0%, except for IMR-90 at D7. However, all LDH values obtained were low, indicating low consistency compared to the viability staining, from which a higher cytotoxicity was expected for IMR-90 and HS-5. Conclusively, the foam did not affect the viability significantly. On the other hand, the morphology was affected. Protruded cells were larger, with more organized actin filament in the foams, while in hydrogels they had a rounded body with thin actin filament branches. NHDFs had the highest cytoskeletal response, elongating the most, and at all timepoints. IMR-90 and HS-5 were mostly rounded in the short-term studies, but some cells exhibited elongation over time. At D21, IMR-90 had formed large, dense cell-structures, especially in hydrogels, while the HS-5 was characterized by clustering, especially in foams. In conclusion, NHDFs were the most viable and stable, and they also interacted the most with the material. NHDFs are primary cells - coming directly from tissue could make it better adapted to 3D life than the cell lines. It could also be that scaffold properties were similar to that of dermis, the origin of NHDF, e.g. regarding stiffness. The fetal lung-derived myoblast-like IMR-90 and the adult bone marrow-derived HS-5 both seemed to prefer cell-cell interaction over material interaction. It is likely that either the stiffness or the

distribution of RGD was not suitable for these cells. The morphological differences induced by the foam are likely responses due to increased stiffness, but to sense stiffness the cell must be able to adhere properly in the first place. These findings show how different cells vary in response to the same material. Though there were some differences in viability between cell types over time, no major differences were seen between foams and hydrogels. Some variances in morphology were seen, but the causes must be explored further. In the future, other strategies for material optimization should be investigated, including degree of stiffness and peptide-grafting, and alternative structural features that provide more accessible surfaces for the cells to attach and interact with the material.

References

1. Green, J.A. and K.M. Yamada, *Three-dimensional microenvironments modulate fibroblast signaling responses.* Advanced Drug Delivery Reviews, 2007. **59**(13): p. 1293-1298.
2. Bott, K., et al., *The effect of matrix characteristics on fibroblast proliferation in 3D gels.* Biomaterials, 2010. **31**(32): p. 8454-8464.
3. Prestwich, G.D., *Evaluating Drug Efficacy and Toxicology in Three Dimensions: Using Synthetic Extracellular Matrices in Drug Discovery.* Accounts of Chemical Research, 2008. **41**(1): p. 139-148.
4. Prestwich, G.D., *Simplifying the extracellular matrix for 3-D cell culture and tissue engineering: A pragmatic approach.* Journal of Cellular Biochemistry, 2007. **101**(6): p. 1370-1383.
5. Andersen, T., P. Auk-Emblem, and M. Dornish, *3D Cell Culture in Alginate Hydrogels.* Microarrays, 2015. **4**(2): p. 133-161.
6. Cukierman, E., et al., *Taking cell-matrix adhesions to the third dimension.* Science, 2001. **294**(5547): p. 1708-12.
7. Andersen, T., et al., *Alginates as biomaterials in tissue engineering.* Carbohydrate Chemistry, 2011. **37**: p. 227-258.
8. Lee, J., M.J. Cuddihy, and N.A. Kotov, *Three-dimensional cell culture matrices: state of the art.* Tissue Eng Part B Rev, 2008. **14**(1): p. 61-86.
9. Gevaert, M., *Engineering 3D Tissue Systems to Better Mimic Human Biology*. 2013. p. 48-55.
10. Baker, B.M. and C.S. Chen, *Deconstructing the third dimension – how 3D culture microenvironments alter cellular cues.* Journal of Cell Science, 2012. **125**(13): p. 3015-3024.
11. Kyburz, K.A. and K.S. Anseth, *Synthetic mimics of the extracellular matrix: how simple is complex enough?* Annals of biomedical engineering, 2015. **43**(3): p. 489-500.
12. Yamada, K.M. and E. Cukierman, *Modeling Tissue Morphogenesis and Cancer in 3D.* Cell, 2007. **130**(4): p. 601-610.
13. Weaver, V.M., et al., *Reversion of the Malignant Phenotype of Human Breast Cells in Three-Dimensional Culture and In Vivo by Integrin Blocking Antibodies.* Journal of Cell Biology, 1997. **137**(1): p. 231-245.
14. Griffith, L.G. and M.A. Swartz, *Capturing complex 3D tissue physiology in vitro.* Nat Rev Mol Cell Biol, 2006. **7**(3): p. 211-24.
15. Anders, M., et al., *Disruption of 3D tissue integrity facilitates adenovirus infection by deregulating the coxsackievirus and adenovirus receptor.* Proceedings of the National Academy of Sciences, 2003. **100**(4): p. 1943-1948.
16. Martin, K.J., et al., *Prognostic Breast Cancer Signature Identified from 3D Culture Model Accurately Predicts Clinical Outcome across Independent Datasets.* PLOS ONE, 2008. **3**(8): p. e2994.
17. Birgersdotter, A., R. Sandberg, and I. Ernberg, *Gene expression perturbation in vitro—A growing case for three-dimensional (3D) culture systems.* Seminars in Cancer Biology, 2005. **15**(5): p. 405-412.
18. Li, S., et al., *Genomic analysis of smooth muscle cells in three-dimensional collagen matrix.* The FASEB Journal, 2003. **17**(1): p. 97-99.
19. Alberts, B., et al., *Cell Junctions and the Extracellular Matrix*, in *Molecular Biology of the Cell*. 2015, Garland Science, Taylor & Francis Group: ew York, US. p. 1035-1089.
20. Geiger, B., et al., *Transmembrane crosstalk between the extracellular matrix and the cytoskeleton.* Nature Reviews Molecular Cell Biology, 2001. **2**(11): p. 793-805.
21. J E Meredith, J., B. Fazeli, and M.A. Schwartz, *The extracellular matrix as a cell survival factor.* Molecular Biology of the Cell, 1993. **4**(9): p. 953-961.
22. Rajagopalan, P., et al., *Direct comparison of the spread area, contractility, and migration of balb/c 3T3 fibroblasts adhered to fibronectin- and RGD-modified substrata.* Biophysical journal, 2004. **87**(4): p. 2818-2827.
23. Akiyama, S.K., et al., *The interaction of fibronectin fragments with fibroblastic cells.* Journal of Biological Chemistry, 1985. **260**(24): p. 13256-13260.

24. Discher, D.E., P. Janmey, and Y.L. Wang, *Tissue cells feel and respond to the stiffness of their substrate.* Science, 2005. **310**(5751): p. 1139-43.
25. Freeman, S. and H. Hamilton, *Biological science*. 2005, Upper Saddle River, N.J.: Pearson Prentice Hall.
26. Lieff, J. *Extra Cellular Matrix Is Critical to Neuroplasticity*. Human Brain [Blog] 2013 [cited 2021; Available from: https://jonlieffmd.com/blog/extra-cellular-matrix-is-critical-to-neuroplasticity.
27. Diekjürgen, D. and D.W. Grainger, *Polysaccharide matrices used in 3D in vitro cell culture systems.* Biomaterials, 2017. **141**: p. 96-115.
28. Kim, J.B., *Three-dimensional tissue culture models in cancer biology.* Seminars in Cancer Biology, 2005. **15**(5): p. 365-377.
29. Andersen, T., et al., *Ionically Gelled Alginate Foams: Physical Properties Controlled by Operational and Macromolecular Parameters.* Biomacromolecules, 2012. **13**(11): p. 3703-3710.
30. Justice, B.A., N.A. Badr, and R.A. Felder, *3D cell culture opens new dimensions in cell-based assays.* Drug Discovery Today, 2009. **14**(1): p. 102-107.
31. Andersen, T., et al., *In situ gelation for cell immobilization and culture in alginate foam scaffolds.* Tissue engineering. Part A, 2014. **20**(3-4): p. 600-610.
32. Slaughter, B.V., et al., *Hydrogels in regenerative medicine.* Adv Mater, 2009. **21**(32-33): p. 3307-29.
33. Hoffman, A.S., *Hydrogels for biomedical applications.* Advanced Drug Delivery Reviews, 2012. **64**: p. 18-23.
34. Nicodemus, G.D. and S.J. Bryant, *Cell encapsulation in biodegradable hydrogels for tissue engineering applications.* Tissue engineering. Part B, Reviews, 2008. **14**(2): p. 149-165.
35. Andersen, T., P. Auk-Emblem, and M. Dornish, *3D Cell Culture in Alginate Hydrogels.* Microarrays (Basel), 2015. **4**(2): p. 133-61.
36. Lee, G.Y., et al., *Three-dimensional culture models of normal and malignant breast epithelial cells.* Nature Methods, 2007. **4**(4): p. 359-365.
37. Kleinman, H.K. and G.R. Martin, *Matrigel: Basement membrane matrix with biological activity.* Seminars in Cancer Biology, 2005. **15**(5): p. 378-386.
38. Ghosh, K., et al., *Cell adaptation to a physiologically relevant ECM mimic with different viscoelastic properties.* Biomaterials, 2007. **28**(4): p. 671-679.
39. Oliver, T., M. Dembo, and K. Jacobson, *Separation of Propulsive and Adhesive Traction Stresses in Locomoting Keratocytes.* Journal of Cell Biology, 1999. **145**(3): p. 589-604.
40. Hadden, H.L. and C.A. Henke, *Induction of lung fibroblast apoptosis by soluble fibronectin peptides.* Am J Respir Crit Care Med, 2000. **162**(4 Pt 1): p. 1553-60.
41. Niland, S., et al., *Contraction-Dependent Apoptosis of Normal Dermal Fibroblasts.* Journal of Investigative Dermatology, 2001. **116**(5): p. 686-692.
42. Bhadriraju, K. and L.K. Hansen, *Extracellular Matrix- and Cytoskeleton-Dependent Changes in Cell Shape and Stiffness.* Experimental Cell Research, 2002. **278**(1): p. 92-100.
43. Schmidt, J.J., J. Rowley, and H.J. Kong, *Hydrogels used for cell-based drug delivery.* Journal of Biomedical Materials Research Part A, 2008. **87A**(4): p. 1113-1122.
44. Liu, Y., et al., *Accelerated repair of cortical bone defects using a synthetic extracellular matrix to deliver human demineralized bone matrix.* Journal of Orthopaedic Research, 2006. **24**(7): p. 1454-1462.
45. Rao, V.V., et al. *Rescuing mesenchymal stem cell regenerative properties on hydrogel substrates post serial expansion*. Bioengineering & translational medicine, 2019. **4**, 51-60 DOI: 10.1002/btm2.10104.
46. Wechsler, M.E., et al., *Engineering the MSC Secretome: A Hydrogel Focused Approach.* Adv Healthc Mater, 2021. **10**(7): p. e2001948.
47. Qazi, T.H., et al., *Biomaterials that promote cell-cell interactions enhance the paracrine function of MSCs.* Biomaterials, 2017. **140**: p. 103-114.
48. Helgerud, T., et al., *Alginates*, in *Food Stabilisers, Thickeners and Gelling Agents*. 2009. p. 50-72.

49. Rehm, B.H.A., *Alginates: Biology and Applications*. Microbiology Monographs, ed. B.H.A. Rehm. Vol. Volume 13. 2009, Berlin, Heidelberg: Springer.
50. Klöck, G., et al., *Biocompatibility of mannuronic acid-rich alginates.* Biomaterials, 1997. **18**(10): p. 707-713.
51. Ingar Draget, K., K. Østgaard, and O. Smidsrød, *Homogeneous alginate gels: A technical approach.* Carbohydrate Polymers, 1990. **14**(2): p. 159-178.
52. Drury, J.L. and D.J. Mooney, *Hydrogels for tissue engineering: scaffold design variables and applications.* Biomaterials, 2003. **24**(24): p. 4337-4351.
53. Shoichet, M.S., et al., *Stability of hydrogels used in cell encapsulation: An in vitro comparison of alginate and agarose.* Biotechnol Bioeng, 1996. **50**(4): p. 374-81.
54. Iansante, V., et al., *A New High Throughput Screening Platform for Cell Encapsulation in Alginate Hydrogel Shows Improved Hepatocyte Functions by Mesenchymal Stromal Cells Co-encapsulation.* Frontiers in Medicine, 2018. **5**(216).
55. Lai, H.L., A. Abu'Khalil, and D.Q.M. Craig, *The preparation and characterisation of drug-loaded alginate and chitosan sponges.* International Journal of Pharmaceutics, 2003. **251**(1): p. 175-181.
56. Skják-Bræk, G., O. Smidsrød, and B. Larsen, *Tailoring of alginates by enzymatic modification in vitro.* International Journal of Biological Macromolecules, 1986. **8**(6): p. 330-336.
57. Draget, K.I., et al., *Effects of molecular weight and elastic segment flexibility on syneresis in Ca-alginate gels.* Food Hydrocolloids, 2001. **15**(4): p. 485-490.
58. Haug, A., et al., *Studies on the Sequence of Uronic Acid Residues in Alginic Acid.* Acta Chemica Scandinavica, 1967. **21**: p. 691-704.
59. Haug, A., et al., *A Study of the Constitution of Alginic Acid by Partial Acid Hydrolysis.* Acta Chemica Scandinavica, 1966. **20**: p. 183-190.
60. Smidsrød, O., *Molecular basis for some physical properties of alginates in the gel state.* Faraday Discussions of the Chemical Society, 1974. **57**(0): p. 263-274.
61. Martinsen, A., G. Skjåk-Braek, and O. Smidsrød, *Alginate as immobilization material: I. Correlation between chemical and physical properties of alginate gel beads.* Biotechnol Bioeng, 1989. **33**(1): p. 79-89.
62. Donati, I., et al., *New Hypothesis on the Role of Alternating Sequences in Calcium−Alginate Gels.* Biomacromolecules, 2005. **6**(2): p. 1031-1040.
63. Grant, G.T., et al., *Biological interactions between polysaccharides and divalent cations: The egg-box model.* FEBS Letters, 1973. **32**(1): p. 195-198.
64. Draget, K.I., et al., *Gel strength of Ca-limited alginate gels made in situ.* Hydrobiologia, 1993. **260**(1): p. 563-565.
65. Smidsrød, O. and G. Skja˚k-Br˙k, *Alginate as immobilization matrix for cells.* Trends in Biotechnology, 1990. **8**: p. 71-78.
66. Nobile, M.R., et al., *Development and rheological investigation of novel alginate/N-succinylchitosan hydrogels.* Journal of Polymer Science Part B: Polymer Physics, 2008. **46**(12): p. 1167-1182.
67. Gombotz, W.R. and S. Wee, *Protein release from alginate matrices.* Advanced Drug Delivery Reviews, 1998. **31**(3): p. 267-285.
68. Lee, K.Y. and D.J. Mooney, *Alginate: properties and biomedical applications.* Progress in polymer science, 2012. **37**(1): p. 106-126.
69. Omtvedt, L.A., et al., *Alginate hydrogels functionalized with β-cyclodextrin as a local paclitaxel delivery system.* Journal of Biomedical Materials Research Part A, 2021. **n/a**(n/a).
70. Boontheekul, T., H.-J. Kong, and D.J. Mooney, *Controlling alginate gel degradation utilizing partial oxidation and bimodal molecular weight distribution.* Biomaterials, 2005. **26**(15): p. 2455-2465.
71. Vold, I.M.N., K.A. Kristiansen, and B.E. Christensen, *A Study of the Chain Stiffness and Extension of Alginates, in Vitro Epimerized Alginates, and Periodate-Oxidized Alginates Using Size-Exclusion Chromatography Combined with Light Scattering and Viscosity Detectors.* Biomacromolecules, 2006. **7**(7): p. 2136-2146.
72. Tam, S.K., et al., *Factors influencing alginate gel biocompatibility.* Journal of Biomedical Materials Research Part A, 2011. **98A**(1): p. 40-52.

73. Strand, B., A.E. Coron, and G. Skjå‹ Braek, *Current and Future Perspectives on Alginate Encapsulated Pancreatic Islet.* Stem Cells Translational Medicine, 2017. **6**: p. 1053 - 1058.
74. Jacobs-Tulleneers-Thevissen, D., et al., *Sustained function of alginate-encapsulated human islet cell implants in the peritoneal cavity of mice leading to a pilot study in a type 1 diabetic patient.* Diabetologia, 2013. **56**(7): p. 1605-14.
75. Legøy, T.A., et al., *Encapsulation boosts islet-cell signature in differentiating human induced pluripotent stem cells via integrin signalling.* Scientific Reports, 2020. **10**(1): p. 414.
76. Hals, I.K., et al., *Alginate Microencapsulation of Human Islets Does Not Increase Susceptibility to Acute Hypoxia.* Journal of Diabetes Research, 2013. **2013**: p. 374925.
77. Rowley, J.A., G. Madlambayan, and D.J. Mooney, *Alginate hydrogels as synthetic extracellular matrix materials.* Biomaterials, 1999. **20**(1): p. 45-53.
78. Leone, G., et al., *Preparation and physico-chemical characterisation of microporous polysaccharidic hydrogels.* Journal of Materials Science: Materials in Medicine, 2004. **15**(4): p. 463-467.
79. Shapiro, L. and S. Cohen, *Novel alginate sponges for cell culture and transplantation.* Biomaterials, 1997. **18**(8): p. 583-590.
80. Catanzano, O., et al., *Macroporous alginate foams crosslinked with strontium for bone tissue engineering.* Carbohydrate Polymers, 2018. **202**: p. 72-83.
81. Huang, Z., et al., *Chondrogenesis of human bone marrow mesenchymal stromal cells in highly porous alginate-foams supplemented with chondroitin sulfate.* Materials Science and Engineering: C, 2015. **50**: p. 160-172.
82. Hwang, C.M., et al., *Fabrication of three-dimensional porous cell-laden hydrogel for tissue engineering.* Biofabrication, 2010. **2**(3): p. 035003.
83. Ceccaldi, C., et al., *Elaboration and evaluation of alginate foam scaffolds for soft tissue engineering.* International journal of pharmaceutics, 2017. **524**(1-2): p. 433-442.
84. Yang, J.-S., Y.-J. Xie, and W. He, *Research progress on chemical modification of alginate: A review.* Carbohydrate Polymers, 2011. **84**(1): p. 33-39.
85. Gomez, C.G., M. Rinaudo, and M.A. Villar, *Oxidation of sodium alginate and characterization of the oxidized derivatives.* Carbohydrate Polymers, 2007. **67**(3): p. 296-304.
86. Alsberg, E., et al., *Cell-interactive alginate hydrogels for bone tissue engineering.* J Dent Res, 2001. **80**(11): p. 2025-9.
87. Alsberg, E., et al., *Engineering growing tissues.* Proceedings of the National Academy of Sciences, 2002. **99**(19): p. 12025-12030.
88. Rowley, J.A. and D.J. Mooney, *Alginate type and RGD density control myoblast phenotype.* Journal of Biomedical Materials Research, 2002. **60**(2): p. 217-223.
89. Ratner, B.D., *The engineering of biomaterials exhibiting recognition and specificity.* J Mol Recognit, 1996. **9**(5-6): p. 617-25.
90. Fonseca, K.B., et al., *Molecularly designed alginate hydrogels susceptible to local proteolysis as three-dimensional cellular microenvironments.* Acta Biomater, 2011. **7**(4): p. 1674-82.
91. Holme, H.K., et al., *Kinetics and mechanisms of depolymerization of alginate and chitosan in aqueous solution.* Carbohydrate Polymers, 2008. **73**(4): p. 656-664.
92. IFF. *NovaMatrix®*. [Homepage] 2021 [cited 2021 14.04.2021]; Available from: https://novamatrix.biz/.
93. AS, D.N.N. *Produksjon av alginat*. [Homepage] 2021; Available from: https://www.stortare.no/produksjon.html.
94. Rueness, J., *stortare*, in *Store norske leksikon*, E. Bolstad, Editor. 2021, Store norske leksikon: www.snl.no.
95. Brouty-Boyé, D., et al., *Chemokines and CD40 expression in human fibroblasts.* European Journal of Immunology, 2000. **30**(3): p. 914-919.
96. Baum, J. and H.S. Duffy, *Fibroblasts and myofibroblasts: what are we talking about?* Journal of cardiovascular pharmacology, 2011. **57**(4): p. 376-379.
97. Fernandes, I.R., et al., *Fibroblast sources: Where can we get them?* Cytotechnology, 2016. **68**(2): p. 223-228.
98. Soundararajan, M. and S. Kannan, *Fibroblasts and mesenchymal stem cells: Two sides of the same coin?* J Cell Physiol, 2018. **233**(12): p. 9099-9109.

99. FRIEDENSTEIN, A.J., et al., *HETEROTOPIC TRANSPLANTS OF BONE MARROW.* Transplantation, 1968. **6**(2): p. 230-247.
100. Friedenstein, A.J., et al., *Precursors for fibroblasts in different populations of hematopoietic cells as detected by the in vitro colony assay method.* Exp Hematol, 1974. **2**(2): p. 83-92.
101. Bernardo, M.E. and W.E. Fibbe, *Mesenchymal stromal cells and hematopoietic stem cell transplantation.* Immunology Letters, 2015. **168**(2): p. 215-221.
102. Caplan, A.I. and J.E. Dennis, *Mesenchymal stem cells as trophic mediators.* Journal of Cellular Biochemistry, 2006. **98**(5): p. 1076-1084.
103. Hass, R., et al., *Different populations and sources of human mesenchymal stem cells (MSC): A comparison of adult and neonatal tissue-derived MSC.* Cell Commun Signal, 2011. **9**: p. 12.
104. Adamo, A., et al., *HS-5 and HS-27A Stromal Cell Lines to Study Bone Marrow Mesenchymal Stromal Cell-Mediated Support to Cancer Development.* Frontiers in Cell and Developmental Biology, 2020. **8**(1227).
105. Murray, L.A., D.A. Knight, and G.J. Laurent, *Chapter 15 - Fibroblasts*, in *Asthma and COPD (Second Edition)*, P.J. Barnes, et al., Editors. 2009, Academic Press: Oxford. p. 193-200.
106. Beacham, D.A., M.D. Amatangelo, and E. Cukierman, *Preparation of extracellular matrices produced by cultured and primary fibroblasts.* Curr Protoc Cell Biol, 2007. **Chapter 10**: p. Unit 10.9.
107. Hossler, F.E., *Connective Tissues*, in *Ultrastructure Atlas of Human Tissues*. 2014, John Wiley & Sons, Inc. p. 77-177.
108. Alberts, B., et al., *The Cytoskeleton*, in *Molecular Biology of the Cell*. 2015, Garland Science, Taylor & Francis Group: New York, US. p. 889-960.
109. Campbell, N.A., et al., *Cell Structure and Function*, in *Biology: A Global Approach*, B. Wilbur, Editor. 2015, Pearson Education Ltd, Laura Dent: Essex, England. p. 167-197.
110. Plikus, M.V., et al., *Fibroblasts: Origins, definitions, and functions in health and disease.* Cell, 2021. **184**(15): p. 3852-3872.
111. Virchow, R., *Die Cellularpathologie in ihrer Begründung auf physiologische und pathologische Gewebelehre*. 1859, **Berlin**: Verlag von August Hirschwals.
112. Chang, H.Y., et al., *Diversity, topographic differentiation, and positional memory in human fibroblasts.* Proceedings of the National Academy of Sciences, 2002. **99**(20): p. 12877-12882.
113. Beningo, K.A., M. Dembo, and Y.-l. Wang, *Responses of fibroblasts to anchorage of dorsal extracellular matrix receptors.* Proceedings of the National Academy of Sciences, 2004. **101**(52): p. 18024-18029.
114. Tang, V.W., *Cell-cell adhesion interface: orthogonal and parallel forces from contraction, protrusion, and retraction.* F1000Research, 2018. **7**: p. F1000 Faculty Rev-1544.
115. Serini, G. and G. Gabbiani, *Mechanisms of Myofibroblast Activity and Phenotypic Modulation.* Experimental Cell Research, 1999. **250**(2): p. 273-283.
116. Masur, S.K., et al., *Myofibroblasts differentiate from fibroblasts when plated at low density.* Proc Natl Acad Sci U S A, 1996. **93**(9): p. 4219-23.
117. Tomasek, J.J., et al., *Myofibroblasts and mechano-regulation of connective tissue remodelling.* Nature Reviews Molecular Cell Biology, 2002. **3**(5): p. 349-363.
118. Haniffa, M.A., et al., *Mesenchymal stem cells: the fibroblasts' new clothes?* Haematologica, 2009. **94**(2): p. 258-63.
119. Haniffa, M.A., et al., *Adult human fibroblasts are potent immunoregulatory cells and functionally equivalent to mesenchymal stem cells.* J Immunol, 2007. **179**(3): p. 1595-604.
120. Ziegler, E., *General pathology; or, The science of the causes, nature and course of the pathological disturbances which occur in the living subject*. 1895, New York: W. Wood and Company.
121. Santiago, R.y.C., *Manual de anatomía patológica general : seguida de un resumen de microscopia aplicada a la histología y bacteriología patológicas*. 1896, Madrid: Moya.
122. Campbell, N.A., et al., *The Animal Body*, in *Biology: A Global Approach*, B. Wilbur, Editor. 2015, Pearson Education Ltd, Laura Dent: Essex, England. p. 933-956.
123. Lonza. *NHDF-Ad - Human Dermal Fibroblasts, Adult*. Primary and Stem Cells [Home page] [cited 2021 26.04.2021]; Available from:

https://bioscience.lonza.com/lonza_bs/NO/en/Primary-and-Stem-Cells/p/000000000000184914/NHDF-Ad---Human-Dermal-Fibroblasts,-Adult.
124. Someya, T. and M. Amagai, *Toward a new generation of smart skins.* Nature Biotechnology, 2019. **37**(4): p. 382-388.
125. Dellambra, E. and G.P. Dimri, *Chapter 7 - Cellular Senescence and Skin Aging*, in *Skin Aging Handbook*, N. Dayan, Editor. 2009, William Andrew Publishing: Norwich, NY. p. 129-148.
126. Boraldi, F., et al., *Normal human dermal fibroblasts: Proteomic analysis of cell layer and culture medium.* ELECTROPHORESIS, 2003. **24**(7-8): p. 1292-1310.
127. ATCC. *IMR-90 (ATCC® CCL-186™)*. Products [Home page] 2016 [cited 2021 29.04.2021]; Available from: https://www.lgcstandards-atcc.org/products/all/CCL-186.aspx?geo_country=no#generalinformation.
128. Nichols, W.W., et al., *Characterization of a new human diploid cell strain, IMR-90.* Science, 1977. **196**(4285): p. 60-3.
129. Nichols, W.W., et al., *Characterization of a New Human Diploid Cell Strain, IMR-90.* Science, 1977. **196**(4285): p. 60-63.
130. Spencer, H., D.B. Flieder, and P.S. Hasleton, *Spencer's Pathology of the Lung*. 2012, Cambridge: Cambridge University Press.
131. Young, C.D., G.W. Moore, and G.M. Hutchins, *Connective tissue arrangement in respiratory airways.* Anat Rec, 1980. **198**(2): p. 245-54.
132. White, E.S., *Lung extracellular matrix and fibroblast function.* Ann Am Thorac Soc, 2015. **12 Suppl 1**(Suppl 1): p. S30-3.
133. Park, H.Y. and D.D. Sin, *Chapter 16 - Stress-Induced Premature Senescence: Another Mechanism Involved in the Process of Accelerated Aging in Chronic Obstructive Pulmonary Disease*, in *Inflammation, Advancing Age and Nutrition*, I. Rahman and D. Bagchi, Editors. 2014, Academic Press: San Diego. p. 193-202.
134. Vij, R. and M.E. Strek, *Diagnosis and treatment of connective tissue disease-associated interstitial lung disease.* Chest, 2013. **143**(3): p. 814-824.
135. ATCC. *HS-5 (ATCC® CRL-11882™)*. Products [Home page] 2016 [cited 2021; Available from: https://www.lgcstandards-atcc.org/products/all/CRL-11882.aspx?geo_country=no#.
136. Roecklein, B.A. and B. Torok-Storb, *Functionally Distinct Human Marrow Stromal Cell Lines Immortalized by Transduction With the Human Papilloma Virus E6/E7 Genes.* Blood, 1995. **85**(4): p. 997-1005.
137. J B Vogler, r. and W.A. Murphy, *Bone marrow imaging.* Radiology, 1988. **168**(3): p. 679-693.
138. Gurkan, U.A. and O. Akkus, *The Mechanical Environment of Bone Marrow: A Review.* Annals of Biomedical Engineering, 2008. **36**(12): p. 1978-1991.
139. Krebsbach, P.H., et al., *Bone marrow stromal cells: characterization and clinical application.* Crit Rev Oral Biol Med, 1999. **10**(2): p. 165-81.
140. Kabrah, S., et al., *The stromal cell line HS-5 is an alternative mesenchymal stem cell source for the development of a 3D bone marrow model.* Mutagenesis, 2015. **30**.
141. Alberts, B., et al., *Analyzing Cells, Molecules, and Systems*, in *Molecular Biology of the Cell*. 2015, Garland Science, Taylor & Francis Group: New York, US. p. 440-528.
142. Kengla, C., A. Kidiyoor, and S.V. Murphy, *Chapter 68 - Bioprinting Complex 3D Tissue and Organs*, in *Kidney Transplantation, Bioengineering and Regeneration*, G. Orlando, G. Remuzzi, and D.F. Williams, Editors. 2017, Academic Press. p. 957-971.
143. Freshney, R.I., *Primary Culture*, in *Culture of Animal Cells: A Manual of Basic Technique and Specialized Applications*. 2011, John Wiley and Sons.
144. Pamies, D., et al., *Advanced Good Cell Culture Practice for human primary, stem cell-derived and organoid models as well as microphysiological systems.* Altex, 2018. **35**(3): p. 353-378.
145. Campisi, J., *The biology of replicative senescence.* Eur J Cancer, 1997. **33**(5): p. 703-9.
146. Jiang, H., Z. Ju, and K.L. Rudolph, *Telomere shortening and ageing.* Z Gerontol Geriatr, 2007. **40**(5): p. 314-24.
147. Cristofalo, V.J., et al., *Replicative senescence: a critical review.* Mechanisms of Ageing and Development, 2004. **125**(10): p. 827-848.

148. Pan, C., et al., *Comparative proteomic phenotyping of cell lines and primary cells to assess preservation of cell type-specific functions.* Molecular & cellular proteomics : MCP, 2009. **8**(3): p. 443-450.
149. Kaur, G. and J.M. Dufour, *Cell lines: Valuable tools or useless artifacts.* Spermatogenesis, 2012. **2**(1): p. 1-5.
150. Cox, T. and J. Erler, *Remodeling and homeostasis of the extracellular matrix: implications for fibrotic diseases and cancer.* Disease models & mechanisms, 2011. **4**: p. 165-78.
151. Butcher, D.T., T. Alliston, and V.M. Weaver, *A tense situation: forcing tumour progression.* Nature Reviews Cancer, 2009. **9**(2): p. 108-122.
152. Tan, J.L., et al., *Cells lying on a bed of microneedles: An approach to isolate mechanical force.* Proceedings of the National Academy of Sciences, 2003. **100**(4): p. 1484-1489.
153. Balaban, N.Q., et al., *Force and focal adhesion assembly: a close relationship studied using elastic micropatterned substrates.* Nature Cell Biology, 2001. **3**(5): p. 466-472.
154. Lim, J.Y. and H.J. Donahue, *Cell sensing and response to micro- and nanostructured surfaces produced by chemical and topographic patterning.* Tissue Eng, 2007. **13**(8): p. 1879-91.
155. Ng, R., et al., *Three-dimensional fibrous scaffolds with microstructures and nanotextures for tissue engineering.* RSC Advances, 2012. **2**: p. 10110-10124.
156. Li, Y. and S.-T. Yang, *Effects of three-dimensional scaffolds on cell organization and tissue development.* Biotechnology and Bioprocess Engineering, 2001. **6**(5): p. 311-325.
157. Takagi, M., T. Sasaki, and T. Yoshida, *Spatial development of the cultivation of a bone marrow stromal cell line in porous carriers.* Cytotechnology, 1999. **31**(3): p. 225-231.
158. Alberts, B., et al., *Visualizing Cells*, in *Molecular Biology of the Cell*. 2015, Garland Science, Taylor & Francis Group: New York, US. p. 529-562.
159. Wang, S. and I.V. Larina, *8 - High-resolution imaging techniques in tissue engineering*, in *Monitoring and Evaluation of Biomaterials and their Performance In Vivo*, R.J. Narayan, Editor. 2017, Woodhead Publishing. p. 151-180.
160. Jonkman, J., et al., *Tutorial: guidance for quantitative confocal microscopy.* Nature Protocols, 2020. **15**(5): p. 1585-1611.
161. Brotchie, A., *3D bioimaging: Cells in gels.* Nature Reviews Materials, 2017. **2**(4): p. 17022.
162. Amos, W.B. and J.G. White, *How the Confocal Laser Scanning Microscope entered Biological Research.* Biology of the Cell, 2003. **95**(6): p. 335-342.
163. Boulesteix, R., et al., *Quantitative characterization of pores in transparent ceramics by coupling electron microscopy and confocal laser scanning microscopy.* Materials Letters, 2010. **64**(16): p. 1854-1857.
164. Anderson, S.I., *11 - Characterisation using imaging techniques*, in *Tissue Engineering Using Ceramics and Polymers*, A.R. Boccaccini and J.E. Gough, Editors. 2007, Woodhead Publishing. p. 226-247.
165. Nygard, K. and N. Bechard, *Confocal Sample Preparation Guide*, in *Preparing Your Sample for a Straight Laser Light Path is Vital to Success*. Integrated Microscopy @ Biotron: University of Western Ontario. p. 9.
166. Alberts, B., et al., *Energy Conversion: Mitochondria and Chloroplasts*, in *Molecular Biology of the Cell*. 2015, Garland Science, Taylor & Francis Group

New York, US. p. 753-808.
167. Probes, M., *LIVE/DEAD ® Viability/Cytotoxicity Kit *for mammalian cells**, in *Invitrogen detection technologies*. 2005, Molecular Probes Inc.: https://www.fishersci.se/shop/products/molecular-probes-live-dead-viability-cytotoxicity-kit-mammalian-cells/10237012. p. 7.
168. *esterase*, in *Miller-Keane Encyclopedia and Dictionary of Medicine, Nursing, and Allied Health*. 2003: https://www.thefreedictionary.com/.
169. Invitrogen, *Calcein AM*. 2020, Thermo Fisher Scientific Inc.: thermofisher.com.
170. Bratosin, D., et al., *Novel fluorescence assay using calcein-AM for the determination of human erythrocyte viability and aging.* Cytometry Part A, 2005. **66A**(1): p. 78-84.

171. Gatti, R., et al., *Comparison of annexin V and calcein-AM as early vital markers of apoptosis in adherent cells by confocal laser microscopy.* J Histochem Cytochem, 1998. **46**(8): p. 895-900.
172. Jonsson, B., et al., *Cytotoxic activity of calcein acetoxymethyl ester (calcein/AM) on primary cultures of human haematological and solid tumours.* European Journal of Cancer, 1996. **32**(5): p. 883-887.
173. Weston, S.A. and C.R. Parish, *New fluorescent dyes for lymphocyte migration studies: Analysis by flow cytometry and fluorescence microscopy.* Journal of Immunological Methods, 1990. **133**(1): p. 87-97.
174. Inc., T.F.S. *Invitrogen™ LIVE/DEAD™ Viability/Cytotoxicity Kit, for mammalian cells*. Cell Growth and Differentiation Reagents and Kits [Page for purchase of lab equipment and supplies] 2001 2021 [cited 2021; Available from: https://www.fishersci.se/shop/products/molecular-probes-live-dead-viability-cytotoxicity-kit-mammalian-cells/10237012.
175. Rye, H.S. and A.N. Glazer, *Interaction of dimeric intercalating dyes with single-stranded DNA.* Nucleic acids research, 1995. **23**(7): p. 1215-1222.
176. Martinez-Madrid, B., et al., *Ficoll density gradient method for recovery of isolated human ovarian primordial follicles.* Fertility and Sterility, 2004. **82**(6): p. 1648-1653.
177. Gaugain, B., et al., *DNA bifunctional intercalators. 2. Fluorescence properties and DNA binding interaction of an ethidium homodimer and an acridine ethidium heterodimer. Appendix: numerical solution of McGhee and von Hippel equations for competing ligands.* Biochemistry, 1978. **17**(24): p. 5078-5088.
178. Lin, Y.-W., T.-C. Chiu, and H.-T. Chang, *Laser-induced fluorescence technique for DNA and proteins separated by capillary electrophoresis.* Journal of Chromatography B, 2003. **793**(1): p. 37-48.
179. Glazer, A.N., K. Peck, and R.A. Mathies, *A stable double-stranded DNA-ethidium homodimer complex: application to picogram fluorescence detection of DNA in agarose gels.* Proceedings of the National Academy of Sciences, 1990. **87**(10): p. 3851-3855.
180. Pasricha, R. and D. Sachdev, *7 - Biological characterization of nanofiber composites*, in *Nanofiber Composites for Biomedical Applications*, M. Ramalingam and S. Ramakrishna, Editors. 2017, Woodhead Publishing. p. 157-196.
181. Narváez, M., et al., *Existence of FGFR1-5-HT1AR heteroreceptor complexes in hippocampal astrocytes. Putative link to 5-HT and FGF2 modulation of hippocampal gamma oscillations.* Neuropharmacology, 2020. **170**: p. 108070.
182. Molecular Probes, I., *DAPI Nucleic Acid Stain*. 2006, Invitrogen detection technologies: www.fishersci.no.
183. Kapuscinski, J., *DAPI: a DNA-specific fluorescent probe.* Biotechnic and Histochemistry, 2009. **70**: p. 220-233.
184. Estandarte, A.K., et al., *The use of DAPI fluorescence lifetime imaging for investigating chromatin condensation in human chromosomes.* Scientific Reports, 2016. **6**(1): p. 31417.
185. Alberts, B., et al., *DNA, Chromosomes, and Genomes*, in *Molecular Biology of the Cell*. 2015, Garland Science, Taylor & Francis Group: New York, US. p. 173-234.
186. Sbirkova-Dimitrova, H.I. and B. Shivachev, *Crystal structure of the DNA sequence d(CGTGAATTCACG)(2) with DAPI.* Acta crystallographica. Section F, Structural biology communications, 2017. **73**(Pt 9): p. 500-504.
187. Larsen, T.A., et al., *The structure of DAPI bound to DNA.* J Biomol Struct Dyn, 1989. **7**(3): p. 477-91.
188. McDermott, M.L., et al., *DNA's Chiral Spine of Hydration.* ACS Central Science, 2017. **3**(7): p. 708-714.
189. Kubista, M., B. Aakerman, and B. Norden, *Characterization of interaction between DNA and 4', 6-diamidino-2-phenylindole by optical spectroscopy.* Biochemistry, 1987. **26**(14): p. 4545-4553.
190. Barcellona, M.L., G. Cardiel, and E. Gratton, *Time-resolved fluorescence of DAPI in solution and bound to polydeoxynucleotides.* Biochemical and Biophysical Research Communications, 1990. **170**(1): p. 270-280.

191. Chazotte, B., *Labeling nuclear DNA using DAPI.* Cold Spring Harb Protoc, 2011. **2011**(1): p. pdb.prot5556.
192. Haines, A.M., et al., *Finding DNA: Using fluorescent in situ detection.* Forensic Science International: Genetics Supplement Series, 2015. **5**: p. e501-e502.
193. Invitrogen, *Phalloidins*. 2019, Thermo Fisher Scientific Inc.: Life Technologies Corporation.
194. *Invitrogen™ Alexa Fluor™ 568 Phalloidin*. Antibody and Dye Based Assays [Page for purchase of Lab Equipment and supplies] [cited 2021; Available from: https://www.fishersci.com/shop/products/molecular-probes-alexa-fluor-568-phalloidin/A12380.
195. Pospich, S., F. Merino, and S. Raunser, *Structural Effects and Functional Implications of Phalloidin and Jasplakinolide Binding to Actin Filaments.* Structure, 2020. **28**(4): p. 437-449.e5.
196. Vandekerckhove, J., et al., *The phalloidin binding site of F-actin.* The EMBO journal, 1985. **4**(11): p. 2815-2818.
197. Mentes, A., et al., *High-resolution cryo-EM structures of actin-bound myosin states reveal the mechanism of myosin force sensing.* Proceedings of the National Academy of Sciences, 2018. **115**(6): p. 1292-1297.
198. Panchuk-Voloshina, N., et al., *Alexa dyes, a series of new fluorescent dyes that yield exceptionally bright, photostable conjugates.* J Histochem Cytochem, 1999. **47**(9): p. 1179-88.
199. Chazotte, B., *Labeling Cytoskeletal F-Actin with Rhodamine Phalloidin or Fluorescein Phalloidin for Imaging.* Cold Spring Harbor protocols, 2010. **2010**: p. pdb.prot4947.
200. Kiernan, J.A., *Formaldehyde, Formalin, Paraformaldehyde And Glutaraldehyde: What They Are And What They Do.* Microscopy Today, 2000. **8**(1): p. 8-13.
201. Jamur, M.C. and C. Oliver, *Permeabilization of cell membranes.* Methods Mol Biol, 2010. **588**: p. 63-6.
202. Cheng, R., et al., *Influence of Fixation and Permeabilization on the Mass Density of Single Cells: A Surface Plasmon Resonance Imaging Study.* Frontiers in Chemistry, 2019. **7**(588).
203. Alberts, B., et al., *Membrane Structure*, in *Molecular Biology of the Cell*. 2015, Garland Science, Taylor & Francis Group: New York, US.
204. Aslantürk, Ö., *In Vitro Cytotoxicity and Cell Viability Assays: Principles, Advantages, and Disadvantages*. 2018.
205. GmbH, R.D. *Cytotoxicity Detection Kit^{PLUS} (LDH)*

[Protocol] 2016 March 2016

[cited 2021; Version 07:[Non-radioactive colorimetric assay suitable for high-throughput quantification of

cell death and cell lysis, based on measurement of lactate dehydrogenase (LDH)

activity released from the cytosol of damaged cells]. Available from: https://www.sigmaaldrich.com/deepweb/assets/sigmaaldrich/product/documents/308/875/cytodetrobul.pdf.
206. KGaA, M. *Trypsin-EDTA solution*. [Page for purchase of products] 2021 [cited 2021 08.08.2021]; Available from: https://www.sigmaaldrich.com/NO/en/product/sigma/t3924?context=product.
207. Carvell, M., I.D. Robb, and P.W. Small, *The influence of labelling mechanisms on the fluorescence behaviour of polymers bearing fluorescein labels.* Polymer, 1998. **39**(2): p. 393-398.
208. Schindelin, J., et al., *Fiji: an open-source platform for biological-image analysis.* Nature Methods, 2012. **9**(7): p. 676-682.
209. Kuo, C.K. and P.X. Ma, *Ionically crosslinked alginate hydrogels as scaffolds for tissue engineering: Part 1. Structure, gelation rate and mechanical properties.* Biomaterials, 2001. **22**(6): p. 511-521.
210. Mushollaeni, W., *The physicochemical characteristics of sodium alginate from Indonesian brown seaweeds.* African Journal of Food Science, 2011. **5**: p. 349-352.

211. McHugh, D.J., *ALGINATE*, in *A guide to the seaweed industry - FAO FISHERIES TECHNICAL PAPER 441*. 2003, FOOD AND AGRICULTURE ORGANIZATION OF THE UNITED NATIONS: School of Chemistry, University College, University of New South Wales and Australian Defence Force Academy, Canberra, Australia.
212. Ehler, E., E. Babiychuk, and A. Draeger, *Human foetal lung (IMR-90) cells: myofibroblasts with smooth muscle-like contractile properties.* Cell Motil Cytoskeleton, 1996. **34**(4): p. 288-98.
213. Hafen, B.B. and B. Burns, *Physiology, Smooth Muscle*, in *StatPearls*. 2021, StatPearls Publishing

214. Bruce, M.C., C.E. Honaker, and R.J. Cross, *Lung fibroblasts undergo apoptosis following alveolarization.* Am J Respir Cell Mol Biol, 1999. **20**(2): p. 228-36.
215. Luo, Y., et al., *Spatial and temporal changes in extracellular elastin and laminin distribution during lung alveolar development.* Scientific Reports, 2018. **8**(1): p. 8334.
216. Ceccaldi, C., et al., *Elaboration and evaluation of alginate foam scaffolds for soft tissue engineering.* International Journal of Pharmaceutics, 2017. **524**(1): p. 433-442.
217. Bohari, S.P., D.W. Hukins, and L.M. Grover, *Effect of calcium alginate concentration on viability and proliferation of encapsulated fibroblasts.* Biomed Mater Eng, 2011. **21**(3): p. 159-70.
218. Kim, C., et al., *In vitro angiogenesis assay for the study of cell-encapsulation therapy.* Lab Chip, 2012. **12**(16): p. 2942-50.
219. Gómez-Florit, M., M. Monjo, and J.M. Ramis, *Identification of quercitrin as a potential therapeutic agent for periodontal applications.* J Periodontol, 2014. **85**(7): p. 966-74.
220. Satué, M., et al., *UV-irradiated 7-dehydrocholesterol coating on polystyrene surfaces is converted to active vitamin D by osteoblastic MC3T3-E1 cells.* Photochemical & photobiological sciences : Official journal of the European Photochemistry Association and the European Society for Photobiology, 2013. **12**.
221. Alberts, B., et al., *How Cells Read the Genome: From DNA to Protein*, in *Molecular Biology of the Cell*. 2015, Garland Science, Taylor & Francis Group: New York, US. p. 299-366.
222. OHSHIMA, S., *Apoptosis and Necrosis in Senescent Human Fibroblasts.* Annals of the New York Academy of Sciences, 2006. **1067**(1): p. 228-234.
223. Ölander, M., N. Handin, and P. Artursson, *Image-Based Quantification of Cell Debris as a Measure of Apoptosis.* Analytical Chemistry, 2019. **91**(9): p. 5548-5552.
224. Kerr, J.F., A.H. Wyllie, and A.R. Currie, *Apoptosis: a basic biological phenomenon with wide-ranging implications in tissue kinetics.* Br J Cancer, 1972. **26**(4): p. 239-57.
225. Alexis, D., et al., *Apoptosis mediates the decrease in cellularity during the transition between granuloma tissue and scar.* The American journal of pathology, 1995. **146**: p. 56-66.
226. Johnson, J.E., *Fine structure of IMR-90 cells in culture as examined by scanning and transmission electron microscopy.* Mechanisms of Ageing and Development, 1979. **10**(6): p. 405-443.
227. Deynoux, M., et al., *A comparative study of the capacity of mesenchymal stromal cell lines to form spheroids.* PloS one, 2020. **15**(6): p. e0225485-e0225485.
228. Stoker, M.G.P. and H. Rubin, *Density Dependent Inhibition of Cell Growth in Culture.* Nature, 1967. **215**(5097): p. 171-172.
229. Abercrombie, M., *Contact inhibition in tissue culture.* In Vitro, 1970. **6**(2): p. 128-142.
230. Grøn, Ø., *brownske bevelgeser*, in *Store norske leksikon*. 2021: snl.no.
231. Hedin, U., et al., *Diverse effects of fibronectin and laminin on phenotypic properties of cultured arterial smooth muscle cells.* The Journal of cell biology, 1988. **107**(1): p. 307-319.
232. Fluck, J., et al., *Normal human primary fibroblasts undergo apoptosis in three-dimensional contractile collagen gels.* J Invest Dermatol, 1998. **110**(2): p. 153-7.

Appendix

A. Light microscopy: Supplementing timepoints

D3

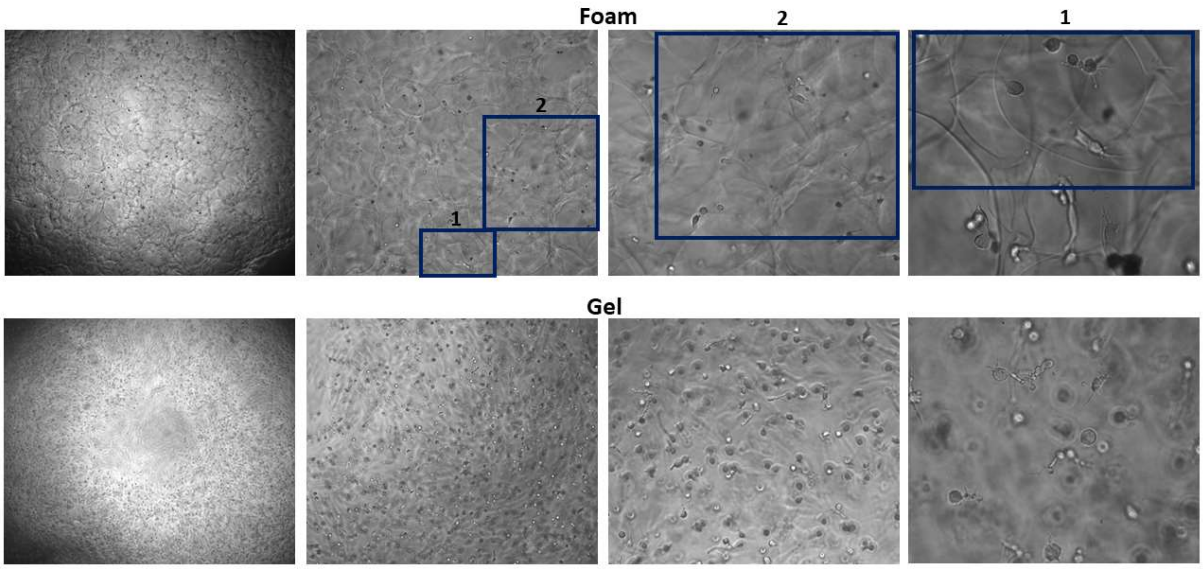

D13

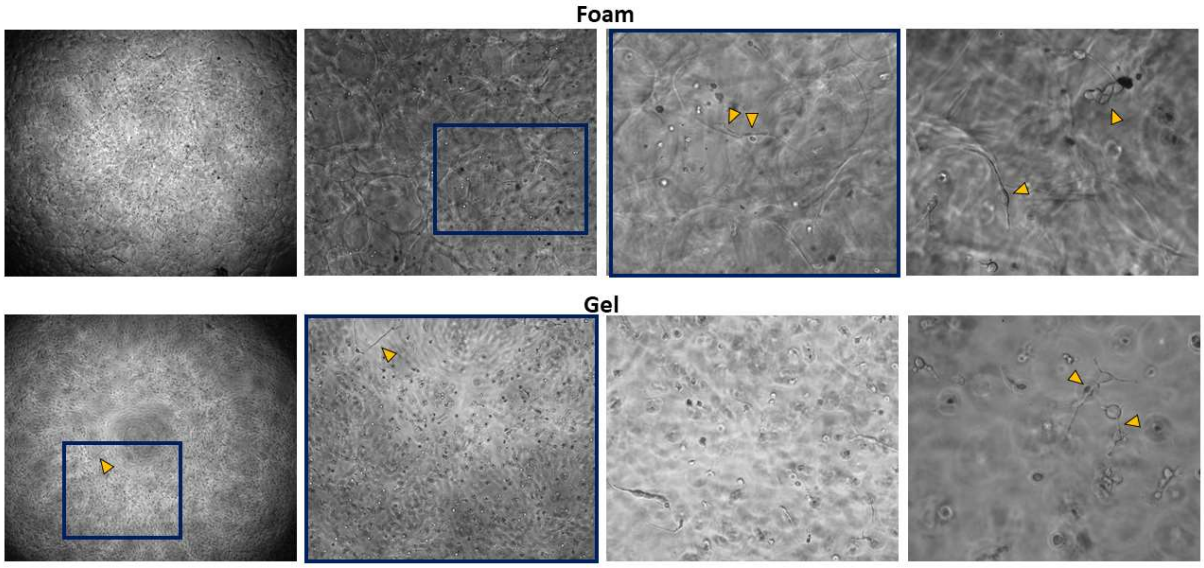

Figure A1: NHDF at D3 and D13 in foams and hydrogels.

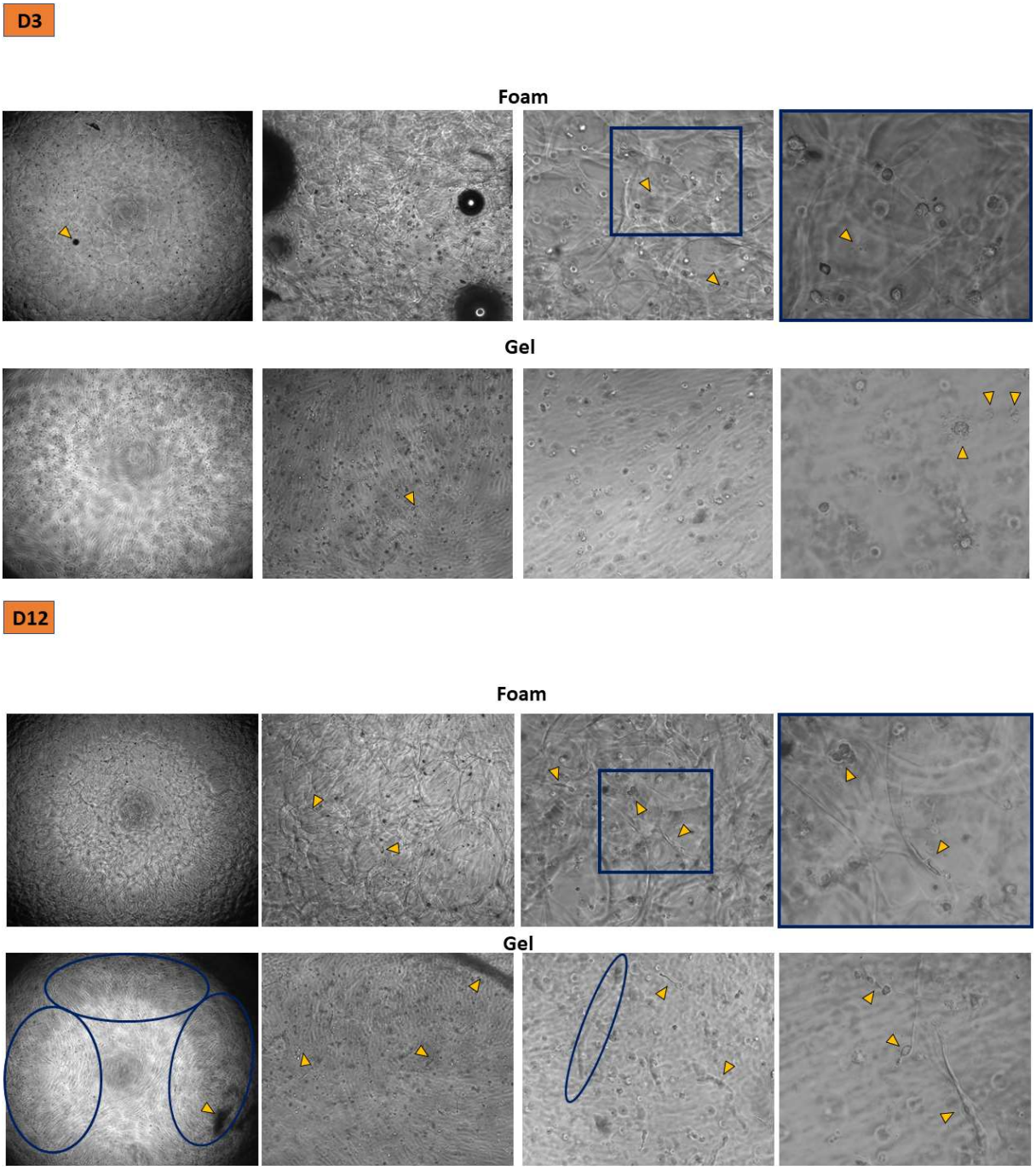

Figure A2: IMR-90 at D3 and D12 in foams and hydrogels. At D12 in hydrogels, a dark spot is observed in the right corner of the 4x image (Gel, D12), which is close to the edge of the hydrogel, as well as a dark line in the right upper corner of the 10x image (Gel, D12). These were probably the beginning of the large, dense cell-structures that were observed in IMR-90 at D21. The blue circle in the 20x image (Gel, D12) encircles a seemingly very long and large cell, but that is out of focus. Better focus is shown in the 40x image (Gel, D12), showing three examples, respectively a connection of three cells, an oval cell body with a long branch and an elongated long and thicker cell.

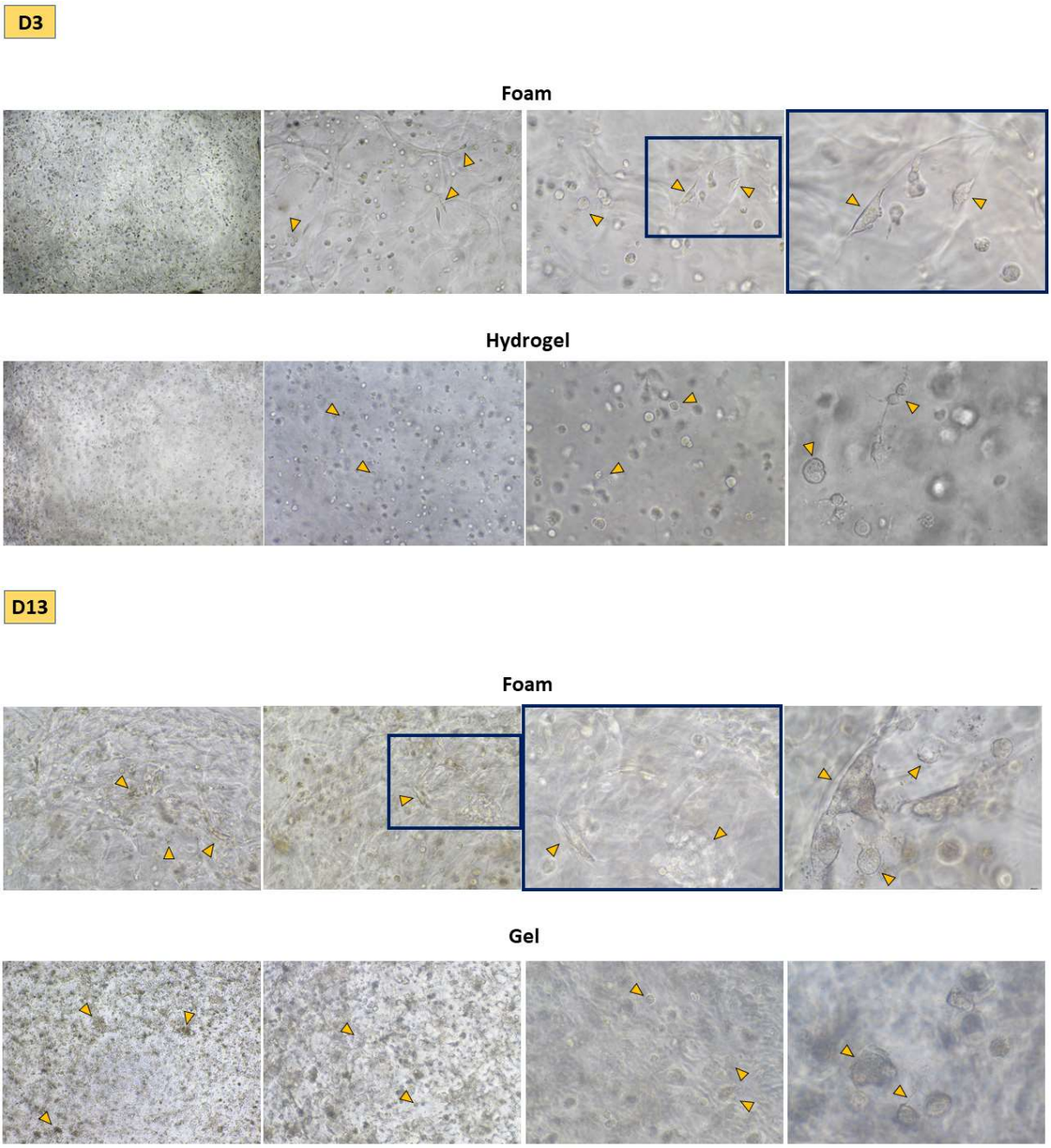

Figure A3: HS-5 at D3 and D13 in foams and hydrogels.

B. Cell morphology in relation to foams

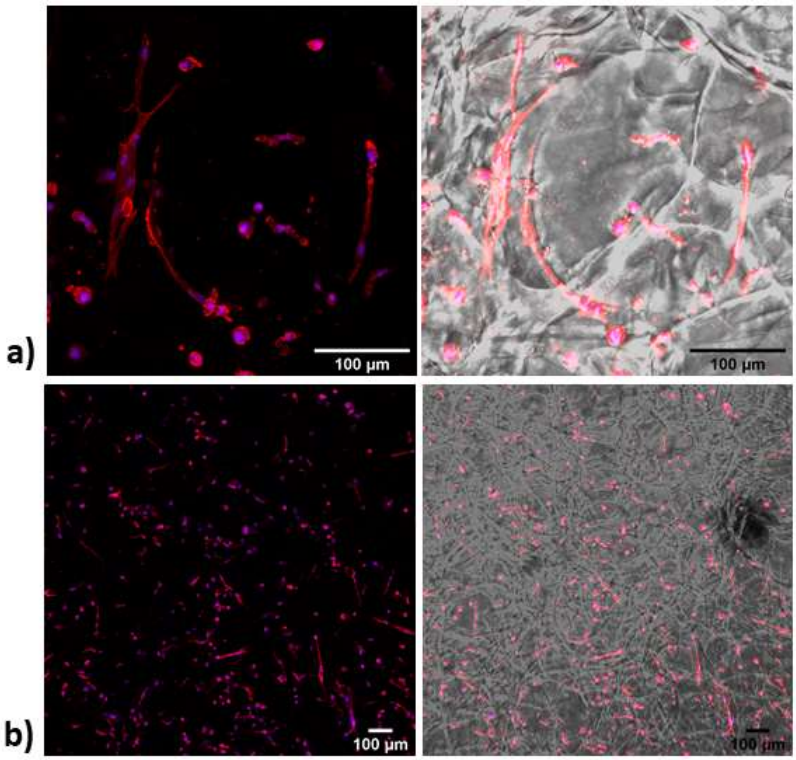

Figure B1: NHDFs stained with DAPI/Phalloidin and imaged with CLSM at D7. Shown in merge with bright field channel, showing cells in 30x that line the foam pores (**a**), in foam structure in 7.5x (**b**).

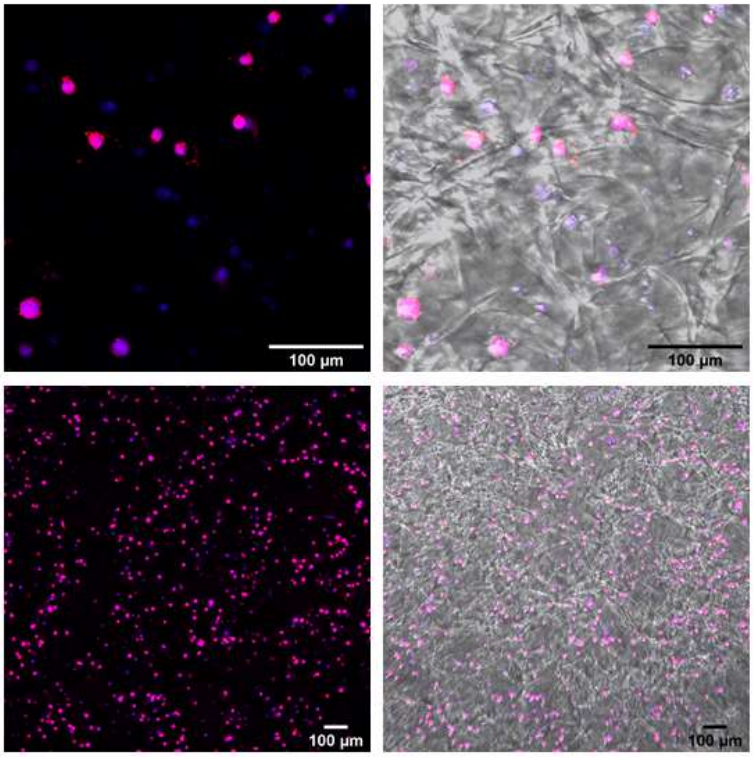

Figure B2: IMR-90s stained with DAPI/Phalloidin and imaged with CLSM at D7. Shown in merge with bright field channel, showing cells in 30x in foam (**a**) and in 7.5x in foam (**b**).

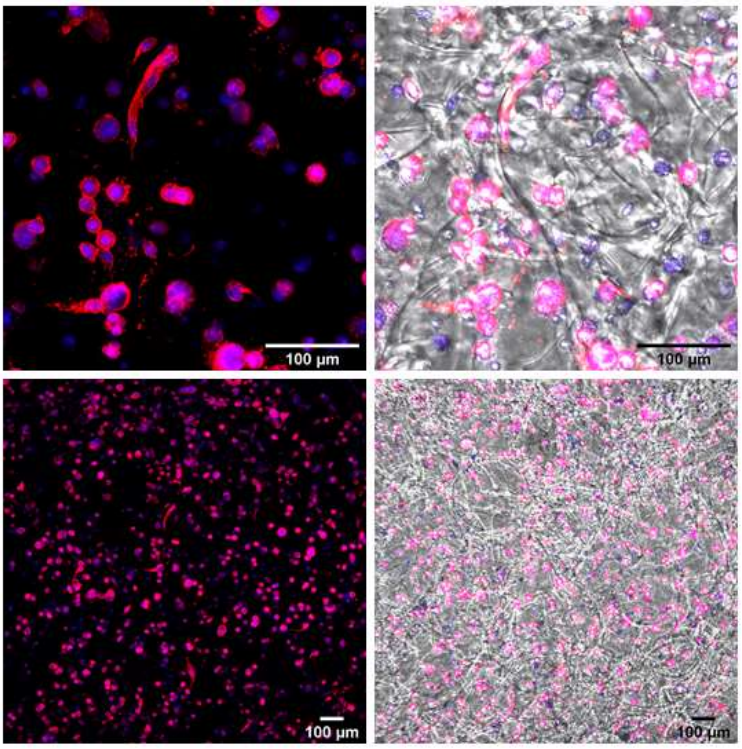

Figure B3: HS-5s stained with DAPI/Phalloidin and imaged with CLSM at D7. Shown in merge with bright field channel, showing a cell in 30x that line the foam pores (top), in foam structure in 7.5x (middle).

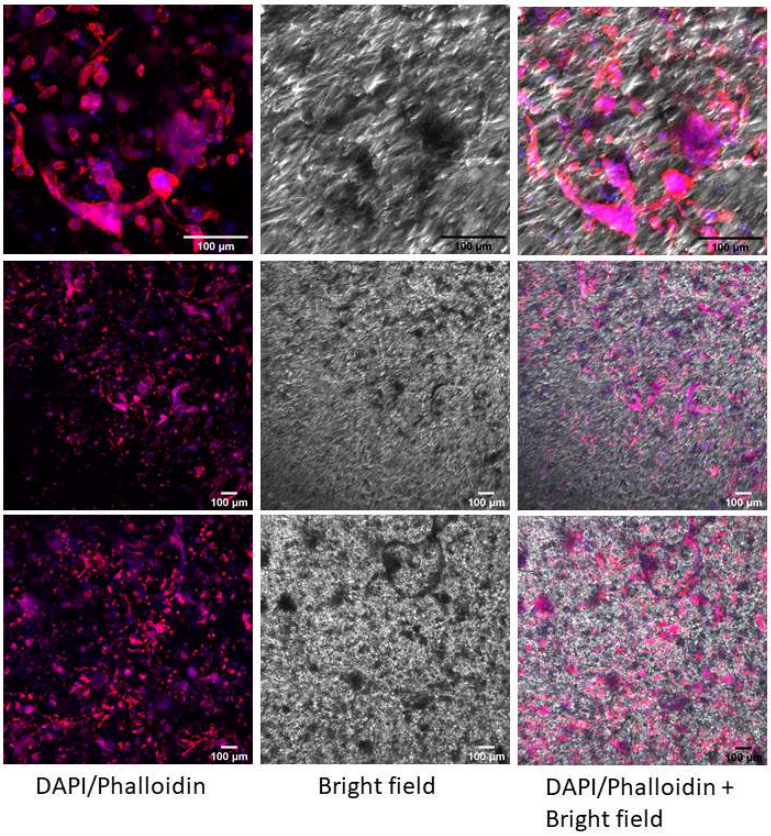

Figure B9: HS-5s stained with DAPI/Phalloidin and imaged with CLSM at D21 in foams. Showing cell clusters and cells in 30x (top) and in in 7.5x (middle and bottom).

C. Large IMR-90-structures at D21

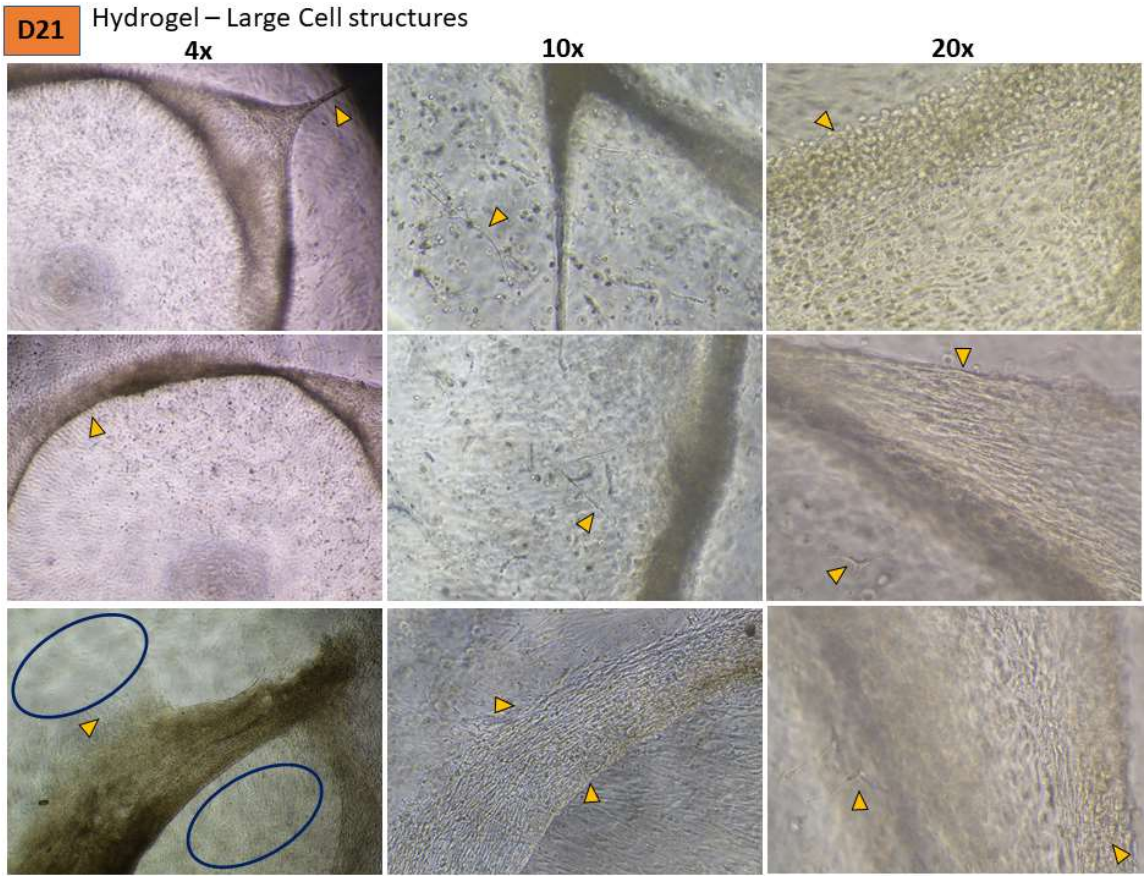

Figure C1: IMR-90 cells in hydrogels at D21, where large dense cell structures had formed. Yellow arrows highlight observations. It could seem that cells were mainly inside the structures, showing bottom-cells "outside" the structure. In the middle upper image (10x), it is shown that in another sample, there were cells seemingly in hydrogel also outside the structure, closer to edge. From the bottom (4x) image, one can see the bottom layer together with the cell structure, and the transition between. The structure is darkest at the top and the bottom (middle, 4x), probably due to density. The middle bottom image (10x) points at what looks like the transition between bottom and start of cell structure, and the border between top of the structure and stretched well-bottom cells, respectively indicated by the arrow to the right and the arrow to the middle. This image corresponds to the one with lower magnification to the left (4x). The image in the very middle (10x) points out an elongated cell. The more magnified images to the right (20x), show how the cells in this wall of cells look in detail. In the top image (20x), the cells look rounded, especially in the densest area. Further down in the image (top, 20x), there are more elongations and space. In the middle image (20x), the arrows point at the structures in focus: an elongated cell with three branches (left arrow), and an area in the cell structure, which indicates that this structure is not horizontal, but rather growing vertically (top arrow, 20x, middle). The cells in the structure here (30x, middle) look more organized, with elongated cells on top of each other. The image at the bottom (20x) shows some of the same, and the part of the cell structure (right arrow) that is on the same level as the two cells that are connected in a square-like structure (left arrow); these also look like they are attached to the cell structure.

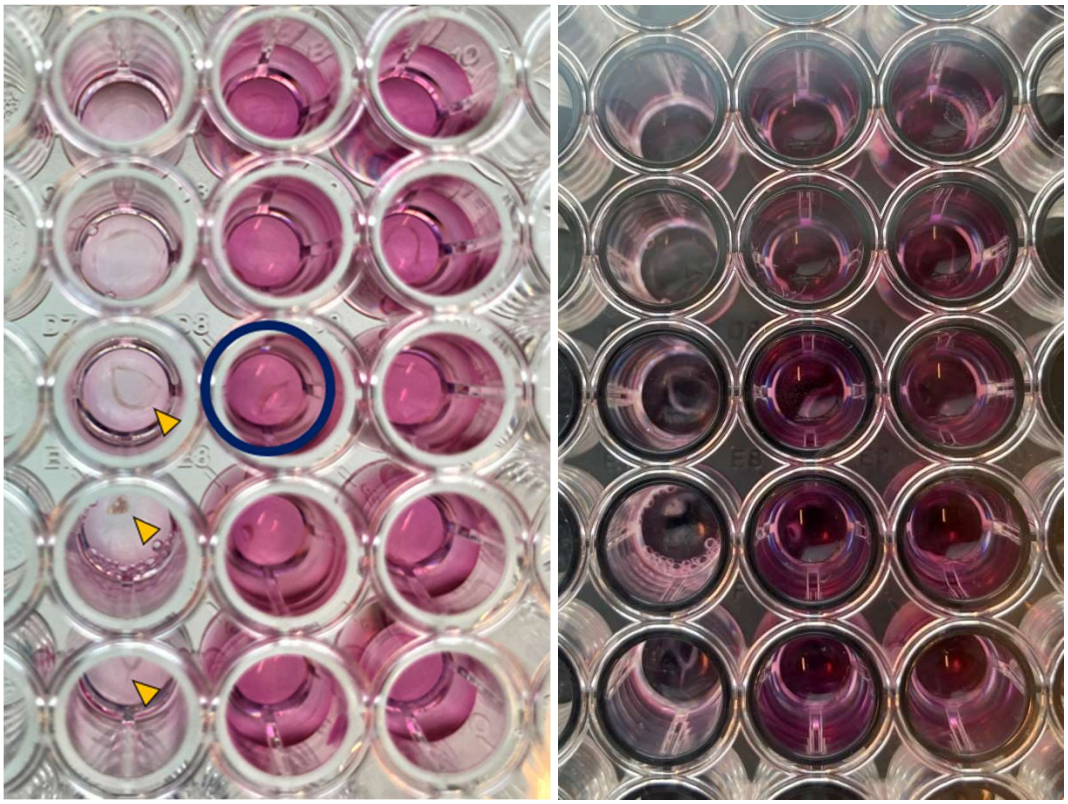

Figure C2: 96-well plate with hydrogel samples with IMR-90, imaged at D21. The same wells are shown with white background (left) and black background (right), for contrast to the cell structures. The large cell structures could also be observed by the naked eye, as pointed out with yellow arrows in the right image.

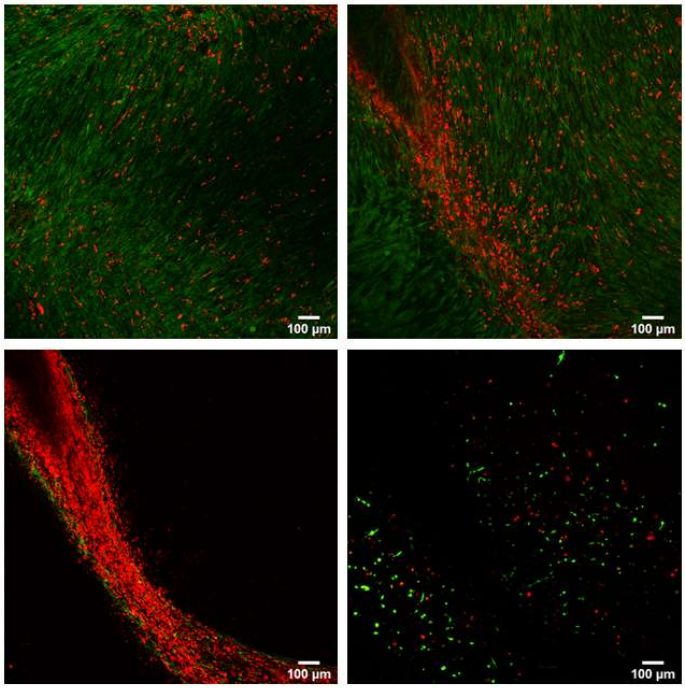

Figure C3: Live/Dead stained IMR-90 at D21, imaged with CLSM, and showing and example of the large cell structures. Comparing the bottom images gives the indication that the cell structures could have been underneath the hydrogel, as it is not visible in the right image where cells in the hydrogel are visible, while the no other cells are visible outside the structure in the left image.

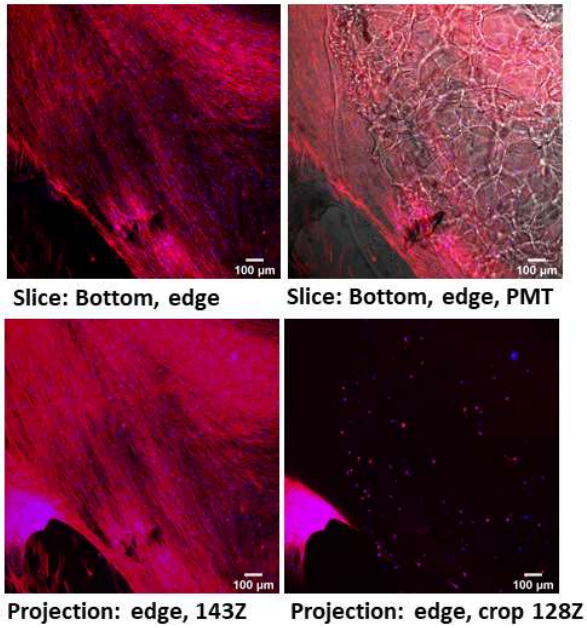

Figure C4: DAPI/Phalloidin stained IMR-90 at D21, imaged with CLSM, and showing an example of the large cell structures in foams. However, these were not so prominent in foams as in hydrogels.

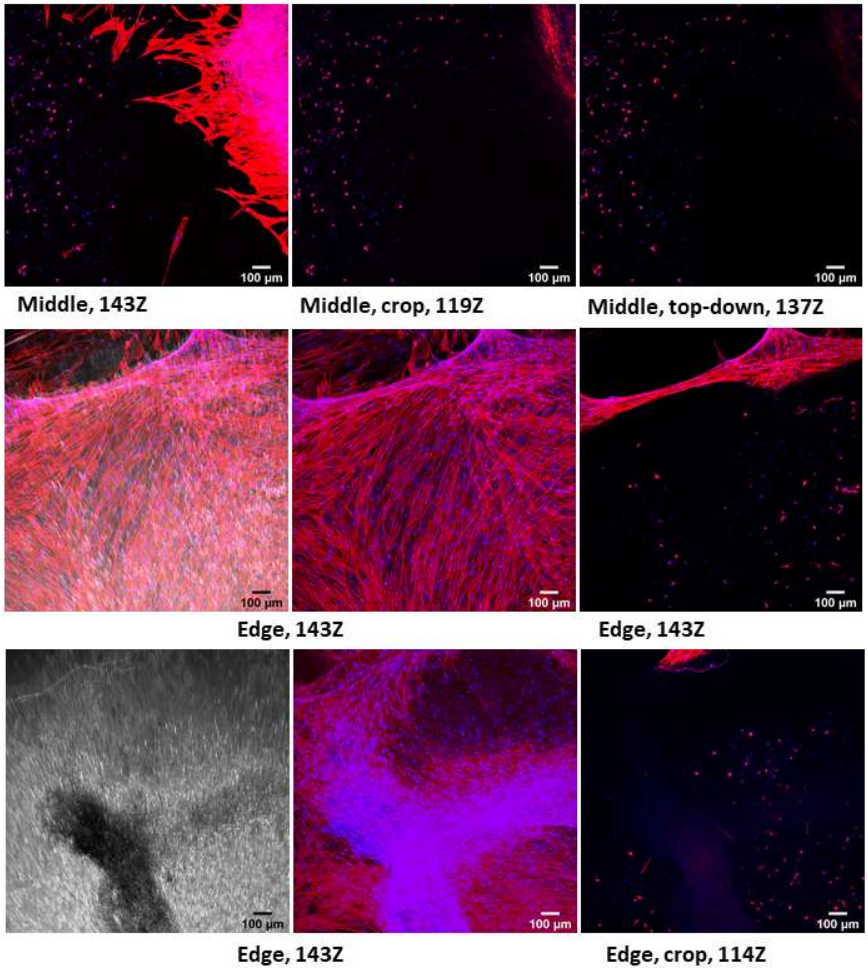

Figure C5: DAPI/Phalloidin stained IMR-90 at D21, imaged with CLSM, and showing an example of the large cell structures in hydrogels. It almost looks as if the structures cut through the hydrogel, as seen in the bottom left image. Thickness of stacks and crops are shown as number of steps in the z-stacks (3.5 µm thick steps).

D. Yellowing of media in long-term HS-5 samples

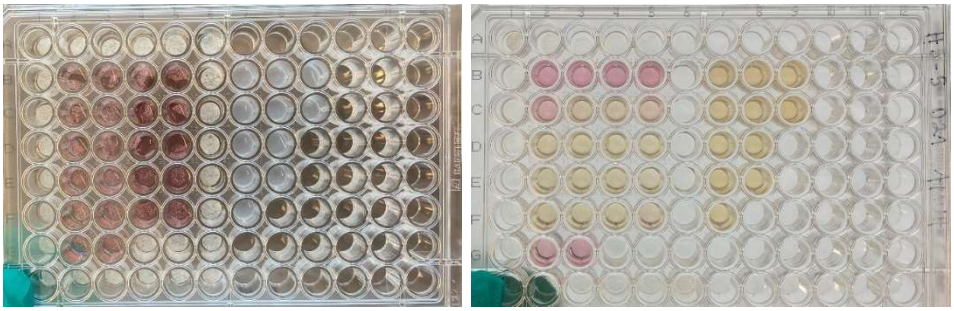

Figure D1: HS-5 samples after casting at D0, where foams are added media and hydrogels are not gelled yet (left image). In the long term (right), media turned yellow quickly. All hydrogels had yellow media, and most of the foams became yellow after a while too (but in a lower degree).

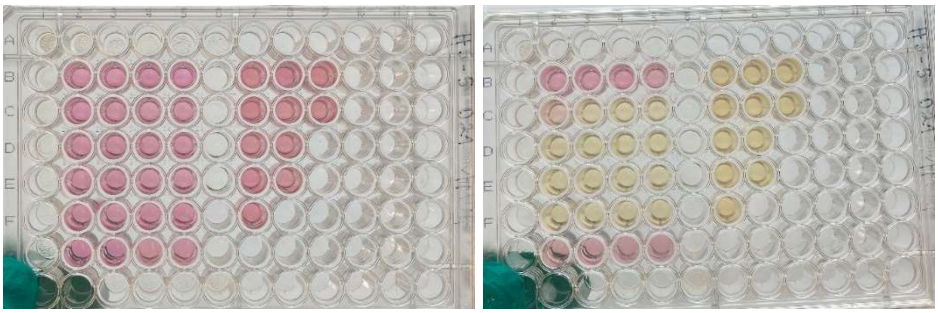

Figure D2: HS-5 samples after removing all media and adding new media, for testing if that would decrease yellowing (left image). The media turned yellow quickly after 1-2 days (right image).

E. Raw data: LDH-absorbance averages in Cytotoxicity testing

Table E1: Absorbance averages (optical density) from LDH-measurement with plate reader (490 nm) for cytotoxicity tests.

Day1	Foam exp.	Gel exp.	Media	Foam neg.	Foam pos.	Gel neg.	Gel pos.
NHDF	0.20684	0.33666	0.117333	0.238767	0.7699	0.4581	1.804833
IMR90	0.33366	0.27664	0.338067	0.3584	0.52953333	0.459633	0.685267
HS5	0.4507	0.53436	0.4661	0.504467	0.7254667	0.637667	1.231333
Day 7							
NHDF	0.12506	0.19076	0.110467	0.153767	1.82696667	0.212567	2.223167
IMR90	0.32106	0.48412	0.27982	0.320667	0.6530333	0.430567	1.1621
HS5	0.6623	1.13114	0.579233	0.90743	1.9533	1.39843	2.75653

F. Additional tests

Comparison of alginate dissolved in media or buffer for foams:

Figure F1: Qualitative comparison of alginate foam gelled with 1% (w/v) alginate in buffer (left) and 1% (w/v) alginate in cultivation media (right) after 48 h. No differences were found.

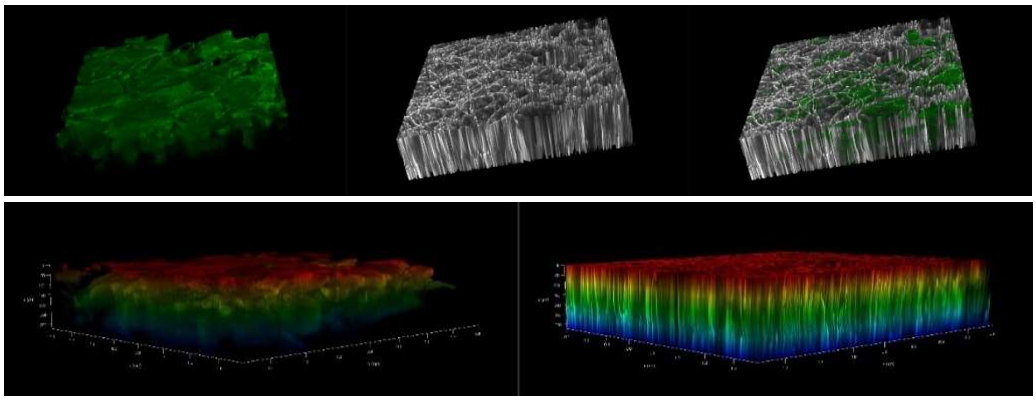

Figure F2: 3D renders of 1% (w/v) alginate in buffer at D7, showing LF200S, foam structure in bright field channel and channel merge (top) and color depth mapping (bottom) of LF200S (left) and foam structure in bright field (right).

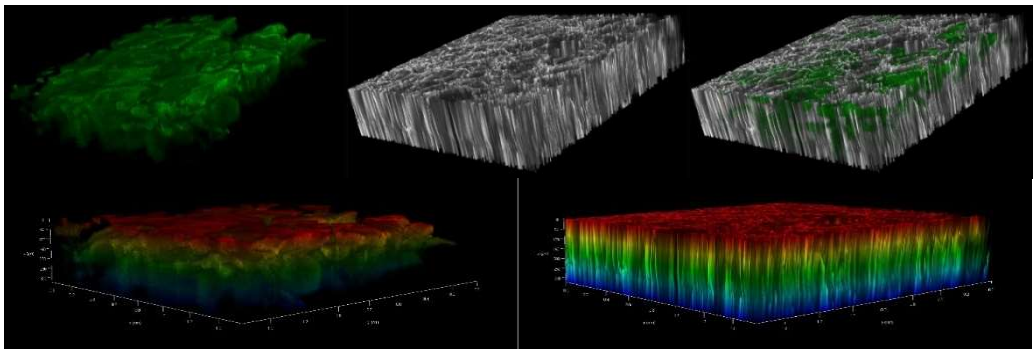

Figure F3: 3D renders of 1% (w/v) alginate in media at D7, showing LF200S, foam structure in bright field channel and channel merge (top) and color depth mapping (bottom) of LF200S (left) and foam structure in bright field (right).

Optimization of cell distribution and investigation of aggregates in foams:

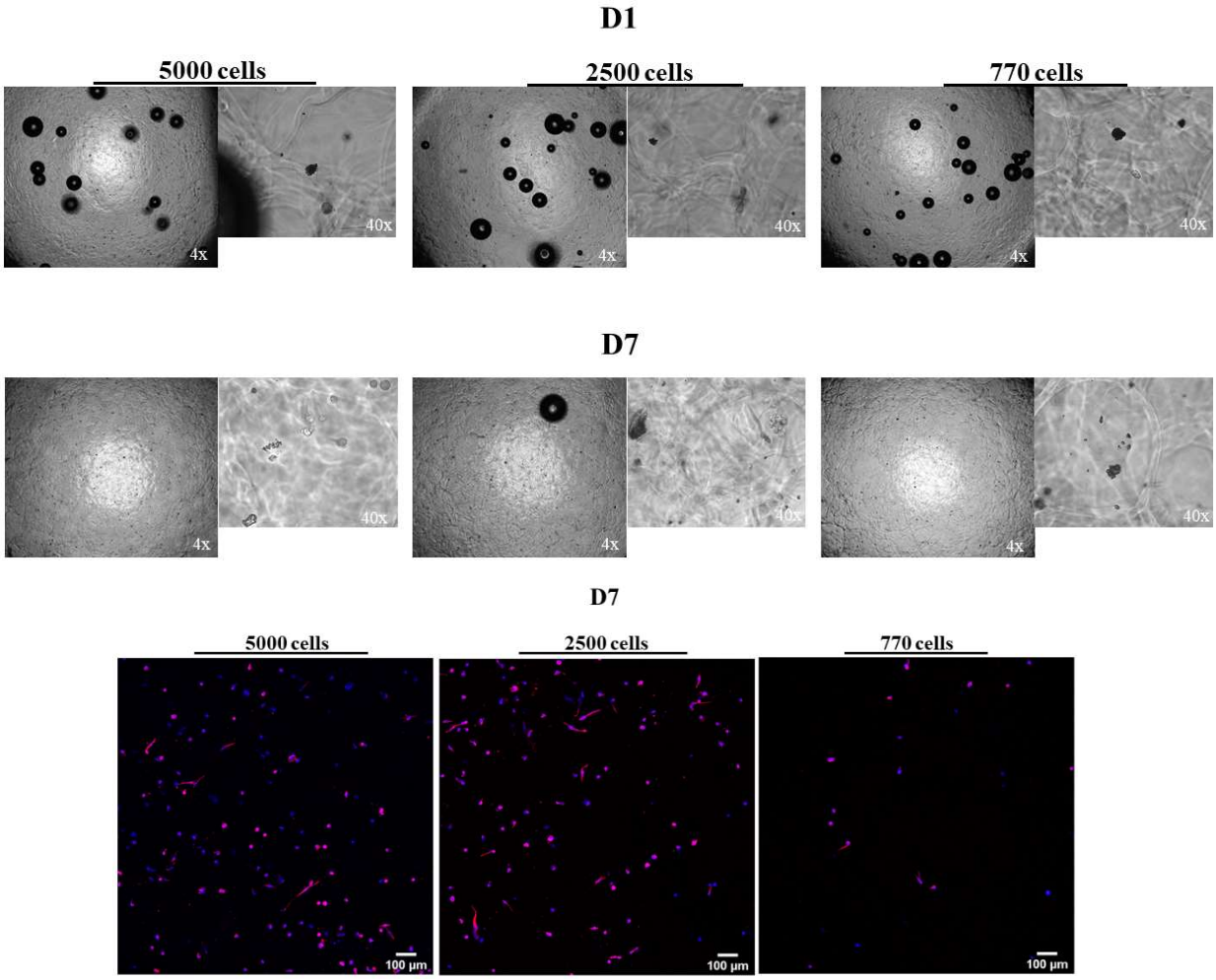

Figure F4: Foams with different cell concentrations (5000 cells/well, 2500 cells/well and 770 cells/well), imaged live with light microscopy at D1 and D7 (top) and from D7 also stained with DAPI/Phalloidin and imaged with CLSM (bottom)

Assessing foam batch differences:

Figure F5: Alginate foams from the first batch used (top row) and later batch (bottom row) taken out of the 96-well plate. Dry foams are shown in the left image, and foams added buffer are shown to the right.

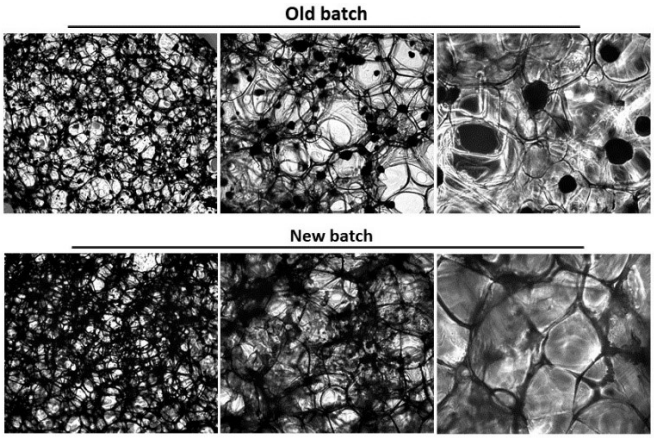

Figure F6: Comparison of dry samples of the first batch used (old batch) and the newer batches, imaged with light microscopy. 4x, 10x and 20x objectives were used. The new batches appear more opaque, and there are fewer black aggregates, however else they look similar in foam structuring.

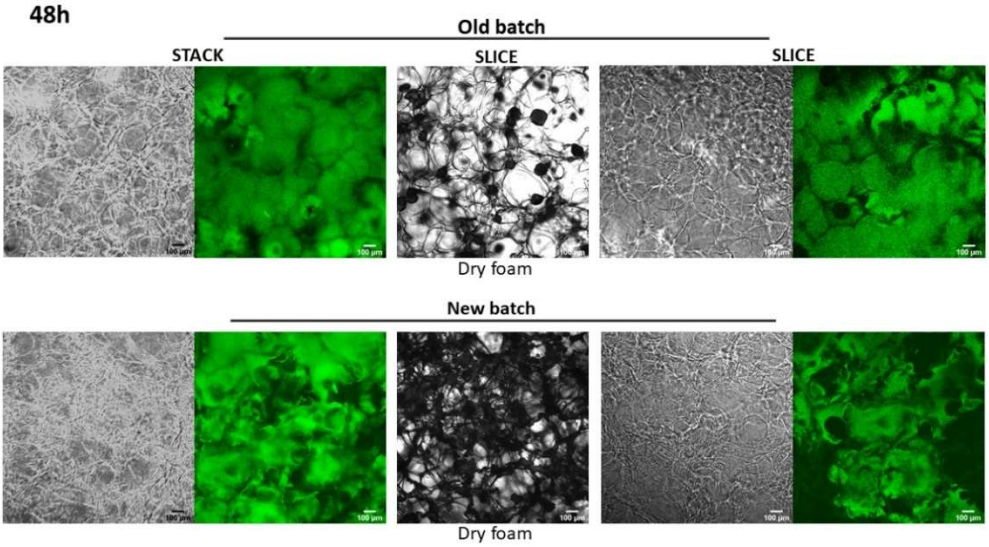

Figure F7: Comparison of samples of the first foam batch used (old batch) and the newer batches, imaged with CLSM and 1% LF200S after 48 h. Bright field channel is shown together with fluorescence channel, and compared to dry samples. Images are shown as both Z-stack projections (left) and slices (right).

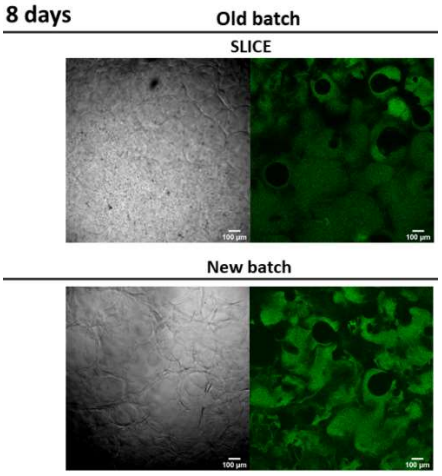

Figure F8: Comparison of samples of the first foam batch used (old batch) and the newer batches, imaged with CLSM and 1% LF200S after 8 days. Bright field channel is shown together with fluorescence channel. Images are slices.

Andrea Mandt-Utbøen Holtermann

NTNU
Norwegian University of
Science and Technology